Subsidence of cover sequences at Kawerau Geothermal Field, Taupo Volcanic Zone, New Zealand

---

A thesis submitted in partial fulfilment of the requirements for the degree

of

Master of Science in Hazard and Disaster Management

at the

University of Canterbury

by

Scott David Kelly

Department of Geological Sciences,

University of Canterbury,

Christchurch, New Zealand

2015

Table of Contents

List of Figures

List of Tables

Abstract

Subsidence occurring at geothermal fields requires monitoring, analysis, and understanding of the mechanisms in order to ensure that it does not affect field operations. This study utilised a broad range of techniques including spatial analysis, three-dimensional modelling, and the comparison of samples of the cover sequences to investigate the subsidence at Kawerau Geothermal Field. Subsidence at Kawerau is of concern because the Tasman Pulp and Paper Mill is located within the geothermal field and utilises machinery with small alignment tolerances that are sensitive to ground deformation. A probabilistic hazard analysis of Kawerau was completed and maps created indicating the potential for subsidence in the future.

Spatial analysis of benchmark re-levelling surveys revealed two types of subsidence features: 1) field wide subsidence and 2) subsidence anomalies. Field wide subsidence, currently covering ~17 km^2, is driven by thermal contraction of reservoir deep formations and/or compaction of the reservoir due to effective stress increases related to pressure drawdown. Four local subsidence anomalies each covering 150 – 400 m^2 are likely driven by varying shallow processes. Two of these features, termed Bowls B and D, south of the Kawerau Geothermal Ltd. power station are the main focus of this thesis along with an assessment of the Tasman Mill site, its potential to develop an anomaly, and the mechanism of subsidence currently occurring across it.

Three-dimensional modelling of the cover sequences to 750 m below relative level was completed in Leapfrog Geo using well logs from Kawerau. Modelling revealed an anomalous thickness of Tahuna Formation below Bowls B and D, and relatively uniform thicknesses across the mill site of other shallow formations. The anomalous thickness of Tahuna Formation was hypothesised as being responsible for the presence of the subsidence bowls by being more compressible than the overlying Caxton Formation which is thicker across the mill site while the Tahuna Formation is thinner. Alternative hypotheses were explored by mapping the relative level of the Matahina ignimbrite, thickness of the Caxton Formation, and distribution of brecciation.

To test the main hypothesis, samples of Tahuna and Caxton formations were collected from the Kawerau Core Shed and tested for their physical properties and relative compressibility. XRD and thin section analysis was also completed on the samples. Tahuna Formation was found to have more than three times the porosity of the Caxton Formation and have smectite clays present. Using a method developed for testing the relative compressibility of weak rock

the Tahuna Formation was found to generally be twice as compressible and elastic as the Caxton Formation when saturated. Samples of Recent alluvium from the mill site were also tested for their physical properties and found not to have the potential to contribute to subsidence across the mill site. However further investigation is required to confirm the mechanisms of Bowls B and D.

A hazard analysis of Kawerau Geothermal Field found that the field has a low annual probability of being impacted by volcanic and volcanogenic, earthquake, and flooding events. Probabilities are calculated based on the reoccurrence intervals for each event. A hazard map for subsidence at Kawerau is also developed and outlines four zones of risk. Infrastructure at risk based on trends of subsidence is also analysed for its susceptibility to subsidence and mitigation methods discussed.

The overall conclusion is that the geological conditions beneath the mill site are unlikely to form a local subsidence anomaly, and the mill site is largely unaffected by the field wide subsidence bowl. Ground tilt values are within mill machinery tolerances, and based on current trends the spatial extent of subsidence anomalies will remain approximately the same into the future.

Acknowledgements

Firstly, I would like to thank Professor Jim Cole. Jim's enthusiasm and encouragement was crucial to this project from the first time I walked into his office and every discussion we had left me with renewed enthusiasm. Thanks also goes to my two co-supervisors, Dr. Paul Siratovich and Dr. Val Zimmer, as well as Dr. Marlène Villeneuve, discussions with you all were vital to the progression of the thesis at various times throughout the year.

I would also like to thank Might River Power Ltd., and in particular John Clark. John was instrumental in the North Island, organising site access, access to reports and data, and provided constant support throughout the project.

I acknowledge that this thesis would not have been possible without funding from a Callaghan Innovation R&D Student Grant, the Source to Surface program, and the Brian Mason Trust. Thanks also to Ben Pezaro at Mighty River Power Ltd. in Auckland who set up the Callaghan Grant.

Thanks to Derrick Hope and Gabriel Anderson at Carter Holt Harvey Tasman, and Joe Hotson and Graeme Everett at Norske Skog Tasman for answering all my questions about the pulp and paper mill processes at Kawerau.

To Peter Joynt and Andrew Cantwell at ARANZ Geo, thanks for tutorials and discussions on Leapfrog Geo. It is an amazing piece of software and the early stages would not have progressed half as quickly or as easily without it or your guidance.

Thanks to Cathy Higgins who helped make testing less than ideal samples possible, and to the rest of the UC technical staff; Chris Grimshaw, Stephen Browne, Rob Spiers, and Dr. Kerry Swanson, for explaining and demonstrating numerous techniques vital to this thesis. Also thanks to Dr. Matthew Hughes, your guidance with ArcGIS over the past two year was crucial.

To all my flatmates over the past five years: Dre, Sam, Leon, Jake, Grace, Emma, Kelsey, Anna, and Ben. I could not have wished for better people to have lived with through my Uni life.

Finally to Mum, Dad, and Elizabeth, thank you for your love, support, and gentle pushes in the right direction to get me where I am today.

1 Introduction

Subsidence is the phenomena when ground level lowers in relation to a fixed datum following a change in subsurface conditions. Subsidence predominantly occurs in oil, gas, and geothermal fields where fluids are extracted from reservoirs resulting in decreased reservoir pressure and higher effective stress from the overlying lithologies (Narasimhan & Goyal, 1982).

In a stable system subsidence is prevented by the lithostatic load being supported by the rock matrix strength and pore fluid pressure. When anthropogenic changes occur and fluids are extracted the pore fluid pressure can decrease, as a result lithostatic load is transferred from the pore fluid to the rock matrix, resulting in compaction of the unit which presents as subsidence at the surface. In geothermal fields another mechanism is the contraction of rock due to a decrease in temperature which results in subsidence at the surface; this is known as thermal contraction (Narasimhan & Goyal, 1982). Compaction can be prevented or reduced by re-injecting fluids into the system to decrease the amount of fluid lost and maintain pore fluid pressure (Sarychikhina et al., 2011). Contraction can be mitigated with sound management of the geothermal field preventing temperature declines in the reservoir.

Subsidence is an issue because the infrastructure required to operate a geothermal field has the potential to be affected by ground deformation. The key parameter is ground tilt which is the difference in rates of subsidence across an area; a high ground tilt can lead to a loss of serviceability - cracking of components such as pipes resulting in leaks, damage to buildings, and in extreme cases result in damage to well bore casings (Bruno, 1992; Bloomer & Currie, 2001). Other effects include a reduction in the reservoir volume due to the compression or contraction of the reservoir unit, changes in reservoir chemistry, flooding because of ground deformation near rivers, and stretching or compression of pipelines because of the movement of foundations (Bloomer & Currie, 2001; Truesdell & Lippmann, 1998).

At Kawerau Geothermal Field (KGF) subsidence is a concern because of the Tasman Pulp and Paper Mill operates within the boundaries of the field. Mill machinery has extremely tight tolerances in order to operate efficiently and subsidence has the potential to misalign mill machinery beyond normal maintenance tolerances. Regular misalignment of machinery will cost time and money to realign. Therefore an analysis of subsidence at KGF is required so mill operators are aware of the likelihood of ground deformation affecting their machinery and KGF tappers can mitigate the development of subsidence features with the potential to impact mill operations.

1.1 Regional Geological Setting

The Taupo Volcanic Zone (TVZ) is a southwest to northeast trending rifted arc (Wilson et al., 1995a) resulting from the subduction of the Pacific Plate beneath the Indo-Australian Plate at 43 mm/year (Beavan, 2002). Extension rates range from ~15 mm/year at the Bay of Plenty coastline to <5 mm/year south of Lake Taupo (Wallace et al., 2004). TVZ is ~60 km wide and ~300 km long, from Mt. Ruapehu in the south to White Island in the north, Wilson et al. (1995a) defined the boundary of the TVZ to encompass all volcanic vents and calderas that have contributed to all the erupted material dispersed in and beyond the TVZ (Fig. 1.1). The concept of a young TVZ boundary is introduced by Wilson et al. (1995a) and includes all the active centres during the Whakamaru-group eruptions around 0.34 Ma, and the vents that have been active through to the present day. The earliest known TVZ activity is andesitic and began at >2 Ma; from ~1.6 Ma activity became predominantly rhyolitic (Darby et al., 2000).

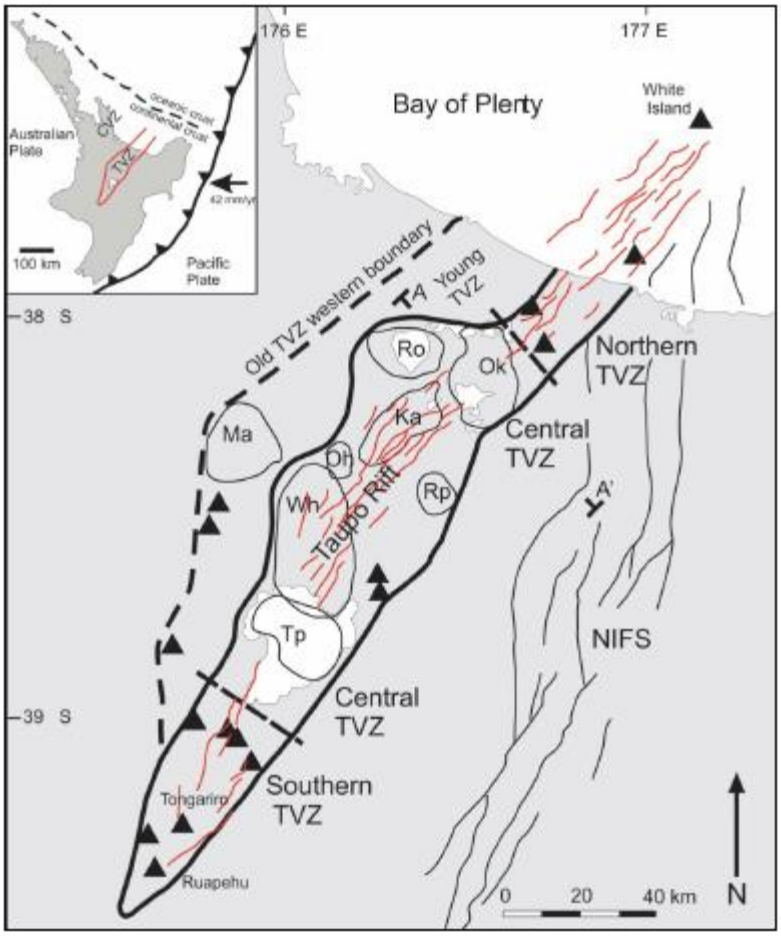

Figure 1.1: Taupo Volcanic Zone with young and old TVZ boundaries (from Cole et al., 2014).

Within the TVZ is a belt of normal faulting along northeast – southwest structures, known as the Taupo Fault Belt, which accommodates northwest – southeast extension (Rowland & Sibson, 2001). Current rates are estimated at 8 ± 2 mm/year based on geodetics (Darby et al., 2000). The heat source for the 23 geothermal fields (Fig. 1.2) is related to the regional TVZ setting, because of the active rifting across the TVZ the crust is stretched and thinned to only 15 km which has led to temperatures of 350 °C at <5 km depth (Wilson et al., 1995a).

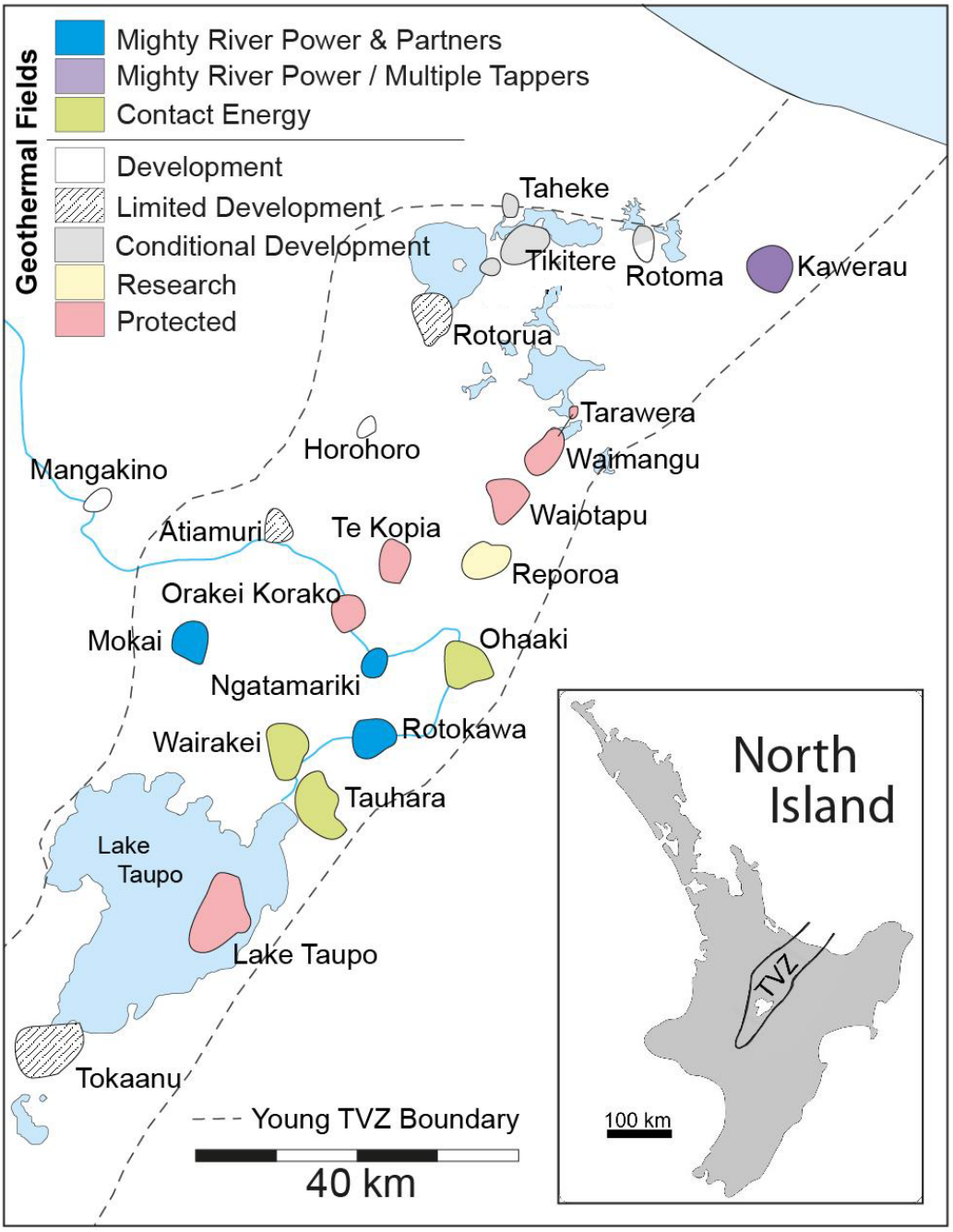

Figure 1.2: Map of Taupo Volcanic Zone geothermal areas (John Clark, pers. comm., 2014).

The Whakatane Graben is the main structural feature occupying the north-eastern area of the TVZ. Following the 1987 Edgecumbe earthquake studies have led to a structural model of the graben, which is made up of a series of normal block faults dipping at 45 ± 10° towards the centre of the graben (Fig. 1.3) (Cole, 1990; Nairn & Beanland, 1989). The structure of the graben results in tectonically driven regional subsidence. Subsidence began ~0.3 Ma continuing to present day at a rate of 1 – 2 mm/year, while the margins of the structure have been uplifted at slightly lower rates (Nairn & Beanland, 1989). Like the rest of the TVZ the Whakatane Graben is actively spreading at several mm/year (Allis, 1997). As a result of the regional subsidence the basement Mesozoic greywacke has been down faulted to ~2 km below ground level (BGL), and the basin has then been in filled by Quaternary volcanics, and sediments from the Tarawera, Rangitaiki and Whakatane rivers as background sedimentary flux and catastrophic events (Milicich, 2013a).

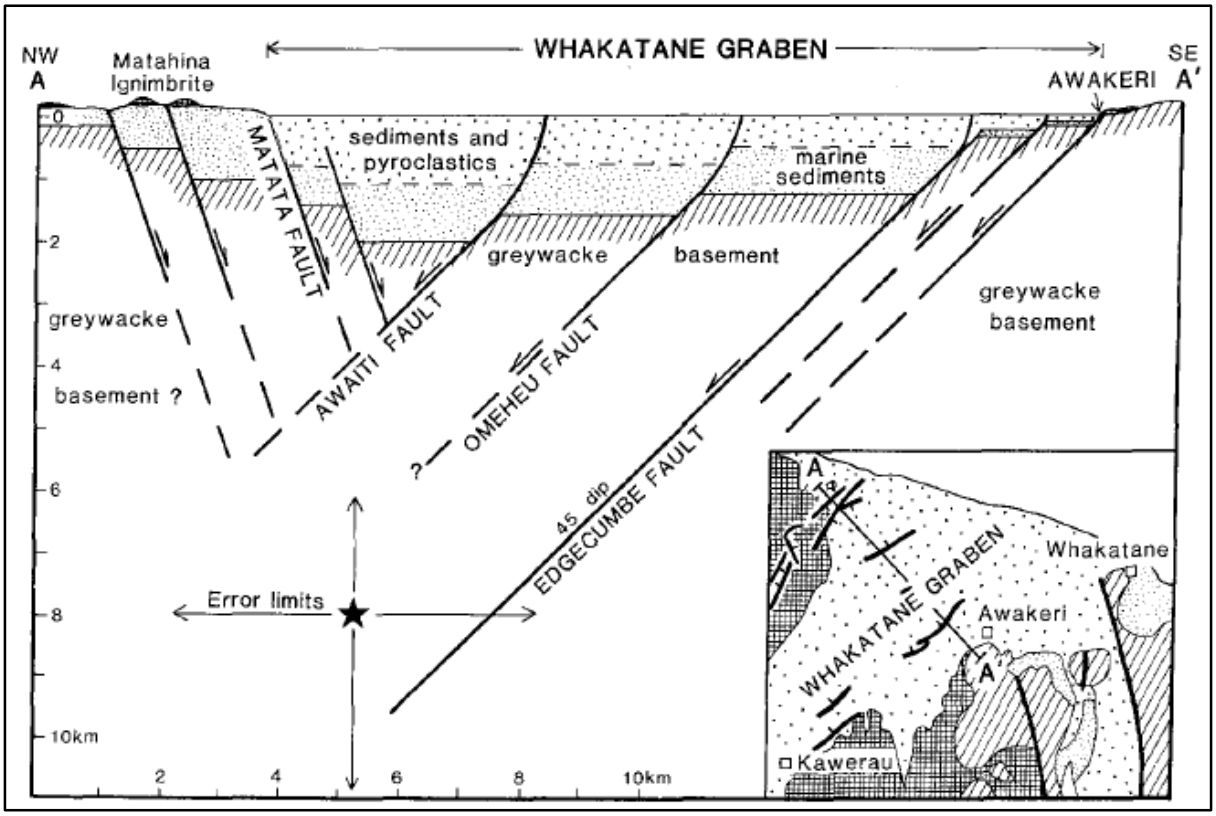

Figure 1.3: Cross section across the Whakatane Graben, star shows location of 1987 Edgecumbe earthquake (from Cole, 1990).

Poor sorting of sands and gravels with interspersed boulders, and angular to sub-angular clasts are typical of catastrophic events which have occurred as breakout floods from Okataina Caldera and Lake Tarawera. Recognised events occurred in c. AD 1315, associated with the AD 1314 Kaharoa eruption, and in AD 1904, associated with the AD 1886 Tarawera basalt

scoria eruption (Ashwell, 2014; Cole et al., 2010; Hodgson & Nairn, 2005). Occurring near the end of the AD 1314 Kaharoa rhyolite eruption, the larger of the two events, was the result of a fan of reworked volcaniclastic material blocking the existing outlet of the Tarawera River. Lake Tarawera rose ~30 m above its present elevation before overtopping the dam and releasing ~1.7 km^3 of water and sediment at a peak rate of ~10^5 m^3/s which scoured the outlet down by >40 m, excavated a 300 m wide channel to the Tarawera Falls, and a 1 km wide channel below the falls (Hodgson & Nairn, 2005). The AD 1904 event was smaller but similar to the c. AD 1315 event and occurred because of the failure of a dam created by the AD 1886 Tarawera eruption, peak discharge of this event is estimated to be ~700 m^3/s (Hodgson & Nairn, 2005).

The surficial formation of the Rangitaiki Plains consists of well sorted, continuous, pockets of similar material which indicates background sedimentation rates from fluvial processes as the Tarawera, Ragitaiki, and Whakatane rivers meander across the Rangitaiki Plains. Deposits include sands derived from pumice, silts, clays, and lenses of organic material (SKM, 2005). Historical river channels are difficult to identify due to reworking of the ground for farming and construction works, but a LiDAR analysis of late Holocene faulting was able to distinguish channel migration assumed to be from faulting processes (Begg & Mouslopoulou, 2010).

1.2 Kawerau Geothermal Field

Kawerau Geothermal Field (KGF) is the north-eastern most geothermal field in the TVZ, located ~20 km from the Bay of Plenty coastline (Fig. 1.4). Unlike many TVZ geothermal fields Kawerau is not located on or in the faulted margins of a rhyolite caldera, instead it is located within an actively extending graben structure overlain by Quaternary volcanics and sediments (Kissling & Weir, 2005). The KGF reservoir is hosted in greywacke basement, unlike many other geothermal fields in the TVZ that are hosted in Quaternary volcano-sedimentary sequences (Wood et al., 2001).

Following successful scientific surveys and shallow drilling in 1951/52 the Tasman Pulp and Paper Mill (now Norske Skog Tasman) was established on the KGF site because of the potential for geothermal heat to be used in the mill processes. Exploration of the geothermal potential at Kawerau began in 1956 and the first geothermal steam was provided to the mill in 1957. The plant currently receives 300 t/h of geothermal steam, accounting for more than half of the direct geothermal heat use in New Zealand (Bloomer, 2011).

The Kawerau Geothermal Limited power station (KGL) is operated by Mighty River Power Ltd. (MRP) and was commissioned in 2008. KGL is a dual-flash separation power plant and

has a net output of 106 MW providing power to the national grid (Transpower, 2014). There are also four binary plants (TG1, TG2, TOPP1 and GDL) under different ownership groups that operate at KGF supplying power to various users including Tasman Mill operators.

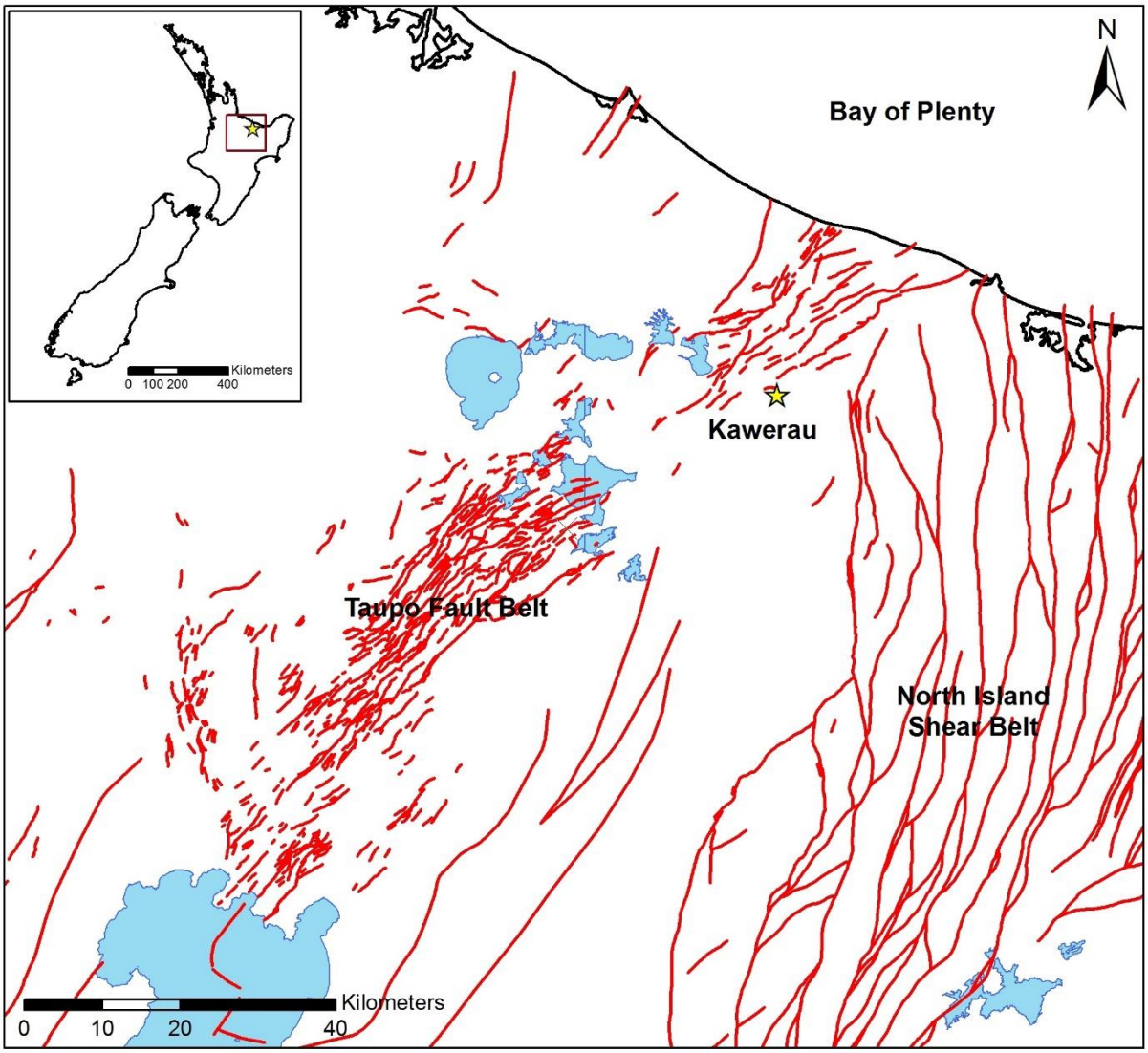

Figure 1.4: Map showing location of Kawerau within New Zealand (inset) with surrounding fault belts and lakes (Leonard et al., 2010).

1.2.1 Wells and KGL Power Station

Since 1952 78 wells have been drilled at Kawerau for production, injection, deep and shallow monitoring, groundwater monitoring, and investigation; currently there are 13 production wells and 11 injection wells in use (Table 1.1). Many of the older, shallow wells developed casing cement issues or suffered cold water invasion and have been grouted up, others are used for monitoring purposes; Figure 1.5 shows the current status and location of all KGF wells. KGL is currently fed by seven ~2000 m deep production wells in a 280 °C reservoir. Reservoir temperatures range from 250 – 310 °C around the field, making Kawerau one of 15 high

temperature geothermal systems in New Zealand (Milicich, 2013a). Fluids from KGL are re-injected into five 2500 m deep wells at 115 – 120 °C in the north of the field, away from the production zone, to prevent pressure drawdown and cooling of the reservoir (Spinks, et al., 2010), waste water is also discharged into the Tarawera River at 40 – 50 °C after flowing through a cooling channel.

	Production	**Injection**
Kawerau Geothermal Limited (MRP)	7	5
Ngati Tuwaretoa Geothermal Assets Limited (NTGA)	6	5
Geothermal Developments Limited (GDL)	1	2

Table 1-1: Developers of KGF and the number of wells utilised.

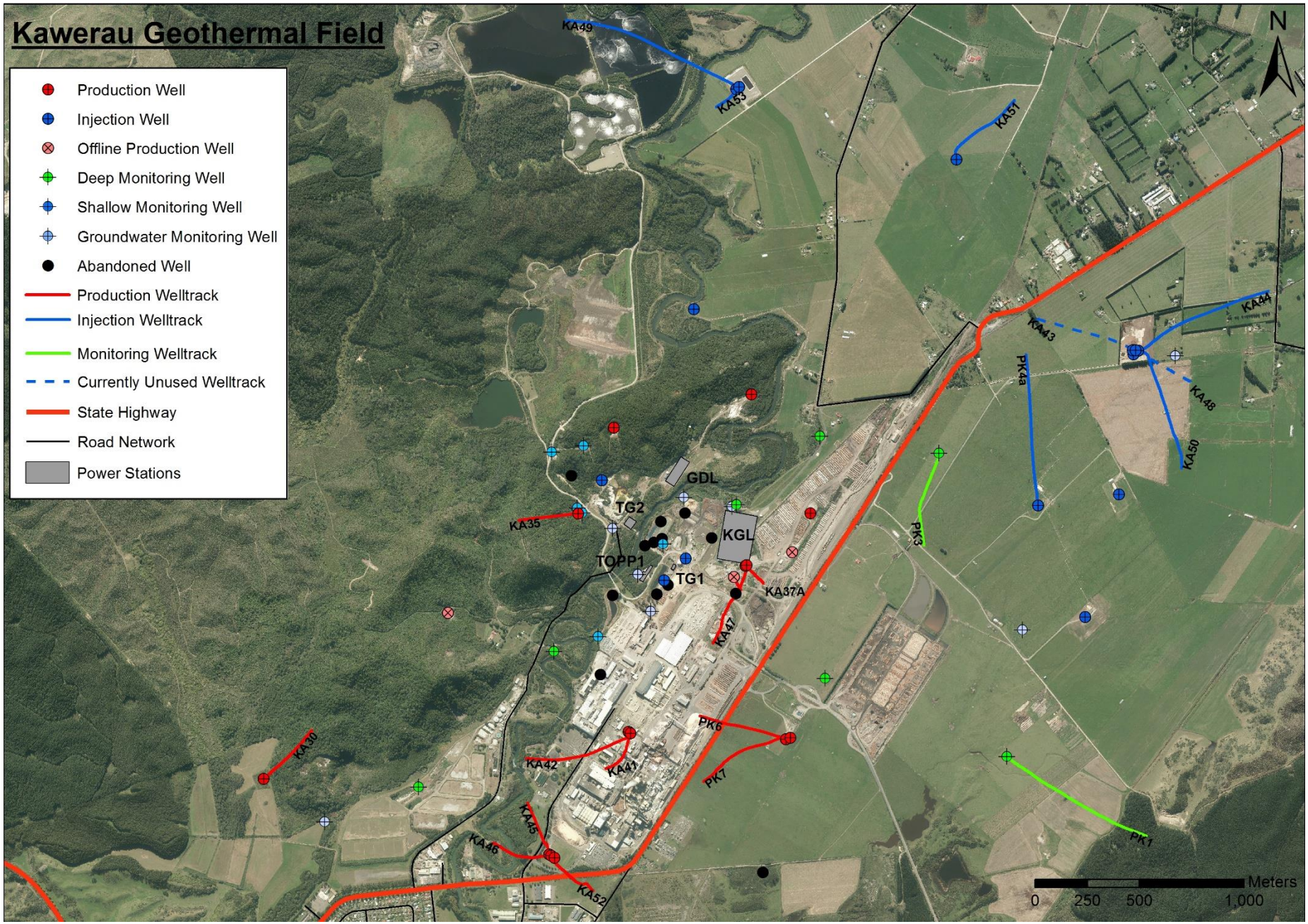

Figure 1.5: KGF wells and power stations.

1.2.2 Geology

The original stratigraphy of an area occupied by a geothermal system is difficult to interpret because high temperature fluids which allow geothermal systems to be utilised also cause extensive hydrothermal alteration of the host rocks (Milicich et al., 2013a). However, exploitation of geothermal systems provides cores and cuttings from wells which provide valuable information on the geological framework of the system. KGF currently has 78 wells to various depths that were analysed in detail by Milicich et al. (2013a). A stratigraphic column and cross section are displayed in Figures 1.6 and 1.7.

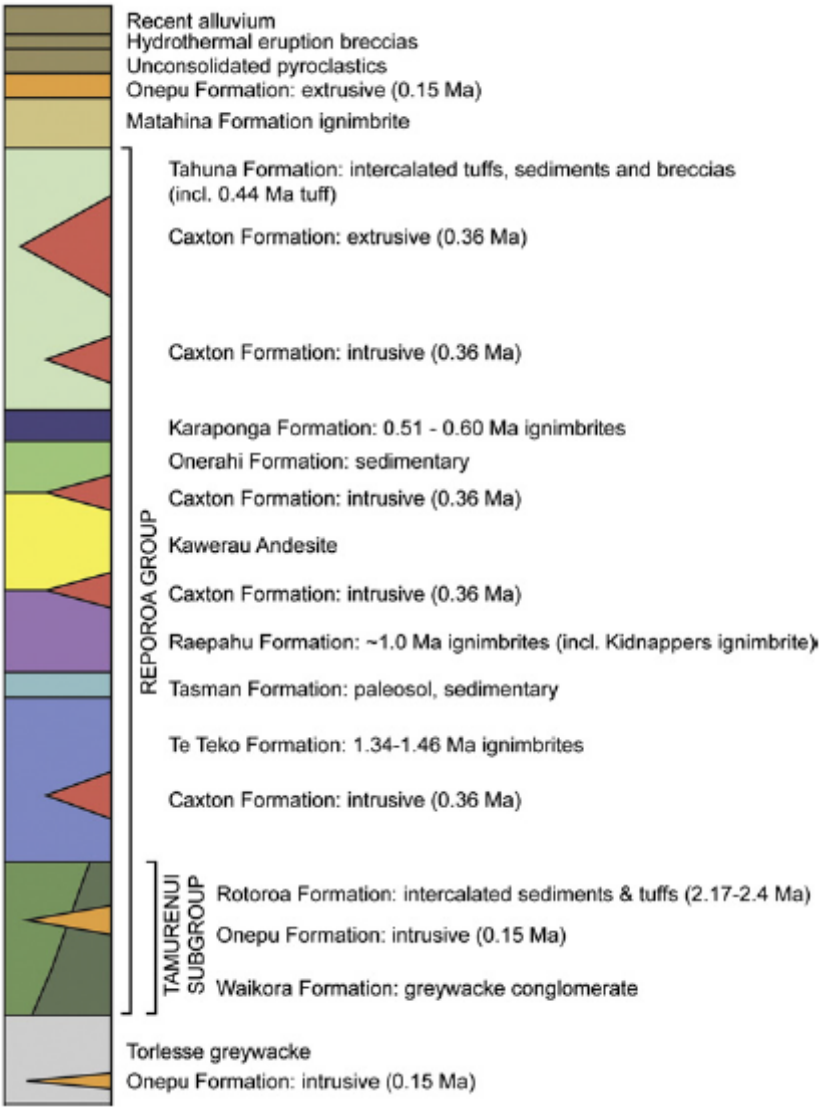

Figure 1.6: Stratigraphy of KGF (from Milicich et al., 2013a)

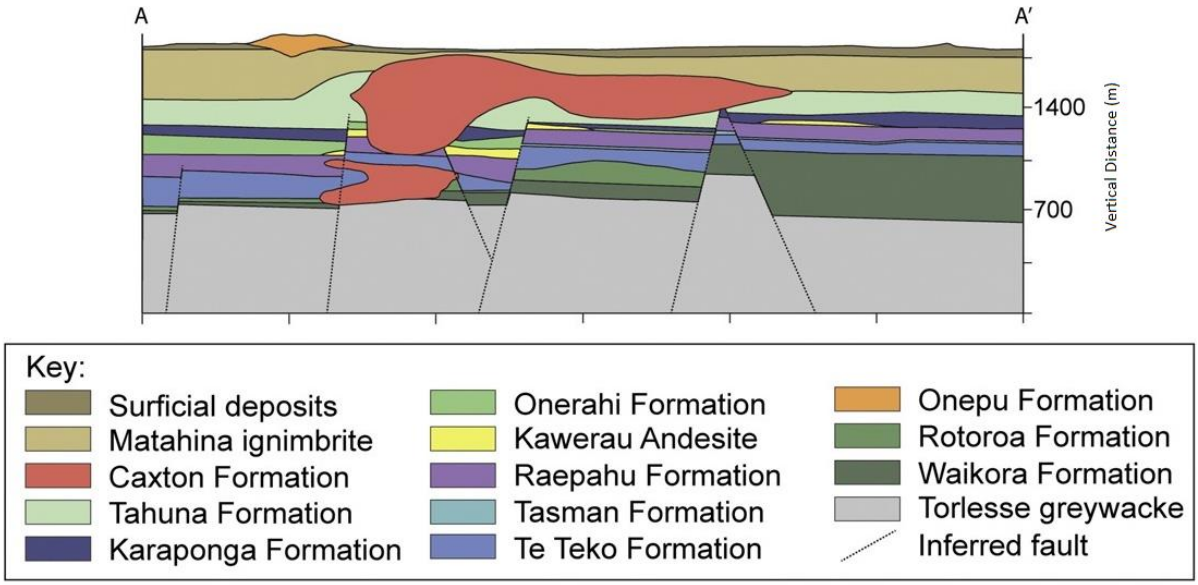

Figure 1.7: West to East Cross section of KGF (from Milicich et al., 2013a).

The following is a summary of the stratigraphy at KGF from Milicich et al. (2013a) from youngest to oldest.

Recent Alluvium

Recent alluvium comprises the top 10 – 80 m of KGF and consists of pumiceous silts, sands and gravels interspersed with clay lenses and peat deposits. The material was deposited by the Tarawera River as it meandered across its flood plain over the past ~60,000 years as background sedimentary flux and catastrophic inundations of the flood plain from break-out floods following eruptions of Okataina Volcanic Centre (OVC) (Hodgson & Nairn, 2004).

Hydrothermal eruption breccias

Two large (10^6 – 10^7 m^3 erupted volume) hydrothermal eruption breccias have been mapped and examined on the south-eastern margin of KGF by Nairn & Wiradiradja (1980). The products of the explosions are interbedded with regionally distributed dateable pyroclastic material. Using ^{14}C dating techniques the deposits are dated at 9,000 and ~14,500 years before present (BP) (Nairn & Wiradiradja, 1980). The eruption breccias contain clasts of hydrothermally altered Matahina ignimbrite and Onepu rhyolite indicating an excavation depth of at least 152 m BGL. The craters left by these eruptions can be seen from high vantage points around at the mill complex. A further seven eruption centres have been inferred; these now consist of shallow depressions occupied by stagnant pools. Features known as Boiling Lake and Lake Pupuwharau, at the base of Putauaki, are also inferred to be the results of hydrothermal eruptions (Christenson, 1987).

Putauaki (Mt. Edgecumbe)

The 821 m high Putauaki is a multiple vent dacite-andesite cone (Carroll et al., 1997) located near the southern boundary of the KGF. The youngest dated eruption of Putauaki is 2400 years BP but the main cone is ~5000 years old making it younger than the Kawerau geothermal system (Browne, 1979; Carroll et al., 1997). Volcanics from Putauaki have been dated at 2400 – 8500 years old but no Putauaki eruptive material has been identified in KGF drillholes (Bignall & Milicich, 2012). Geothermal exploration and production, and the conceptual model of the modern Kawerau geothermal system indicates that intrusive igneous rocks associated with the Putauaki complex may be the heat source and upflow area of KGF as the highest temperatures (up to 310 °C) occur along the southern part of KGF near Putauaki (Bignall & Milicich, 2012). Deep, hot fluids move upwards through basement greywacke via widely spaced, steeply dipping faults and/or fractures with high local permeability in an otherwise highly impermeable rock (Allis et al., 1993; Bignall & Milicich, 2012).

Unconsolidated pyroclastics

KGF has received numerous fall deposits, not all of which are preserved and identified as continuous units within the stratigraphy. On the edges of KGF are two ignimbrite deposits from nearby OVC which are thick enough to form mappable deposits; the c. 64 ka Rotoiti Formation, and c. 26.5 ka Mangaone Subgroup ignimbrites (Jurado-Chichay & Walker, 2000). Neither formation is included in the KGF stratigraphy due to their discontinuity in well logs.

Matahina Ignimbrite

The Matahina ignimbrite was erupted from OVC at 0.322 ± 0.007 Ma (Leonard et al., 2010) and covers ~2000 km^2 out cropping to the north, south, and east of KGF; it is encountered at 10 – 330 m beneath the geothermal field (Milicich, 2013b). Matahina ignimbrite is a partially welded and jointed fall deposit and hosts a shallow aquifer that flows as near-surface cold groundwater across the field (Milicich et al., 2013b). The thickness and depth varies across the field because deposition was controlled by the topographic relief of the Caxton rhyolite dome complex and Tahuna Formation that underlie it. Beneath the Tasman Mill complex the ignimbrite is found at 69 m BGL in G1 and G2, and 60 – 65 m BGL in KA41 and KAM11 (SKM, 2005).

Tahuna Formation

The Tahuna Formation is made up of sedimentary units and intercalated tuffs which are grouped together because of their contemporaneous deposition. The formation is dominated by intercalated carbonaceous siltstones and crystal-rich sandstones with breccias, tuffs, ignimbrites, and shallow marine deposits with shell deposits. Lithological variation in the sedimentary horizons are gradual and lateral variability in thickness makes the formation difficult to correlate between wells. The sediments do however form a discontinuous, relatively impermeable aquaclude at ~400 m BGL across the field. Zircons within a tuff toward the bottom of the formation have yielded an eruption age of 0.44 ± 0.02 Ma (Milicich et al., 2013b).

Caxton Formation

The Caxton Formation is a brecciated to massive series of flow banded rhyolites that are considered to form extrusive and intrusive bodies that are interbedded with Kawerau Andesite and other ignimbrites (Milicich et al., 2013a) (Fig. 1.6 & 1.7). Within both the extrusive and intrusive members of the formation are crystal-poor and crystal-rich variants; the crystal-poor member is found to be the most extensive and age estimates for both members are almost identical (0.36 ± 0.02 – 0.03 Ma (Milicich et al., 2013b)).

Karaponga Formation

The Karaponga Formation consists of three ignimbrites from explosive rhyolitic volcanic events approximately 0.5 – 0.6 Ma. The ignimbrites are separated by U-Pb dating on zircons, estimated ages are 0.60 ± 0.05 Ma, 0.57 ± 0.02 Ma, and 0.51 ± 0.02 Ma (Milicich et al., 2013b). The middle ignimbrite outcrops to the southwest of Kawerau and is also located on the Bay of Plenty coast in fluvial sequences. The formation is inferred to have been erupted from a now buried source beneath OVC, where it has been labelled Utu ignimbrite (Cole et al., 2010).

Onerahi Formation

Composed of tuffaceous to muddy breccias and coarse tuffaceous sandstones the Onerahi Formation was one of the formations previously included with the Huka Falls Formation (HFF). Occurring sporadically below the Karaponga Formation age data from units above and

below infer that the Onerahi Formation was deposited during a long period when a small amount of material was available for depostition around the time the Kawerau Andesite was erupted.

Kawerau Andesite

The Kawerau Andesite consists of multiple lava flows and tuffs at ~600 – 1000 m BGL and forms a NW – SE elongated body in the central and northwest part of the field thickening towards an inferred vent-zone in the northwest of the field. Many early wells at KGF produced from the Kawerau Andesite utilising its fracture permeability, and maximum well temperatures were found in KA8, KA35 and KA37 where the andesite is also cut by faults. To be able to support fracture permeability the Kawerau Andesite is dense and hard, like the older Te Teko Formation (Allis et. al, 1993) and greywacke basement (Wood et al., 2001). In parts of the field the andesite is intercalated with pyroclastic units, implying episodic emplacement.

Raepahu Formation

The Raepahu Formation is made up of two deposits from eruptions that are ~1 Ma in age; the Kidnappers and Rocky Hill ignimbrites (Edbrooke, 2005). Milicich et al. (2013b) took samples from KA23 and correlated it directly with the Kidnappers ignimbrite (0.95 ± 0.05 Ma) using age data, primary mineralogy, and by identifying the presence of altered biotite. Rocky Hill ignimbrite is not directly identifiable at Kawerau, however a second ignimbrite was sampled from KA26 and KA48, and was dated at 0.98 ± 0.04 Ma and 1.00 ± 0.03 respectively. The relationship between these two ignimbrites at Kawerau is still unknown as there are no wells where both deposits occur, they are therefore grouped into one formation.

Tasman Formation

The Tasman Formation is a new addition to the stratigraphy at Kawerau, including sediments previously logged as HFF and Tasman Breccia (Milicich et al., 2013a). The sedimentary component of the Tasman Formation (previously HFF) contains muddy breccia, sandstone, and siltstone and is identified by a 5 – 20 m thick interval of fine-grained, reddish brown sediments, which is inferred to represent a break in time when a paleosol was able to develop. The volcanic component (ex-Tasman Breccia (Browne, 1978)) contains rhyolite lava, pumice, ignimbrite, greywacke, basalt, granophyre clasts, and crystal fragments. The formation has been inferred to predate proposed activity at OVC based on its relative age below the 1 Ma Raepehu Formation and not be hydrothermal in origin. Its actual age and origin is yet to be determined (Cole et al., 2010; Milicich et al., 2013a).

Te Teko Formation

All units that are stratigraphically below the Tasman or Raepahu formations and above the Tamurenui Subgroup form the Te Teko Formation. Throughout most of KGF the Te Teko Formation is represented by a single ignimbrite with an estimated age of 1.46 ± 0.01 Ma. Two other ignimbrites separated by 25 m of sediments and/or paleosols are present in KA23, the upper ignimbrite has an estimated age of 1.34 ± 0.04 Ma and the lower of 1.46 ± 0.01 Ma (Milicich et al., 2013b).

Rotoroa Formation

Below the Te Teko Formation several lithologies exist separating it from the Basement Greywacke, however none can be correlated across KGF. Lithologies include sandstone, siltstone, and tuff; these units make up the Rotoroa Formation. Two pyroclastic units have been dated as 2.17 ± 0.05 Ma and 2.38 ± 0.05 Ma. Both are inferred to be sourced from the Kaimai area, near Tauranga, on the basis of their ages and petrology (Milicich et al., 2013b). Along with the Waikora Formation the Rotoroa Formation is part of the Tamurenui Subgroup.

Waikora Formation

In TVZ geothermal fields the term Waikora Formation is typically applied to greywacke pebble conglomerates. At KGF the formation is up to 450 m thick (KA44) and is predominantly present in the north and northeast of the field, the formation thins towards the southwest and is coeval with the Rotoroa Formation sediments and tuffs. Deposition of the formation was controlled by strike-slip generated half-grabens and associated with the uplift of axial greywacke ranges east of Kawerau (Milicich et al., 2013a).

Basement Greywacke

The basement material at KGF is a hydrothermally altered, and faulted greywacke of the Torlesse supergroup. Hydrothermal alteration is moderate with 30 – 60% replaced by chlorite and faulting is consistent with the regional northeast-southwest normal faulting structures. The greywacke at Kawerau is a medium-grained sandstone dominated by sub-angular volcanic clasts of andesite, rhyolite lava, and ignimbrite, with minor argillite and chert (Milicich et al., 2013a), detrital crystal clasts include plagioclase, quartz, K-feldspar, biotite, epidote, and rarely muscovite (Wood et al., 2001). Basement at Kawerau is encountered at a range of depths, from -667 mRL in KA29, in the southeast of the field, to -1268 mRL in KA17 on the northwest margin of the field, this lead Allis et al. (1993) to suggest that basement drops from SE to NW

across NE-trending normal faults bounding a series of blocks that are back-tilted to the SE, this is however unconfirmed as faults cannot be located with any accuracy from basement surface morphology. The ability to sustain a fracture network in basement materials allows KGF to have more fault-related permeability in comparison to the more ductile granite-rhyolite derived greywacke at other TVZ geothermal fields (Wood et al., 2001).

1.2.3 Permeability

Permeability in a geothermal system can come from two sources, the first is matrix permeability of the rock mass; microscopic gaps between the individual grains allow fluids to flow through the system, the second is through faults and fractures in the rock mass. The basement greywacke reservoir at Kawerau utilises faults and fracture derived permeability due to its andesite-dacite composition. Drilling at KGF indicates that the main lateral permeability is located toward the north of the field, this is controlled by active faults and fracture networks. Production at Kawerau occurs in the southern area of the field where the highest temperatures are recorded (up to 310 °C), reinjection occurs north of production with a small amount of overlap in the central part of the field where shallow injection occurs. Fluid flows laterally from southeast to northwest with progressive cooling of the fluid northwards as it mixes with groundwater accompanied by dilution of the waters; this is consistent with regional groundwater flows (Bignall & Milicich, 2012; Bromley, 2002; White, 1995). Tracers placed in injected fluids have been found in production fluids (John Clark, pers. comm., 2014) indicating that re-injected fluids in the north are contributing to the recharge of the reservoir in the south.

1.2.4 Surface Geology

The surface geology of the Kawerau region is primarily Holocene alluvial sediments (Recent alluvium) that have been deposited across the Rangitaiki Plains by the Tarawera River (Fig. 1.8). Gravels and sands dominated by pumice clasts have been deposited during times of background sediment flux or by outbreak floods from Lake Tarawera. Around the margins of the alluvial plain is the Rotoiti Formation, a non-welded rhyolite ignimbrite with a moderate to high crystal content; two extrusive rhyolite domes rising 160 m above the plains outcrop in the west of KGF (Onepu Formation); Tasman Mill waste dumped near Lake Rotoitipaku; Putauaki in the south of the field made up of the Edgecumbe Group; and the Mangaone Subgroup. Mapped surface fault traces include the Onepu Fault which was displaced during the 1987 Edgecumbe earthquake, the Edgecumbe Fault which appears along a similar strike to the

Onepu Fault, and the Rotoitipaku Fault Zone in the northwest; and the Te Teko Fault and northwest tip of North Island Shear Belt in the northeast.

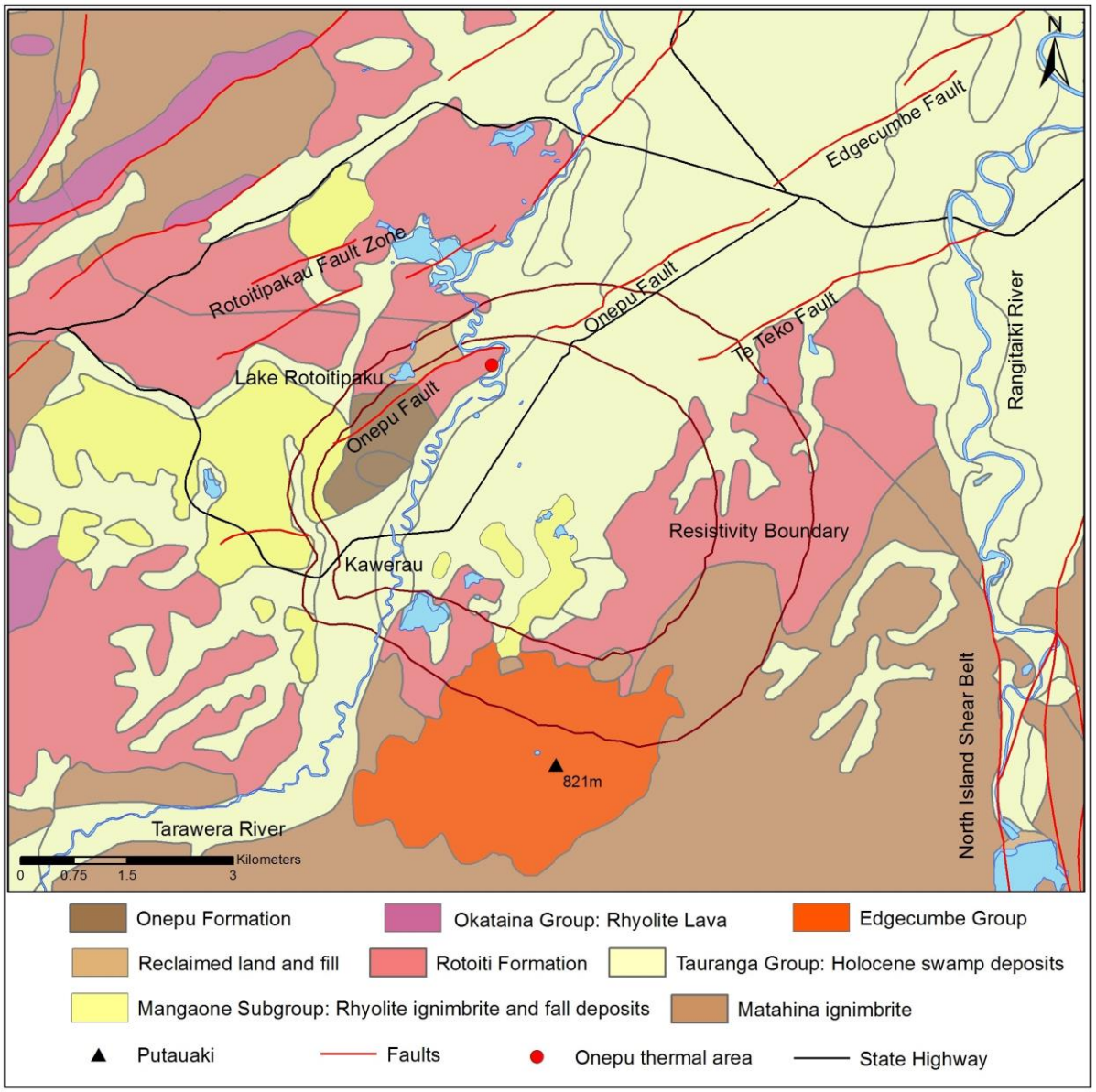

Figure 1.8: Surface geology of the Kawerau region showing labelled surface fault traces, KGF resistivity boundary and State Highway (modified from Leonard et al., 2010).

1.2.5 Surface Thermal Features

During the early 1900's surface thermal features at Kawerau included hot springs, seepages and associated sinters, altered and steaming ground with small fumeroles, and hydrothermal eruption vents. The springs and seepages were concentrated along the banks of the Tarawera River, and around the southern shore of Lake Rotoitipaku in an area called the Onepu thermal area (Fig. 1.8). By the 1950's many of these surface features had been lost, this was attributed to the downcutting of the Tarawera River by three metres which also lowered the groundwater

level (Studt, 1958). Patches of steaming ground occur south of the Onepu thermal area along the Onepu Hills, along the west edge of Kawerau town, and in an area ~1 km east of the mill (Allis, 1997). Current monitoring of thermal features in Kawerau includes photographic and sampling surveys of all thermal features, geochemical analysis of accessible flowing springs, ground temperature surveys, and vegetation surveys. A scenic reserve in the southwest of the field containing natural surface features required a specific monitoring program; a purpose-designed monitoring well was installed to monitor temperature, water level, and allow chemical analysis of fluids from the shallow thermal aquifer. Springs are sampled at six-monthly intervals, and photographic and vegetation surveys carried out biennially (Spinks et al., 2010).

1.3 Scope

Many reports and publications attempt to address or describe subsidence at Kawerau (Allis, 1982a; Allis et al., 2009; Berry & Denton, 1985; Bloomer, 1997; SKM, 2005; Spinks et al., 2010; White et al., 2005). This project was undertaken following discussions with MRP and follows on from Mackenzie (2011) which investigated the localised subsidence bowls in the north of the field using geophysics, field investigation methods, and laboratory testing. This thesis focuses on the pulp and paper mill site within the KGF and the potential for mill operations to be affected by subsidence.

The thesis objectives are:

1) Spatially analyse the extent of the subsidence and produce a hazard map.
2) Define a rate of subsidence for the mill site.
3) Define the contribution to overall subsidence from the cover sequences across the mill complex.
4) Define the mechanisms of the subsidence in the mill area.

1.4 Methodology

To assess the potential for the cover sequences of KGF to contribute to subsidence three overarching approaches are used.

1) The assessment of benchmark re-levelling surveys and other available datasets from KGF.
2) Modelling of the shallow cover sequences using Leapfrog Geo and MRP well logs from KGF (Milicich, 2013b).
3) Testing of available core material to assess each shallow units potential to contribute to subsidence.

Assessment of benchmark surveys and datasets

Benchmark levelling surveys at KGF have been completed annually or biennially since 1970, soon after it was identified that geothermal fields are prone to subside due to fluid withdrawal. The benchmark data consists of an Excel spreadsheet with raw elevation data and calculated annual rates of subsidence (expressed in mm/year) which is updated following each survey, and a point shapefile which consists of the benchmark network. Using the join tool in ArcMap the shapefile and Excel file can be joined together for analysis in ArcMap. The analysis consists of identifying all the benchmarks consistently re-levelled in the 2007 to 2013 surveys, and using ArcMap tools the point data is contoured presenting annual contour maps of the rate of subsidence across KGF. The benchmarks used in the analysis were only those which had been annually re-levelled from 2007 – 2013 to maintain the dataset (benchmark) density and output (contour maps) resolution. The date range for the analysis is chosen because 2007 is the year the number of benchmarks began to increase. Furthermore in July 2008 KGL was commissioned resulting in increased annual production and injection totals, therefore by including the 2007 survey subsidence can be assessed pre and post KGL. An analysis of the ground tilt beneath sensitive mill machinery is then completed.

Other datasets analysed that have the potential to be correlated with subsidence are pressure and pressure drawdown, enthalpy, and production and injection. Pressure drawdown has been identified at geothermal, oil, and gas fields as being responsible for subsidence (Bloomer & Currie, 2001; Nagel, 2001) and is therefore monitored within all geothermal fields where fluid is being extracted. At KGF pressure is monitored in five wells with the equipment set at different depths in each well, one well monitors shallow groundwater pressures while the other four monitor deeper reservoir pressures. Pressure is analysed since the commissioning of KGL in June, 2008.

Enthalpy is monitored in the seven MRP production wells, six of which have been producing since 2008 and one since mid-2013. Enthalpy is the thermodynamic potential of the production fluid and consists of the internal energy of the system plus the product of the pressure and volume of the system. Enthalpy of the production fluid is recorded at the surface and does not represent a specific depth but the combined mass flow weight temperatures of the feed zones and is recorded as an average over a period of time. Changes in the pressure and volume of the system can cause subsidence, therefore enthalpy is a relative dataset to assess. Finally to evaluate whether production is related to subsidence, the production and injection data will be

assessed between 27/06/2007 and 31/07/2013 to correspond with benchmark levelling survey dates. Production and injection data is recorded as average rate over a period of time, since mid-2012 an average rate is recorded daily, prior to that it was averaged over a 2 week period. Calculations must then be completed to determine the approximate annual totals.

Modelling of shallow cover sequences

Over the lifetime of KGF more than 70 wells have been drilled and logged, Milicich (2013b) re-logged the wells providing an up to date dataset that can be imported into Leapfrog Geo, three-dimensional geological modelling software by ARANZ Geo. The purpose of modelling is to determine whether there is an anomalous thicknesses of a particular unit which could be responsible for the presence of the subsidence anomalies and whether one exists beneath the mill site which could contribute to subsidence. Three shallow (<120 m) geotechnical bores below the mill site are also modelled in Leapfrog Geo. From the modelling a hypothesis will be formed to determine the units responsible for the subsidence anomalies.

Testing of samples

Following the Leapfrog Geo modelling samples are collected from KGF to test the properties of the cover sequences to determine whether they are responsible for subsidence. Testing includes recording the physical properties, compressibility, thin section analysis, XRD, and laser sizing.

Using the above methods a conclusion will be drawn about the potential for the shallow cover sequences to subside, in particular around the mill site, and mechanisms for the subsidence occurring at KGF proposed.

1.5 Thesis Structure

Chapter 1 – Introduction

Chapter 2 – A Review of Production Induced Subsidence

Chapter 3 – Spatial Analysis of Subsidence using Benchmarks

Chapter 4 – Modelling of the Cover Sequences

Chapter 5 – Properties of the Cover Sequences

Chapter 6 – Hazard analysis of Kawerau Geothermal Field

Chapter 7 – Discussion and Management of Subsidence at Kawerau

Chapter 8 – Conclusions

2 A Review of Production Induced Subsidence

Vertical ground deformation can be caused by natural processes such as tectonics, earthquake activity, volcanic activity, isostatic phenomena, and compaction from overburden loading; or by anthropogenic causes such as fluid extraction, fluid injection, cooling causing thermal contraction, pressure drawdown causing effective stress increases, and underground mining (Nagel, 2001). Subsidence is present in oil, gas, and geothermal fields around the world because the extraction of fluids results in changes at depth that can cause subsidence at the surface. The following case studies provide useful analogies to Kawerau Geothermal Field:

2.1 Wilmington Oil Field, California, United States

Wilmington Oil Field is located on the south-western margin of the Los Angeles Bain in Southern California and has been producing oil since 1932. The field is hosted in a broad asymmetrical anticline which is broken by a series of transverse normal faults and covered in Pliocene and Quaternary sediments over a Pliocene unconformity at ~600 m BGL (Mayuga & Allen, 1969). Oil is produced from five main sand intervals at depths of 600 – 3350 m, and to date over 2.5 billion barrels have been produced from the 6,150 wells drilled, making it the third largest oil field in the United States (Long Beach, 2014).

Subsidence at Wilmington was first definitively recognised in 1941 and re-levelling surveys of lines between San Pedro and Long Beach showed increasing maximum subsidence which formed a broad elliptical bowl (Table 2.1). Early production at Wilmington was associated with 10 MPa (100 bar) of pressure drawdown due to the extraction of oil, water, and gas (Nagel, 2001). The subsidence was also accompanied by large horizontal displacements of up to 3.66 m (Kosloff et al., 1980; Mayuga & Allen, 1969). Subsidence and horizontal displacement occurred in a mostly continuous manner, however small earthquakes in 1947, 1949, 1952, 1955, and 1961 caused abrupt strain release with associated ground deformation (Kosloff et al., 1980).

Year	Total observed subsidence (m)
1947	2.4
1951	4.0
1954	6.1
1958	7.9
1965	8.8

Table 2-1: Total observed subsidence at Wilmington Oil Field 1947 – 1965 (Kosloff et al., 1980)

The subsidence and horizontal movement at Wilmington caused substantial damage to surface and near-surface structures at the Port of Long Beach, one of California's largest industrial areas and a United States Navy shipyard. Remedial measures costing US$100 million up to 1969 included construction levees, retaining walls, and filling to prevent flooding of land and structures. To prevent further subsidence a re-pressurisation program was started in 1958 and by 1968 the subsidence rate had decreased from 750 mm/year to zero; areas with the greatest amount of water re-injected experienced surface rebound of 45 cm, and the area of the subsidence bowl decreased from ~50 km^2 to 8 km^2 (Kosloff et al., 1980; Mayuga & Allen, 1969) To prevent a reoccurrence of subsidence at Wilmington the operators are required to maintain 105% water reinjection (Nagel, 2001). The anthropogenic subsidence is therefore largely attributed to the 10 MPa of pressure drawdown.

Wilmington Oil Field is an example of how subsidence can have a large effect on other operations and how expensive repairs can be. Knowledge of the effect production can have on ground deformation was in its infancy when Wilmington was subsiding but it was shown that while subsidence cannot be reversed it can be prevented.

2.2 Cerro Prieto Geothermal Field, Mexico

Cerro Prieto Geothermal Field (CPGF) is the second largest geothermal field in the world in terms of power generated. Located in the Mexicali Valley, north-eastern Baja California, CPGF has been producing electricity since 1973 and has a current capacity of 720 MW across five power houses. In 2005 72 million tons of fluids were extracted from 1500 – 3000 m, but only 20% were re-injected at 500 – 2600 m (Armienta et al., 2014; Glowacka et al., 2010; Lippmann et al., 2004; Sarychikhina et al., 2011).

CPGF is hosted in sedimentary and metasedimentary rock underlain by Upper Cretaceous granitic bedrock with a mudstone and brown shale cap rock. CPGF is a high temperature system with fluid extracted at 250 – 350 °C from grey shales. Faulting in the system is a part of the San Andreas tectonic system and has a NW – SE strike combined with SW – NE cross faulting (Puente & De La Peña, 1979). The combination of these faulting systems has produced step-faulted horst and graben basement topography.

Subsidence at CPGF has an elliptical shape with a NE-SW major axis which coincides with the thermal anomaly, production borefield, and the orientation of a pull-apart basin located between the strike-slip, right lateral Cerro Prieto and Imperial faults (Glowacka et al., 1999). Levelling surveys performed since 1977 have detected subsidence with a maximum rate of

~120 mm/year, and subsidence rates have been shown to increase following large increases in fluid extraction (Glowacka et al., 2000). Natural tectonic subsidence from the pull apart basin and soil compaction should be on the order of millimetres/year, 10 times less than the measured subsidence rates (Glowacka et al., 1999). All indications at CPGF are that subsidence is mostly driven by fluid extraction.

Long term reinjection of fluid began in 1989 to maintain reservoir pressures, however this had a strong effect of the chloride content of the fluids due to the fluids being evaporated before injection resulting in Cl-rich fluid being injected. Evaporation also reduced the amount of fluid available for reinjection. CPGF also has issues with localised boiling of fluid as a result of pressure drawdown. Boiling resulted in high gas contents in the steam and the production of corrosive HCl. Natural and injection-related recharge of cooler waters are designed to decrease the amount of boiling but will ultimately cool the reservoir (Lippmann et al., 2004).

CPGF is an example of how fine the balance of all aspects of a geothermal field must be for it to operate efficiently; highlighting how pressure changes can affect ground deformation, chemical and physical characteristics, and groundwater conditions with the field.

2.3 Reykjanes Peninsula, Iceland

Reykjanes Peninsula is a small peninsula on the southwest tip of Iceland that hosts six high temperature geothermal fields and four power stations (Fig. 2.1). Geothermal energy accounts for 25% of electricity generation and nearly all heating in Iceland (NEA, 2015). The Reykjanes Peninsula geothermal fields are surrounded by a large number of NE-trending eruptive fissures and fractures that are grouped into four swarms. The fissures are intersected by a series of N-S orientated right-lateral strike-slip faults that are surface expressions of the left-lateral E-W shear at depth. The fields are primarily located at the intersections of eruptive fissures and strike-slip faults (Keiding et al., 2010).

Pressure drawdown has been found to be diminishing the productivity of Reykjanes wells, to remediate this injection is carried out at Svartsengi with around 50% of produced fluid re-injected as of 2008. At Hellisheidi all production waste fluids are re-injected, but this does not make up 100% of production fluids due to steam losses. As of 2009 systematic reinjection in the Reykjanes field had not started (Keiding et al., 2010). Subsidence at Svartsengi field was first documented following levelling and gravity surveys based on repeated measurements from 1975 – 1999 which showed subsidence rates of 7 – 14 mm/year, with the highest rates during the first years of production.

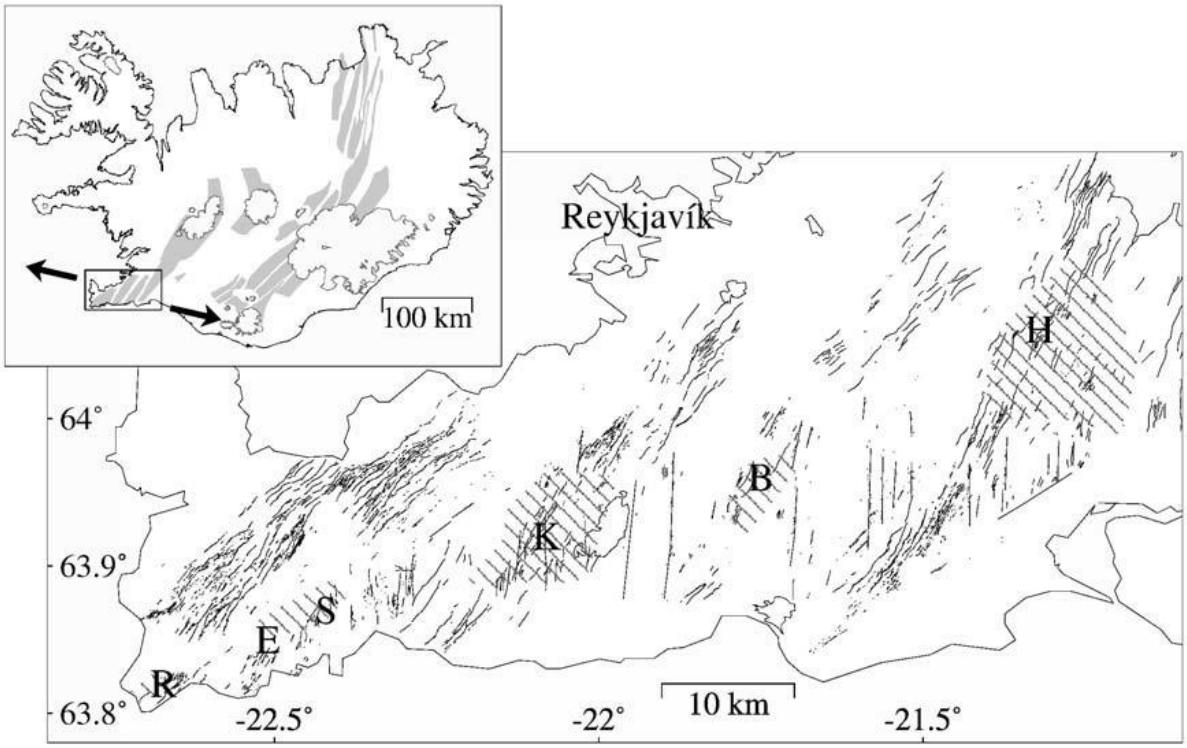

Figure 2.1: Tectonic map of Reykjanes Peninsula showing NE-SW trending normal faults. Inset map shows spreading direction of 2 cm/year across the peninsula. Geothermal fields are hatched areas; R: Reykjanes, E: Eldvorp, S: Svartsengi, K: Krisuvik, B: Brennistiensfjoll, and H: Hengill (from Keiding et al., 2010).

Subsidence on the Reykjanes Peninsula is concluded to be both fault induced and anthropogenic related to production. The main anthropogenic subsidence bowl around Reykjanes Field is elongated NE-SW aligning with the main trend of fractures in the area and rates are estimated to be ~10 mm/year. Anthropogenic subsidence is due to a compaction of the reservoir due to a decrease in pressure from fluid losses (Keiding et al., 2010).

2.4 New Zealand Geothermal Fields

New Zealand has eight operating geothermal fields, seven of which are located in the TVZ (see Fig. 1.2). Geothermal energy currently provides almost 17% of New Zealand's electricity (Bromley, 2014); and the first generator was commissioned at Wairakei in 1958. Early development focused on maximising output with little thought given to the effects of extraction, because of this large amounts of ground deformation have occurred at Wairakei. Subsidence at Ohaaki Geothermal Field and in the Wairakei-Tauhara Geothermal System are outlined below.

2.4.1 Ohaaki Geothermal Field

Ohaaki Geothermal Field is located ~25 km northeast of Taupo. Exploratory drilling began in 1965 followed by extensive field testing from 1967 – 1971 when extraction averaged 25,000 tonnes per. day (tpd) with no reinjection, this resulted in pressure decline of 1.5 MPa (15 bar) in four years (Rissmann, 2010). In 1988 the 116 MW Ohaaki Power Station was commissioned and production increased to 45,000 tpd with 28,000 tpd re-injected (White et al., 2010). Reservoir pressure declined by 2.5 MPa (25 bar) by 2000 and thermal features of Ohaaki West previously flowing at 9 – 23 l/s ceased (Hunt & Bromley, 2000).

Subsidence was first observed at Ohaaki following production testing in 1969 and rates measured at 150 mm/year from surveys of benchmarks. By the late 1990's rates had accelerated to 500 mm/year across the NW borefield. The subsidence feature occupied an area of ~1.5 km^2, as defined by the 100 mm/year contour and was ~3 m deep. Broad, low amplitude subsidence extended across the remainder of the field, declining towards the inferred margins of the reservoir (Rissmann, 2010).

Production at Ohaaki occurs in Wairoa Formation pumice and lapilli tuff. Overlying this is the Huka Falls Formation (HFF) composed of mostly mudstone and siltstone which is up to 300 m thick. It is the compaction of HFF that is inferred to have been the cause of the high rate of subsidence at Ohaaki (Allis & Zhan, 2000).

Effects of subsidence at Ohaaki include well damage, stretching and compression of pipelines, the geothermal field being threatened by a relative rise in river levels, flooding of Ohaaki Marae, and tilting of separation plants 1 and 2 by 3% (Bloomer & Currie, 2001; White et al., 2005).

2.4.2 Wairakei-Tauhara Geothermal System

The Wairakei-Tauhara geothermal system is located on the northern and eastern edge of Taupo in the centre of the TVZ and hosts two fields, Wairakei and Tauhara, the boundary between them is the Waikato River (Fig. 2.2). The two fields are considered to be part of the same system because they are in pressure communication with each other through the Waiora Formation where production occurs. The Waiora Formation is present between 300 and 2400 m BGL and is a varied sequence of volcanic deposits with interlayered sandstone and mudstone (Rosenberg et al., 2009).

Wairakei and Tauhara geothermal fields were the subject of a geotechnical investigation into the source of subsidence bowls in both fields after subsidence had been an issue during resource consent processes related to the ongoing development of the system. The investigation consisted of the recovery of >4 km of core from inside and outside the recognised bowls (Fig. 2.2) which was then tested for its geotechnical properties to explain the mechanisms for the subsidence bowls and propose mitigation methods (Bromley et al., 2010).

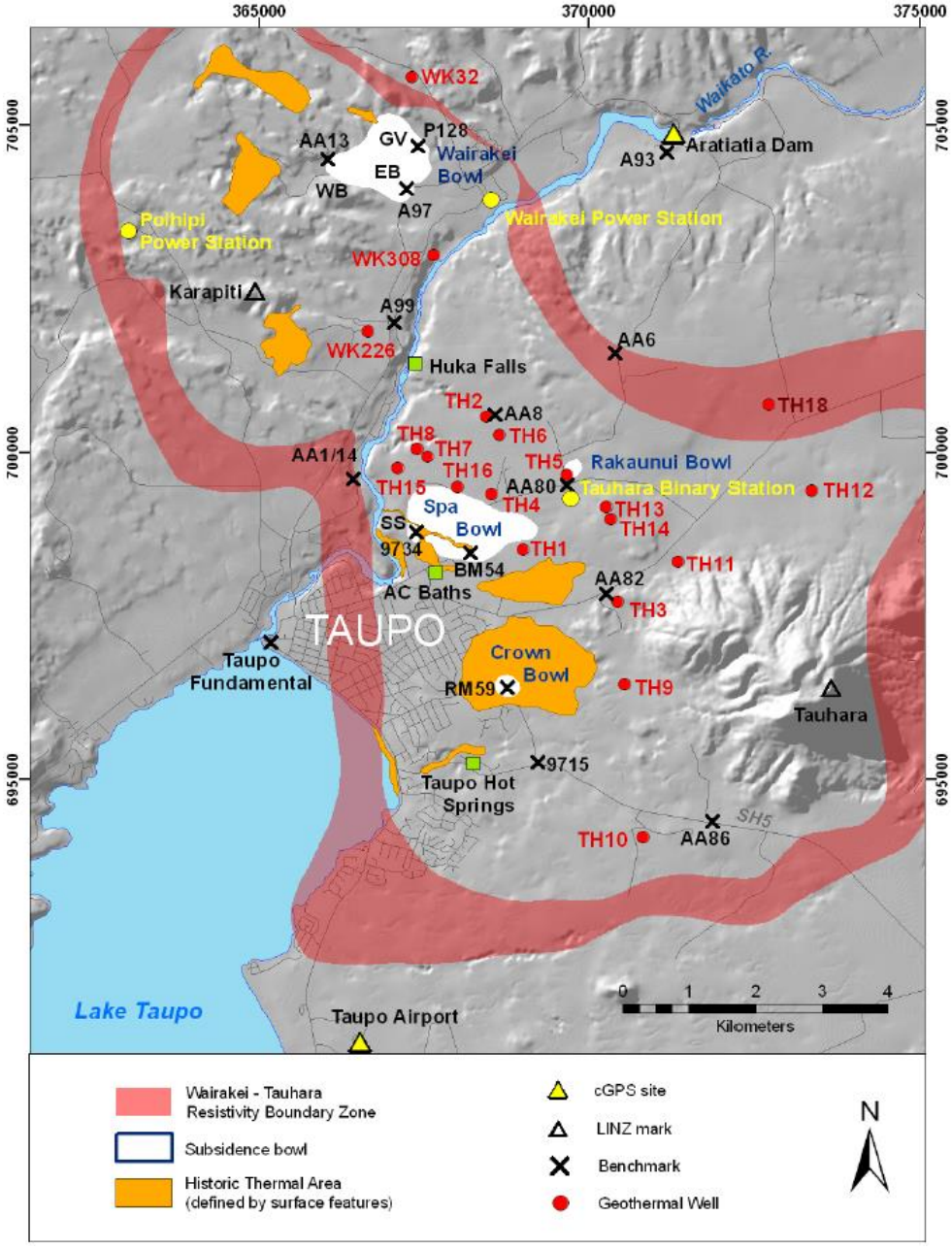

Figure 2.2: Map of the Wairakei-Tauhara geothermal system showing the location of subsidence bowls (from Bromley et al., 2010).

Wairakei Geothermal Field

Subsidence at Wairakei was detected soon after testing of exploration wells in the early 1950's (Allis, 2000). It is concentrated in a 2 km^2 bowl on the northeastern boundary of the field outside of the production borefield (Allis, 1982a). There has now been 15 ± 0.5 m of subsidence in the centre of the bowl with peak rates of 480 mm/year reached in the 1970's. The current trend of subsidence at Wairakei is of decreasing rates in the recognised bowls. The most recent subsidence rates come from re-levelling surveys carried out in 2001, early 2005, and 2009. Rates show a decline from 70 mm/year (2001 – 2004) to 45 mm/year (2004 – 2009) (Bromley et al., 2010). Maximum rates are believed to have been reached in the 1990's (Allis et al., 2009).

Results of the geotechnical investigation found that compressible HFF sub-units (75 -230 m BGL), altered tuff and breccia at the top of the Waiora Formation (230 – 330 m BGL), and possibly decaying peat and vegetation layers (30 – 45 m BGL) are responsible for Wairakei Bowl (Bromley et al., 2010).

Tauhara Geothermal Field

Subsidence at Tauhara was first detected in the 1960's and occurred because of pressure communication with Wairakei; early rates were between 20 and 40 mm/year. Maximum total accumulated subsidence back calculated to 1955 at Tauhara is ~2.9 m to 2009. Latest maximum subsidence rates from benchmark re-levelling surveys occur in the Spa Bowl at a rate of 105 mm/year (2008 – 2009) (Bromley et al., 2010).

Results from the geotechnical investigation found that sub-units of HFF at 130 – 400 m BGL are responsible for Spa Bowl, and a hydrothermal eruption breccia with a strongly altered hydrothermal clay matrix between 35 and 200 m BGL is responsible for Crown Bowl.

Effects of subsidence at Wairakei-Tauhara include; ponding of Wairakei Stream, well casing damage, tension cracks, sliding joints in the main drain, and removing/adding steam main section pipes (Bloomer & Currie, 2001).

Because of the increased understanding of the source depth and mechanisms for subsidence at Tauhara an injection strategy was developed to mitigate the subsidence. Current injection at Wairakei-Tauhara is designed to maintain deep pressure, therefore passing the compressing units responsible for subsidence without affecting them. Targeted injection into the formations responsible for the subsidence bowl is the recommended method to locally increase pressure,

thereby reducing and controlling future subsidence rates (Bromley et al., 2010). Thought however still needs to be given to the consequences of adjusting the injection strategy from deep to shallow injection, which has been shown to affect production well temperatures (Itoi et al., 2014).

2.5 Conclusions

Literature studies of oil, gas, and geothermal fields that have subsidence occurring due to fluid withdrawal reveal that subsidence is largely due to pressure drawdown within either shallow compressible units or the reservoir. Reservoir pressure drawdown produces a field wide elliptical bowl with relatively low rates of subsidence. In the case of the Reykjanes Peninsula geothermal fields subsidence rates were found to increase significantly after production was increased indicating an associated decrease in reservoir pressure.

A second type of subsidence feature is also distinguishable; a subsidence anomaly. Subsidence anomalies are superimposed on the field wide bowl and are driven by shallow processes. In the case of Wairakei-Tauhara geothermal fields the anomalies are driven by pressure drawdown in shallow, anomalously compressible units. The amount of subsidence experienced is therefore a combination of geologic conditions and the amount of pressure drawdown. Tectonically active geothermal fields, such as Cerro Prieto, also experience fault induced subsidence where extension of the area results in subsiding graben structures. Care must therefore be taken to interpret subsidence that is anthropogenic and that which is natural.

Whilst broad conclusions can be made about production induced subsidence, each case is ultimately different. No field is the same as structural, geological, and chemical characteristics vary locally within the field and between fields, which will affect the amount of subsidence experienced.

3 Spatial Analysis of Subsidence using Benchmarks

Benchmark levelling surveys are a standard subsidence monitoring technique in geothermal, oil, and gas fields around the world. The Geysers, North California, Wairakei-Tauhara and Broadlands geothermal fields, New Zealand, Reykjanes Peninsula Geothermal Fields, Iceland, and Wilmington Oil Field, California all use or have used benchmark levelling surveys to track ground deformation (Allis, 1982a; Allis et al., 2009; Bromley et al., 2010; Geri et al., 1985; Kosloff et al., 1980; Mossop & Segall, 1997). Since 2008 Mighty River Power Ltd. (MRP) have operated a 106 MW power station at Kawerau Geothermal Field (KGF) under resource consent conditions from Environment Bay of Plenty, one of the conditions is that annual re-levelling surveys (completed by Energy Surveys Ltd.) of a subsidence benchmark network are completed (BOPRC, 2013). Since 2007 the benchmark network has been significantly expanded (Table 3.1) which has resulted in higher resolution surveys and a greater understanding of the ground deformation ocurring; there are currently 844 benchmarks around KGF, of which 577 were surveyed in 2013, covering an area of 75 km^2 (Fig. 3.1).

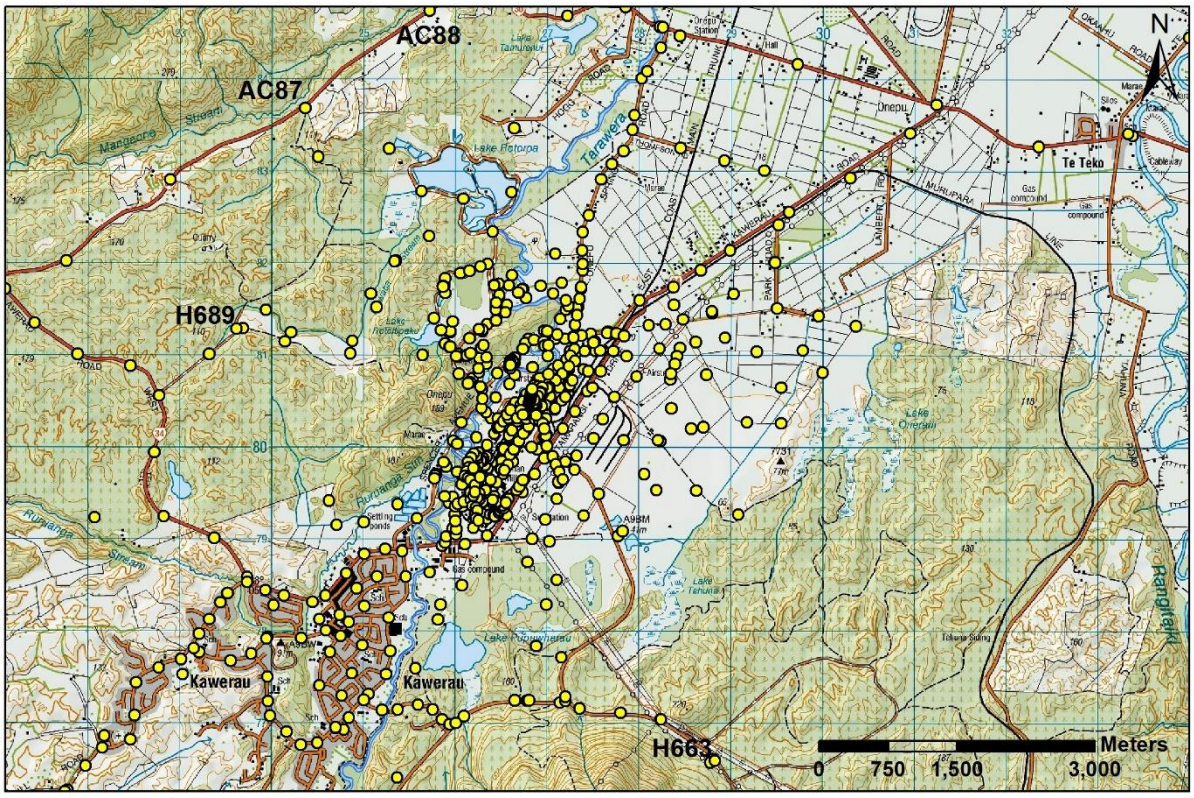

Figure 3.1: All KGF benchmarks. Benchmarks indicated by yellow circles and benchmarks referenced in text are included here.

Month-Year	Benchmarks surveyed	Corrected subsidence rate (mm/year)		
		Mean	Maximum	Minimum
May-70				
Apr-72	58	-1.47	-23.96	11.46
Jul-76	30	-5.47	-16.31	0.75
Sep-77	1	-2.39	-2.39	-2.39
Oct-78	1	-2.13	-2.13	-2.13
Apr-79	2	-0.80	-1.40	-0.20
Jan-81	22	-8.47	-15.43	-2.29
Jan-82	22	-5.33	-19.70	1.00
Jan-83	91	-7.94	-31.00	0.00
Jan-84	103	-5.22	-22.70	4.00
Jan-85	124	-12.25	-37.20	-2.10
Jan-86	122	-6.86	-22.40	11.50
Jan-87	121	-7.45	-42.60	0.60
Apr-87	129	-904.21	-1252.40	-523.60
May-88	169	-10.51	-32.22	18.06
Jan-90	130	-8.91	-31.02	7.72
Jan-92	127	-9.06	-26.95	-2.45
Feb-94	141	-12.05	-78.61	-2.36
Feb-96	145	-11.25	-55.35	-3.35
Jan-98	158	-12.76	-32.52	-3.41
Feb-00	154	-9.93	-30.34	-2.30
Jan-02	148	-9.45	-34.96	-1.03
Feb-04	146	-11.45	-38.45	-1.85
Feb-06	146	-5.97	-17.85	0.94
Jun-07	275	-9.51	-37.01	1.97
Jun-08	328	-6.24	-33.95	1.50
Jun-09	401	-9.73	-48.12	25.59
Jun-10	429	-9.88	-63.06	3.61
Jul-11	442	-12.46	-49.63	7.17
Aug-12	496	-15.38	-53.19	3.48
Jul-13	577	-18.53	-59.16	0.00

Table 3-1: Summary table of corrected rates of subsidence at KGF from benchmark levelling data. Note: The large amount of subsidence recorded in the Apr-87 survey is related to the 1987 Edgecumbe Earthquake.

Subsidence at KGF occurs on three different scales, with each scale the result of a different mechanism. Regional subsidence is the largest scale, occurring across the Whakatane Graben which is actively spreading and subsiding; the most recent example resulting from the 1987 Edgecumbe earthquake which caused widespread deformation. Field wide subsidence is the broad, low tilt subsidence occurring across KGF and is the result of deep reservoir processes associated with production. Finally, localised subsidence features, often called subsidence anomalies are the bowls that occur across a small area at a higher rate than field wide subsidence and are superimposed on the field wide bowl. The mechanisms of subsidence anomalies can vary with detailed investigation required to be certain of the mechanism.

Rates of subsidence across KGF are analysed to establish a trend in ground deformation and track the development of features. To do this benchmarks re-levelled annually from 2007 to 2013 are used to create contour maps detailing subsidence. Each survey is individually mapped, and features and trends in subsidence are explained.

The main subsidence related concern at KGF is the effect subsidence may have on the Tasman Mill complex; a site specific analysis is therefore carried out to identify the effect subsidence is having on mill machinery. To do this specific benchmarks are analysed to establish differential subsidence beneath sensitive structures within the mill complex. Ground tilt values are also analysed to establish a trend in the severity of subsidence across the mill complex.

Finally subsidence trends are compared with pressure and pressure drawdown, production and injection, and enthalpy datasets to correlate the subsidence to measureable parameters from KGF. By doing this the likely cause of subsidence at KGF may be identified.

3.1 Regional Subsidence

The TVZ is an area of active rifting and subsidence resulting from the oblique subduction of the Pacific plate beneath the North Island (Wood et al., 2001). Subsidence across the Rangitaiki Plains has been inferred from geodetic surveys and the known regional structure of the Whakatane Graben. The Edgecumbe earthquake demonstrated that subsidence caused by the development of the geothermal field is superimposed on the tectonic subsidence of the Whakatane Graben, with evidence suggesting that the graben is subsiding intermittently at an average rate of several mm/year (Allis, 1997).

The effect of regional tectonic subsidence from the Whakatane Graben must be considered when analysing the KGF benchmark surveys. The network origin benchmark for the KGF

surveys (AC88) is located north of KGF on SH34 (Fig. 3.1) and is the single network origin for each KGF survey as is now best practice in New Zealand geothermal fields (Abele and Currie, 2012). Benchmark AC88 is located within the Whakatane Graben but outside the KGF subsidence bowl, therefore ground deformation measured in KGF surveys does not include the effect of regional tectonic subsidence due to both the origin benchmark and survey benchmarks being affected by approximately the same amount of regional subsidence.

3.2 Field Wide Subsidence

Field wide subsidence (Fig. 3.2) associated with fluid withdrawal is a side effect at many geothermal fields around the world (Bromley et al., 2013; Eysteinsson, 2000; Geri et al., 1985; Truesdell and Lippmann, 2000), and KGF is no different. Field wide subsidence can occur by two mechanisms, compaction or contraction of the reservoir. Compaction occurs because the weight of sediments overlying the geothermal reservoir are supported by both the rock matrix and pore fluid pressure. During production pressure drawdown of the pore fluids occurs, and the overburden load is transferred from the pore fluid pressure to the rock matrix, resulting in reservoir compaction. Thermal contraction of reservoir rock occurs when the reservoir is cooled by either meteoric water or re-injected fluids making their way back to the reservoir too quickly. Field wide subsidence at KGF is a low amount of subsidence over a large area. The affected area spreads beyond the production wells forming an elliptical SW-NE orientated bowl. The large area and low amount of subsidence indicate that the source of the subsidence is relatively deep.

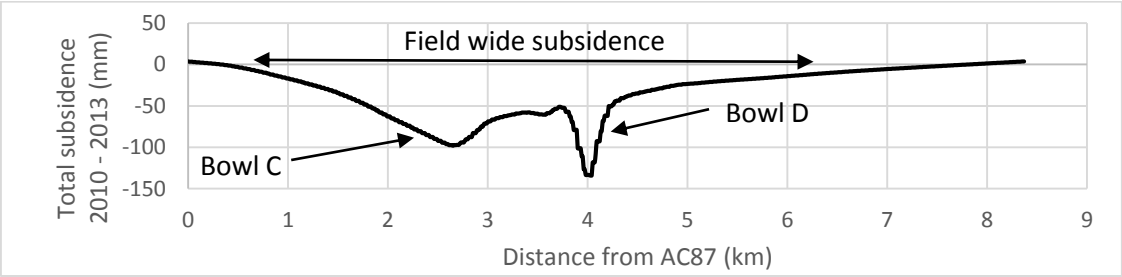

Figure 3.2: Northwest – Southeast cross section of KGF subsidence from benchmark AC87 to H663 (Figure 3.1 shows benchmark locations)

Average subsidence rates across the KGF benchmark network have recently been increasing in response to an increase in size of the field wide feature (Table 3.1). Figure 3.5 shows the migration of the 5, 10 and 15 mm contours across the mill site indicating an increase in the size of the field wide feature. Furthermore Energy Surveys Ltd. annual reports on the subsidence at

KGF includes the area bounded by the -10 mm/year contour which shows this increase and are as follows:

Survey period	Area covered by 10 mm/year contour
2012 – 2013	17 km^2
2011 – 2012	8 – 11 km^2
2010 – 2011	5 – 8 km^2
2009 – 2010	5 km^2
2008 – 2009	6 km^2
2007 – 2008	2 km^2
2006 – 2007	5 km^2
2004 – 2006	1 km^2
2002 – 2004	7 km^2
2000 – 2002	5 km^2
1998 – 2000	4 km^2

Table 3-2: Area covered by -10 mm/year contour in each of the last 11 surveys (Abele & Currie, 2013).

It should be noted that the calculated area affected by the -10 mm contour can be a product of the numbers of benchmarks re-levelled and the area they cover (John Clark, pers. comm., 2014). With the number of benchmarks being surveyed increasing annually (Table 3.1) this likely has an effect on the calculated area. However Figure 3.5 still shows an increasing of the field wide bowl.

3.3 Localised Subsidence Features

Localised subsidence features are the anomalies which are superimposed on the field wide subsidence and are where the maximum rate of subsidence occurs, at KGF there are four subsidence anomalies termed Bowls A – D by MRP and Energy Surveys Ltd. (Fig. 3.3) which have been present for more than 20 years (GeoMechanics Technologies, 2013). Cumulative subsidence from 2010 to 2013 is chosen to best show localised subsidence features because it shows a well constrained long term accumulation of subsidence across the field. Subsidence anomalies require investigation to be certain of the causes. Reasons for anomalies in geothermal fields include, but are not limited to, anomalously soft zones altered by fluids, steam zones, voids created by hydrothermal eruptions, cooling because of an invasion of meteoric waters, and the settling of shallow river sediments (see Chapter 2).

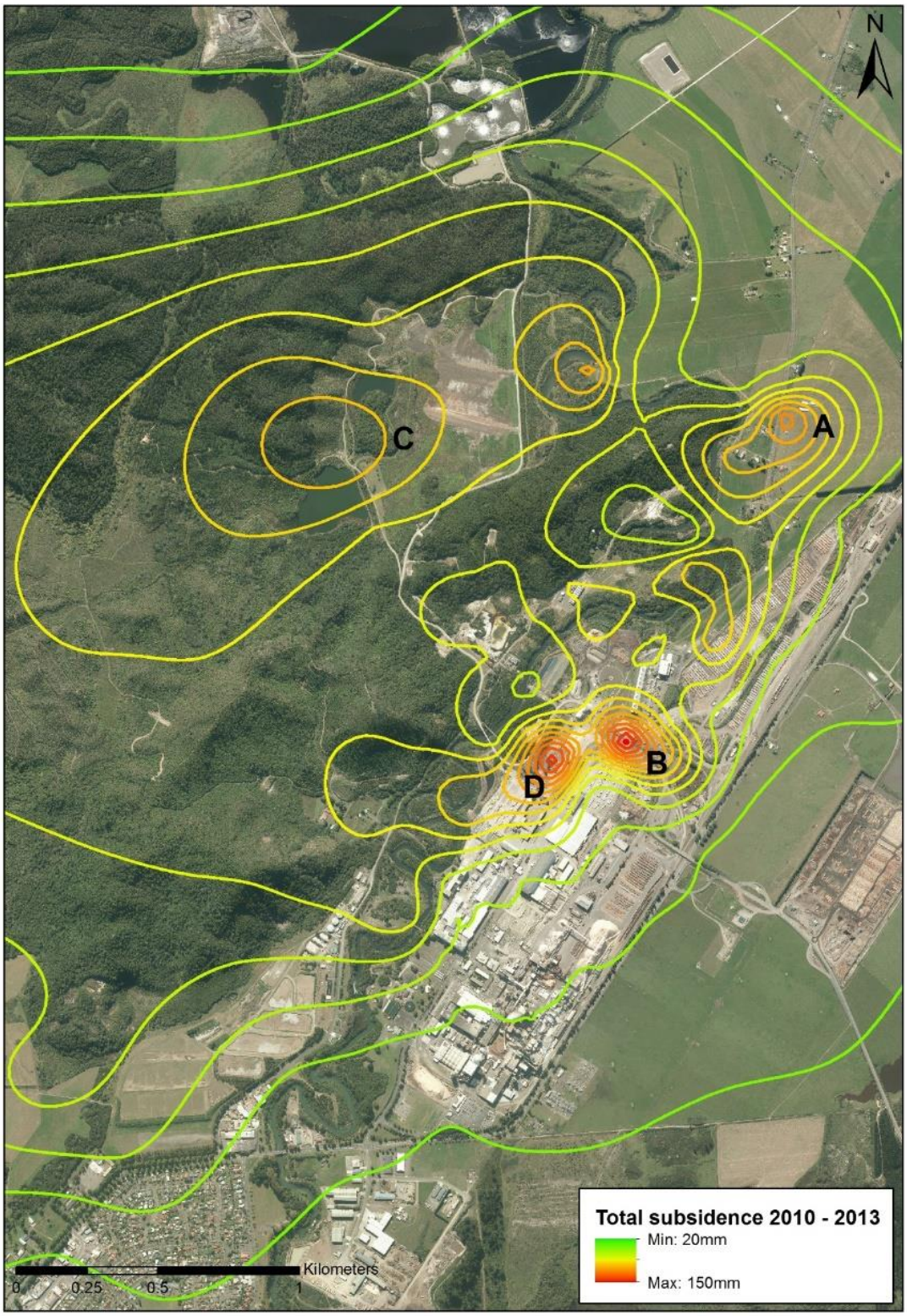

Figure 3.3: Total subsidence from 2010 – 2013 showing the locations of the four anomalies with 10 mm contour spacing.

Before the development of KGF a hot spring area near Lake Rotoitipaku and Bowl C existed; due to a decrease in pressure this has since ceased to exist (Allis, 1997). Extinct hot spring areas often become subsidence anomalies due to pressure drawdown and the compaction of weak highly altered rock resulting from hot spring fluid flow (Allis, 2000; Narasimhan and Goyal, 1982). The area was also once used by the mill operators to dump mill waste which is likely to be steadily compressing under its own weight (John Clark pers. comm., 2014), an area of reclaimed land and fill which matches the outline of Bowl C is shown on the surface geology map (see Fig. 1.8). Onepu thermal area (see Fig. 1.8) and the associated hydrothermal alteration at depth is most likely responsible for the feature at the north-eastern tip of Bowl C.

A shallow site investigation of Bowls A and B was completed by Mackenzie (2011) this included aerial photo interpretation, geophysics with reliable interpretation to ~5 m, hand augurs and face logs to <3 m BGL, and laboratory testing of collected samples. Mackenzie (2011) concluded that geothermal operations are not the primary driver of localised subsidence features at Kawerau. GeoMechanics Technologies (2013) completed modelling of ground deformation at KGF and proposed three potential causes for the anomalies:

1) Pressure changes (groundwater level changes) in soft materials in buried alluvial channels and/or zones of hydrothermal alteration.
2) Cooling due to the downflow and/or lateral inflow of groundwaters.
3) Settlement of shallow sediments related to changes in historical river flow.

Evidence over the past 10 years increasingly points to shallow mechanisms not directly related to geothermal production and injection operations in the greywacke reservoir. A discussion on the likely causes of subsidence anomalies at KGF is given in Chapter 7.

3.4 Rates of Subsidence

From the benchmark levelling surveys the ground deformation at KGF can be illustrated for a chosen time frame. Because of the increased survey resolution from 2007 onwards, this is chosen as the first survey to best represent ground deformation in response to the commissioning of the Kawerau Geothermal Limited power station (KGL) in 2008. To maintain the contour resolution the benchmarks that are consistently re-levelled from 2007 – 2013 are used (Fig. 3.4), this ensures that in each output (Fig. 3.5) the density of the points from which the contours are drawn is identical and the contours are drawn from the same benchmarks in each output.

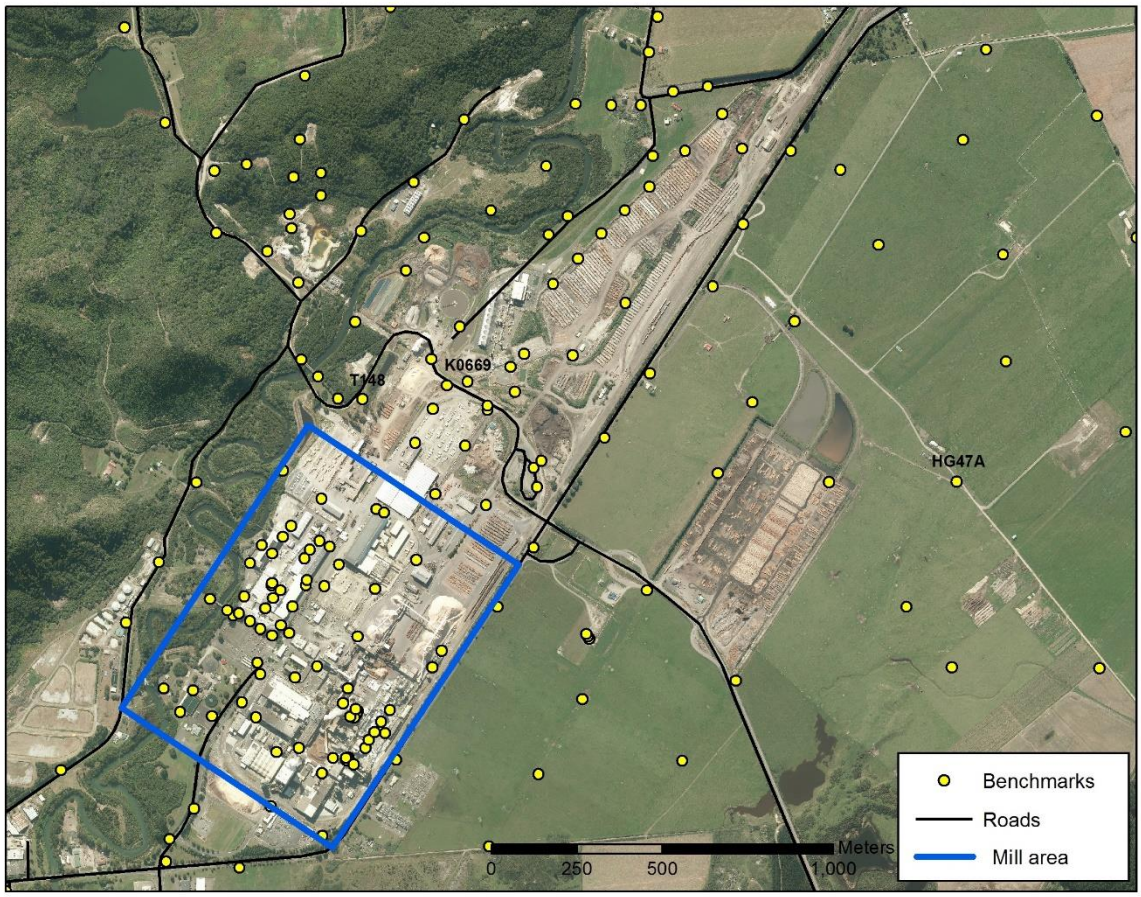

Figure 3.4: Benchmarks consistently re-levelled from 2007 – 2013 from which the contours in Figure 3.5 are derived.

Figure 3.5 shows annual changes in subsidence rates across the selected benchmarks from 2007 – 2013 (Fig. 3.4). Important features in these images is the rates of bowls B and D south of KGL, the lack of a subsidence feature beneath the mill area (Fig. 3.4), and the apparent subsidence anomaly in the east of the 2007 – 2008 image.

From 2008 onwards the continuation of a subsidence anomaly can be seen south of KGL centred on benchmark K0669 (Fig. 3.4), this anomaly has been termed Bowl B (Fig. 3.3) by Energy Surveys and MRP and will be referred to as Bowl B hereinafter. From 2010 onwards Bowl B is seen to extend in a westerly direction towards benchmark T148, the extension of Bowl B is termed Bowl D. Given the proximity of Bowls B and D to each other the likelihood that the two bowls are being driven by the same process is high. Following analysis of earlier benchmark re-levelling surveys back to 1972 it is found that the area of Bowls B and D has always been prone to greater subsidence than the rest of KGF. This indicates that there may be an anomalous material at depth with different properties to the surrounding area causing Bowls B and D. The increase in the intensity of Bowl B coincides with the increase in production

from the commissioning of KGL. Another increase in production with a subsequent increase the intensity of subsidence bowls could confirm a link between shallow and deep processes.

The mill complex area (Fig. 3.4) does not display a subsidence anomaly, instead the area is only affected by the broad, field wide subsidence bowl and current rates within the mill complex are 10 – 15 mm/year (2012 – 2013 surveys). The development of a subsidence anomaly within the mill complex area could have a negative effect on the operations of at least one of the three companies operating in the area (Carter Holt Harvey Tasman, Norske Skog Tasman and SCA) depending on its location, and on the geothermal tappers because of the Resource Consents they operate under. A subsidence anomaly occurring within the mill complex has the potential to damage assets within the complex due to its high ground tilt, and prevent normal operations. Mill site subsidence is analysed further in section 3.7.

In the 2007 – 2008 survey an anomaly is detected east of the mill complex, but does not develop, nor is it detected in any of the following surveys. This is most likely because the benchmark (HG47A, Fig 3.4) at the centre of the anomaly has been disturbed by processes outside of those affecting the rest of the benchmark network, for example it may have been run over by a vehicle. This benchmarks predecessor (HG47), which was surveyed in 2006 and 2007, did not record an anomalous rate of subsidence during this period and the surrounding benchmarks do not reflect this anomalous measurement. Consistent rates across benchmarks close to each other over successive re-levelling surveys are key to distinguishing between apparent subsidence and true subsidence. The feature detected in the 2007 – 2008 survey is the only apparent subsidence feature detected from 2007 – 2013 despite Bowls A, B and D being described as potentially apparent subsidence features in previous studies (Mackenzie, 2011).

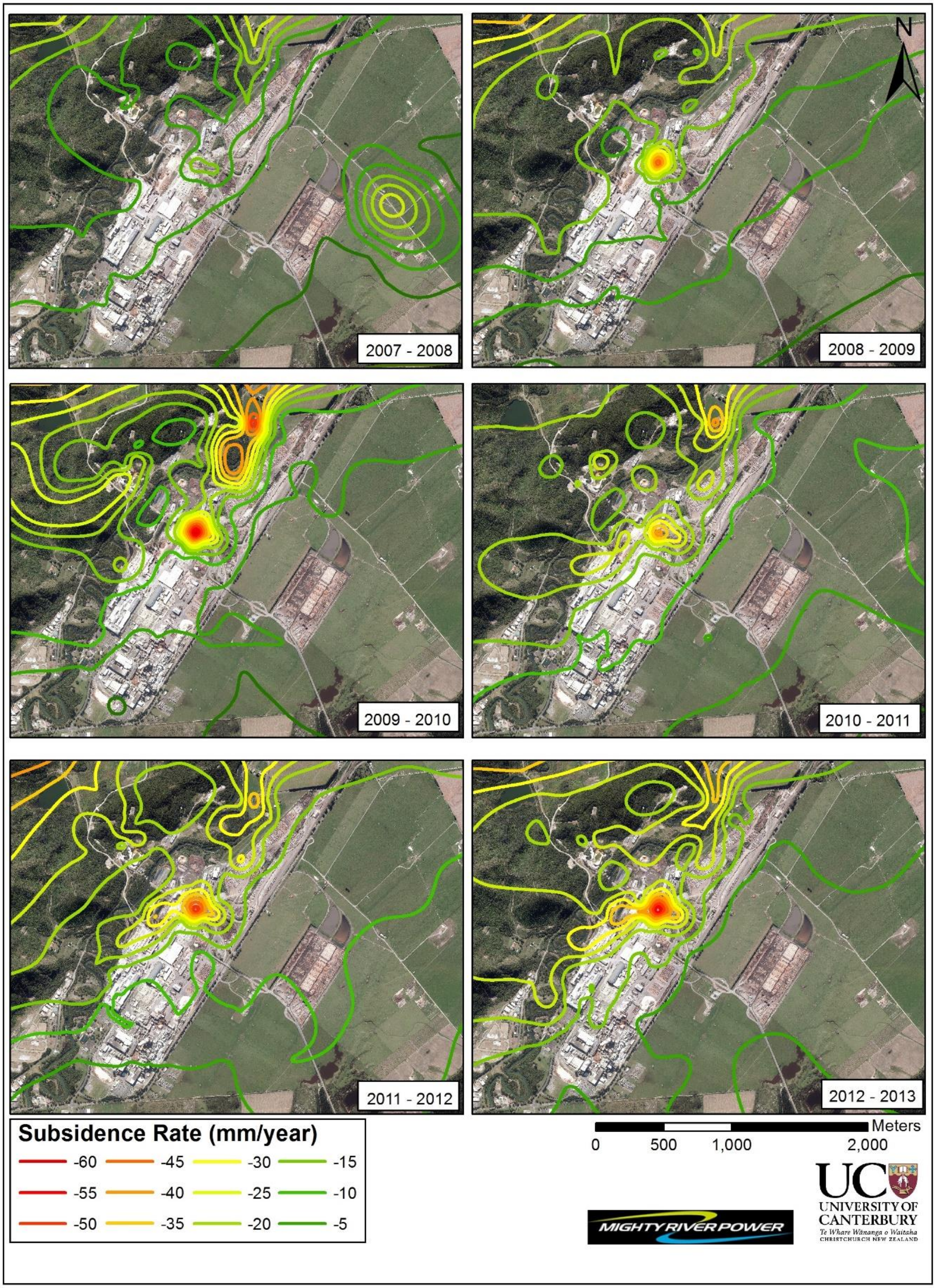

Figure 3.5: Contours derived from selected benchmarks that are re-levelled from 2007 to 2013 showing the change in rates of subsidence around the field.

3.5 Mill Site Subsidence

The mill site is defined by the presence of the three operating companies; Carter Holt Harvey Tasman (CHH), Norske Skog Tasman (NSK), and SCA Hygiene Australasia (SCA) and is located south of KGL. The site is bounded by State Highway 34 (SH34) in the east and south, and the Tarawera River in the west (Fig 3.4).

Over the mapped period from 2007 to 2013 (Fig. 3.5) the mill site shows very little change in its subsidence trend, the general trend is of uniform subsidence across the mill site and the noticeable lack of a subsidence anomaly which would cause issues for operations. Figure 3.5 indicates that the rate the mill site is subsiding is slowly increasing, this is due to the broadening of the field wide bowl. The 2007 – 2008 subsidence map shows the -5 mm contour going through the mill complex in a SW-NE orientation, the following two surveys (2008-09 and 2009-10) also have the -5 mm contours going through the mill site but it is located further south-east each time, indicating a broadening of the field wide bowl. In the 2010-11 survey the -10 mm contour is located through the mill complex at the same orientation. The 2011-12 survey shows a decrease in the rate of subsidence of the field wide bowl, indicated by the -5 mm contours crossing through the southern area of the mill site. Finally the 2012-13 survey shows an overall broadening of the field wide bowl with the mill site in between the -15 mm contour in the north-west and -10 mm contour in the south-east.

Ground tilt across the mill site is a concern due to the sensitive machinery operating within the mill site. If tilt is greater than the tolerances of the machinery there will be a negative effect on operations costing time and money to remediate. Ground tilt is represented by the closeness of subsidence contours on a plane (Abele & Currie, 2013), the closer the contours, the greater the ground tilt. Tilt is calculated as part of Energy Surveys annual reports on the subsidence levelling reports.

Throughout all the surveys from 2007 to 2013 the spacing of the contours remains approximately the same indicating little change in ground tilt across the mill site. Tilt within the mill site is calculated between three benchmarks surrounding the NST paper machines (Fig 3.6) and is included in each Energy Surveys report. Average tilt rates are as follows:

Year	Average Tilt rate (mm/100 m/year)	Direction
1998 – 2008	0.7	332°
2008 – 2009	1.6	330°
2009 – 2010	1.1	333°
2010 – 2011	1.2	253°
2011 – 2012	2.2	16°
2012 – 2013	1.4	336°
2009 – 2013	1.5	324°
Total since 1982	21.8mm/100m*	314°

*Table 3-3: Tilts rates in the Norske Skog paper machine area. *: of which 17% occurred in the 1987 Edgecumbe earthquake. (Abele & Currie, 2012 and 2013)*

Overall the tilt rates show that the subsidence across the mill site is regular with low tilt gradients.

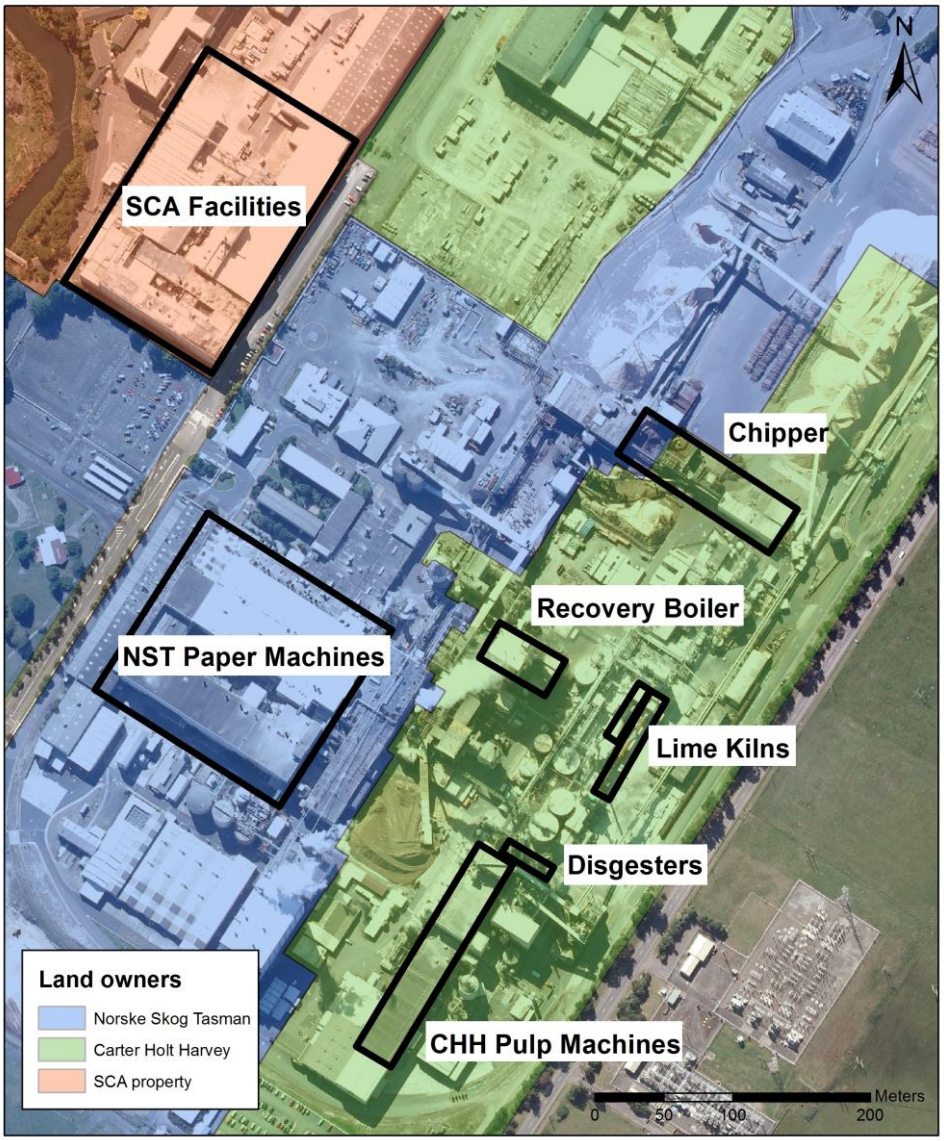

Figure 3.6: Tasman mill site, features shown include; land owners and structures sensitive to ground tilt.

3.5.1 Norske Skog Tasman Paper Mill

The Norske Skog Tasman paper machine building (Fig. 3.6) houses three paper machines that run in a south-east to north-west direction. Due to product demand only paper machine three at the south end of the building is currently in use (Joe Hotson, pers. comm., 2014). Using the recorded values from 2009 to 2013 from four benchmarks at the corners of the building the approximate ground tilt direction can be shown (Fig. 3.7). The graph shows that the north-west corner (K0908) is subsiding at a slightly higher rate than the other three benchmarks. Over the four years the benchmarks have been re-levelled the range between the most effected and least effected benchmarks (K0908 and K0911 respectively) is 6.5 mm, the benchmarks are ~170 m apart, further highlighting the low tilt rates across the mill site.

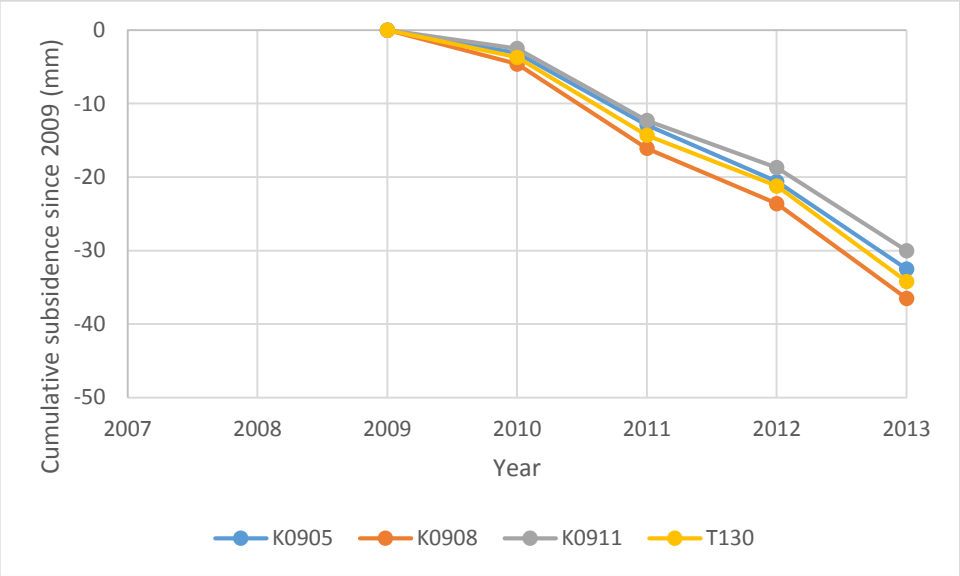

Figure 3.7: Norske Skog Tasman paper machine benchmarks. K0905 - North-east corner, K0908 - North-west corner, K0911 - South-east corner, T130 - South-west corner.

3.5.2 Carter Holt Harvey Structures

Due to the chemical process required to produce Carter Holts Harvey's pulp product there are a greater number of structures sensitive to ground tilt at CHH than at NST. These include: the chipper, recovery boiler, lime kilns, digesters, and pulp machines (Fig. 3.6). Of these structures the lime kilns, recovery boiler, and digesters have benchmarks on their foundations that can be used to measure subsidence.

The Lime Kilns are located in the north area of CHH and run parallel with SH34. There are four benchmarks evenly spaced along the base of Lime Kiln 2 which were installed in 2007 and re-levelled annually through to the current 2013 survey. Figure 3.8 shows the differential subsidence across the four benchmarks, the graph shows that the north end of the Lime Kiln is

subsiding at a slightly higher rate than the south end. The north and south benchmarks are spaced approximately 90 m apart and the northern benchmark (K0744) has subsided 2.9 mm more than the southern benchmark (K0740) over a five year period (0.64 mm/100 m/year).

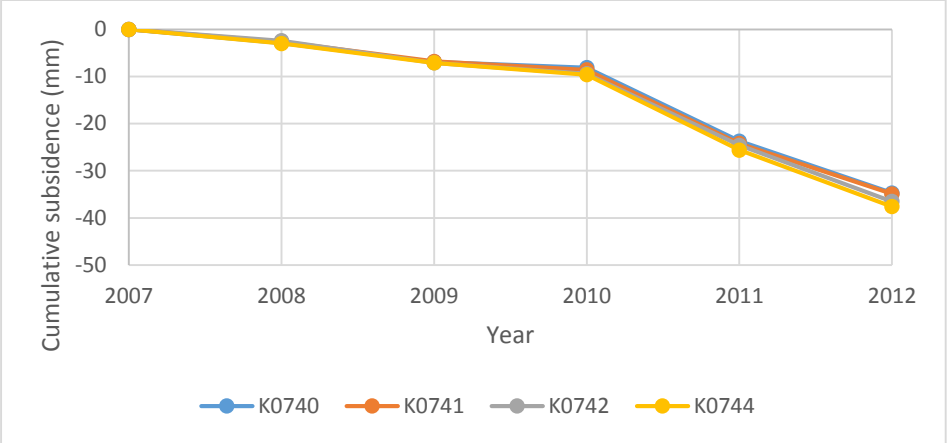

Figure 3.8: Carter Holt Harvey Lime Kiln 2 benchmarks. K0744 - North, K0742 - Centre north, K0741 - Centre south, K0740 - South.

The recovery boiler is located 80 m northwest of the Lime Kilns and is a 1000 T top hung boiler housed within a structure, supported by seismic guides that were retrofitted in 2011 to meet NZS 1170.5 and the Building Act 2004 (Beca, 2011). The housing structure has a footprint of ~947 m^2 and has four benchmarks on the four corners, one of which is labelled as destroyed in the 2011 annual survey (K0754). The benchmarks show that ground beneath the recovery boiler has subsided 5.6 mm more in the northwest (K0755) than in the southeast (K0752) across 45 m over five years (Fig. 3.9). Because the recovery boiler is housed in a multi-storey structure ground tilt is amplified at the top of the structure as a function of its height.

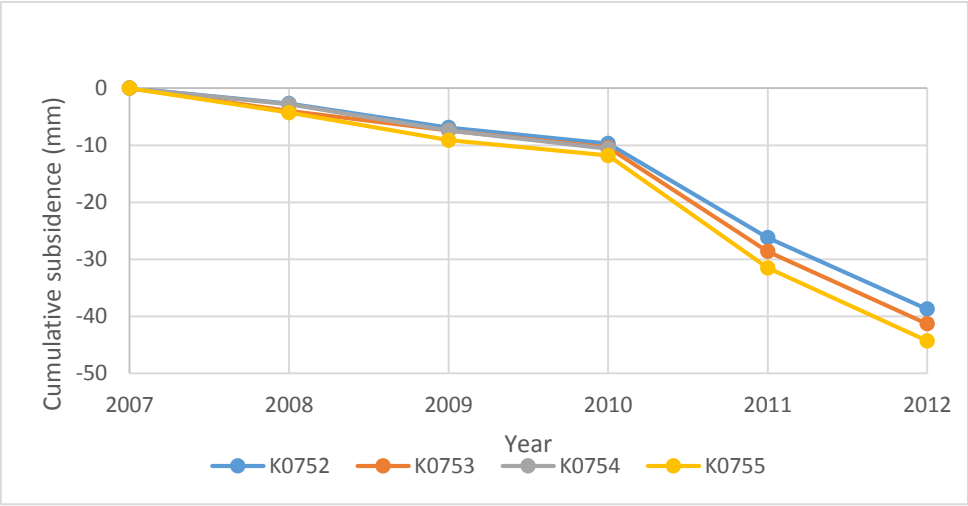

Figure 3.9: Carter Holt Harvey Recovery Boiler #2 benchmarks. K0755 - Northwest, K0754 - Southwest, K0752 - Southeast, K0753 - Northeast

The digesters are located at the south end of the lime kilns and the north end of the CHH pulp machines. There are three digesters situated perpendicular to SH34 and digesters one and two, the two western digesters, have benchmarks at their bases. Because of the digesters small footprints the effect of ground tilt on them is minimal. Digester 1, in the middle, has a footprint of ~54 m^2 and four benchmarks at the base which have been re-levelled annually since 2009. To date after four surveys there is 0.3 mm range in the four benchmarks (Table 3.4).

Benchmark	2009	2010	2011	2012
K0736A	0	-1.6	-15.6	-26.9
K0737A	0	-1.8	-15.8	-26.9
K0738A	0	-1.3	-15.4	-26.6
K0739A	0	-1.7	-15.6	-26.8

Table 3-4: Carter Holt Harvey Digester 1 cumulative ground deformation across surrounding benchmarks, measurements in millimetres.

Digester 2, located west of Digester 1, is a similar height and has approximately the same footprint. It has four benchmarks at the base orientated 45° differently to Digester 1 that have been re-levelled annually since 2007. Of the six surveys completed on the Digester 2 benchmarks to date there is a 0.3 mm range in the four benchmarks (Table 3.5).

Benchmark	2007	2008	2009	2010	2011	2012
K0732	0	-3.1	-6.8	-8.2	-22.5	-33.8
K0733	0	-3	-6.9	-8.1	-22.3	-33.5
K0734	0	-3.1	-6.9	-8	-22.2	-33.5
K0735	0	-2.8	-6.9	-8	-22.4	-33.8

Table 3-5: Carter Holt Harvey Digester 2 cumulative subsidence across surrounding benchmarks, measurements in millimetres.

Because the digesters are multi-storey structures ground tilt is amplified as a function of the building height at the top of the structure. To measure this Carter Holt Harvey have placed a simplistic gauge at the top of Digester 3 (Fig. 3.10) which measures the amount of lateral movement at the top of the digester.

Figure 3.10: Simplistic gauge to measure the amount of movement at the top of Carter Holt Harvey's digesters.

Overall, due to the small footprint of the Carter Holt Harvey structures, ground tilt has little effect on them. With many of the structures housing or supporting rotating or vibrating machinery the shaking from the machinery likely has just as much effect in machinery becoming misaligned as ground tilt. Furthermore the measured differences in the benchmarks around the structures are within the error range at the 95% confidence level.

3.6 Subsidence Compared with Monitoring Data

Subsidence at geothermal fields has been correlated with monitored parameters since the 1950's when it was first noticed that Wairakei Geothermal Field had subsided as much as 0.25 feet from 1950 – 1956 (Hatton, 1970), since then all operating geothermal fields in New Zealand have been monitored for subsidence. Along with this, certain parameters that effect the availability of the resource and parameters that are bound by resource consent conditions are monitored. These include pressure and pressure drawdown, production and injection, and enthalpy. These parameters also have the potential to be correlated with subsidence and they are analysed here.

To compare the benchmark levelling data to other datasets the benchmarks must be limited to those that are constantly re-levelled. A further constraint added is that any outlying benchmarks are omitted from the calculation of the average rate as they do not represent ground deformation within the area of concern and can affect the results by drawing contours between two benchmarks over a large distance where there is no data in between. For example when calculating the average rate of subsidence rate in Figure 3.13 and 3.14 only those benchmarks

levelled annually from 2007 – 2012 and those around the mill site are used to calculate the average rate of subsidence (Fig. 3.4).

Pressure and Pressure drawdown

Pressure drawdown is a decrease in pressure as a result of extraction and is the primary cause for field wide subsidence in geothermal fields around the world (Allis et al., 2009; Carnec and Fabriol, 1999). Pressure drawdown occurs because the system is unable to recharge the reservoir at an equal rate to production. Injection is designed to minimise pressure drawdown but is not always equal to production due to the potential for reservoir cooling, loss of fluid as steam into the atmosphere (KGL), loss of steam through silencers, and discharge of fluid into the Tarawera River (NTGA) (John Clark pers. comm., 2014). Pressure drawdown within the reservoir is linked to subsidence because the pressure of the fluids along with the reservoir rock supports the cover sequences of the reservoir. When pressure drawdown occurs the lithostatic load from the cover sequences effectively increases resulting in the compaction of the reservoir and is represented at the surface as a broad field wide subsidence bowl. Subsidence anomalies can occur when shallow groundwater pressures decline due to fluids being drawn into deeper lithologies, e.g. the drying up of surface thermal features.

Pressure at KGF is monitored in five monitoring wells, four deep and one shallow (KA14) using downhole capillary tubing (Spinks et al., 2010). Three of the wells monitor pressure within the producing basement greywacke (KA23, KA25 and PK3) and one each are located in the extrusive and intrusive members of the Caxton Formation (KA14 and KA31 respectively). Monitoring equipment in the four deep wells is set at different depths and while pressure increases with depth the pressure changes reflect each other in their response to changes in the reservoir. The consistent response across the four monitoring wells indicates a large, distributed, and permeable reservoir (Spinks et al., 2010). The shallow groundwater monitoring well, KA14, shows no response to reservoir pressure changes indicating that the aquifer monitored by KA14 is not connected to the deeper reservoir or any response is muted due to pressure support from NTGA's shallow injection. Meanwhile KA31 shows a small amount of response to reservoir pressure changes (Fig. 3.11).

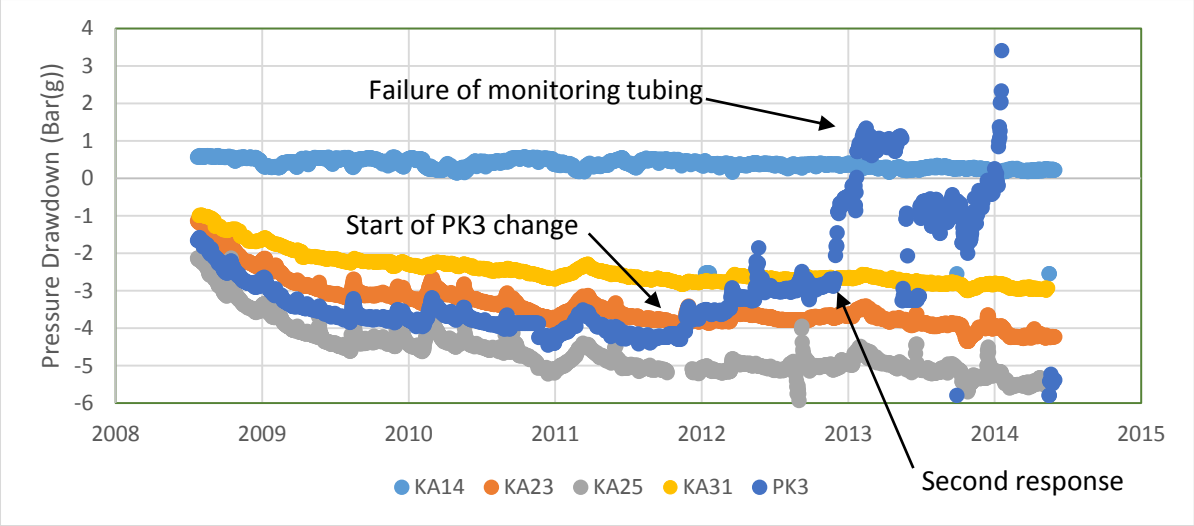

Figure 3.11: KGF pressure drawdown from monitoring well data. KA14 (shallow, Caxton Formation - extrusive), KA31 (Caxton Formation - intrusive) and KA23, KA25, PK3 (deep, Greywacke).

PK3 shows a different response towards the end of 2011 compared with the other three deep monitoring wells. The first response change correlates with a brine-condensate switch between PK8 and PK5, the second change at the end of 2012 correlates with the brine-condensate switch between PK5 and KA50. Both of these response changes suggest there is a flow path between these wells and PK3. The pressure response change in early-mid 2013 is associated with a failure of the pressure monitoring tubing. The tubing in PK3 has since been fixed and reset, and appears to be working correctly again (Clark et al., 2014).

Pressure monitoring at KGF began in July, 2008, coinciding with the commissioning of KGL. Pressure began with a steady decrease of nearly 2 bar over the first year before levelling out to an average rate across the three functional wells of 0.16 bar/year over the following four years. The initial drop in pressure compares favourably with numerical modelling completed before KGL commissioning which showed a decline of 4 – 8 bar over the same period (Spinks et al., 2010). The initially higher rate of pressure drawdown is to be expected because of the initial shock to the system of increased production from 2007 to 2008 when production nearly tripled (Fig. 3.13). In comparison Wairakei Geothermal Field had 25 bar of pressure decline from 1950 to 1980, an average rate of 0.8 bar/year, across the production zone which resulted in maximum subsidence of 14 metres in the Wairakei subsidence bowl (Allis, 2000). The average rate of pressure drawdown at Wairakei during the cited 30 year period is five times greater than the pressure drawdown currently occurring at Kawerau.

When viewing the total pressure in the monitored wells (Fig. 3.12) as opposed to pressure drawdown (Fig. 3.11), the graph shows that pressure drawdown as a fraction of the total

pressure is very small. Very little change in pressure is able to be distinguished in the chart. The issues previously explained in PK3 however are visible in the downhole pressure chart from late 2011 onwards, where PK3 does not reflect the other deep monitoring wells.

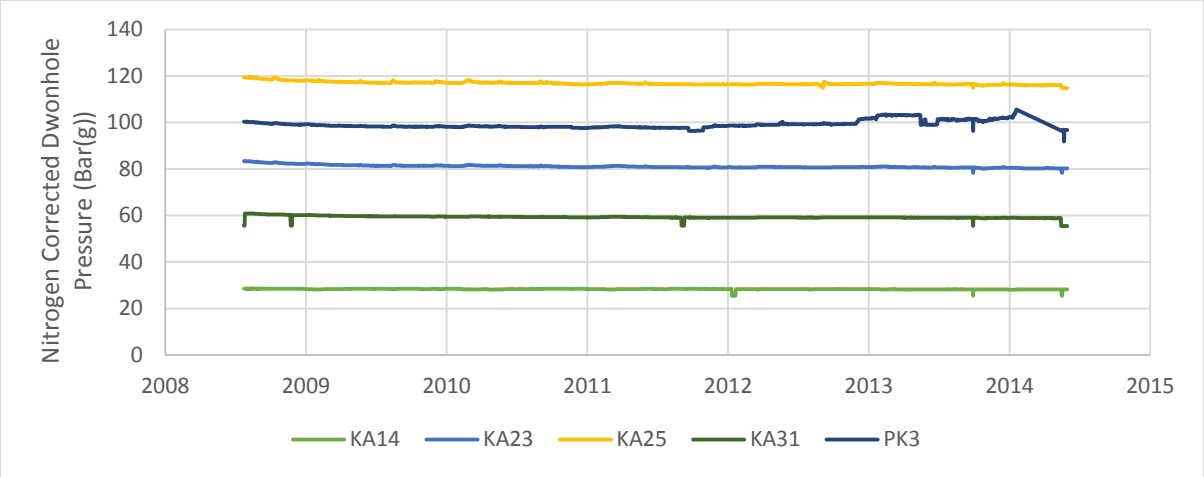

Figure 3.12: Kawerau Nitrogen Corrected Downhole Pressure from monitoring well data. KA14 (Caxton Formation - extrusive), KA31 (Caxton Formation - intrusive) and KA23, KA25, PK3 (Reservoir Greywacke).

Production and Injection

At KGF production and injection is recorded as a daily average in tonnes/hour in all production and injection wells since 1st June, 2012, before this recordings were taken as an average for a variable period of time, typically 2 – 3 weeks. Production and injection totals include all geothermal tappers at KGF. Currently there are 14 production wells and 12 injection wells in use at KGF. To compare the amount of production and injection with subsidence the total amount of fluid extracted and injected is calculated for an annual period to match the re-levelling surveys and compared with the average annual subsidence rate across selected benchmarks (Fig. 3.13).

Following the commissioning of KGL production increased from 11.5 Mt/year in 2007 to 29.7 Mt/year in 2008 and in the following four years (2009 – 2012) has remained stable at ~35 Mt/year, total injection also increased following the commissioning of KGL from 4.5 Mt/year in 2007 to 16.7 Mt/year in 2008 in response to the increased production required for KGL. Since 2009 production and injection totals have remained fairly consistent, with any slight production changes reflected by injection, keeping the net loss consistent. An example of this is the increase and decrease in production and injection from 2010 – 2011 and 2011 – 2012 (Fig. 3.13).

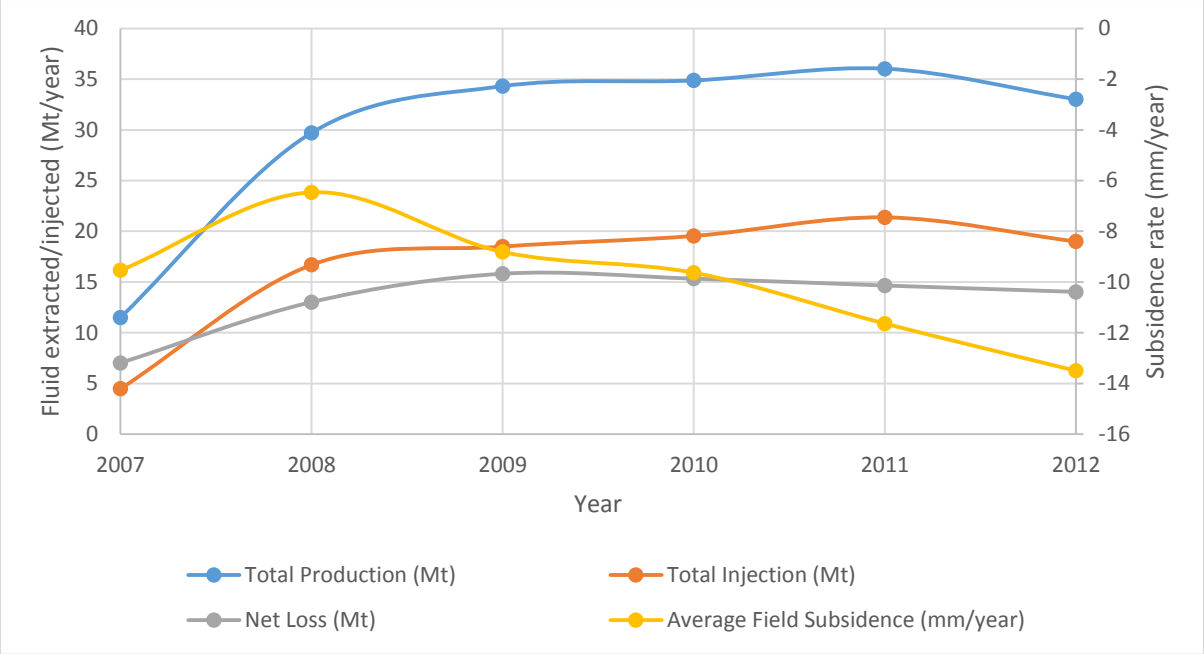

Figure 3.13: Total annual production, injection and net loss values at KGF, compared with the average annual subsidence rate across selected benchmarks.

Figure 3.14 shows the annual percentage of production fluids that are re-injected across all KGF wells. The graph shows that since 2008 the percentage of fluid re-injected has been between 50% and 60%, while the average field subsidence across selected benchmarks (Fig. 3.4) has steadily increased since 2009. The increasing average field subsidence is due to the broadening of the field wide subsidence bowl, as the bowl size increases higher subsidence values are recorded on more benchmarks, increasing the average value.

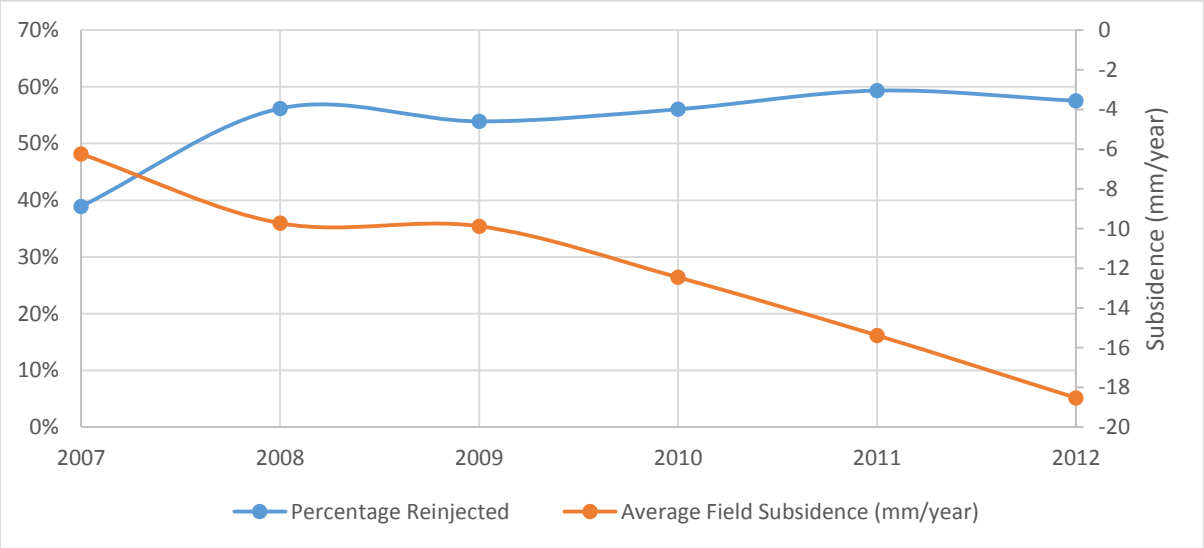

Figure 3.14: Annual percentage of fluids re-injected vs. Average field subsidence across selected benchmarks.

While production and injection levels have remained stable since the commissioning of KGL the average rate of subsidence has continued to increase; this suggests that production and

subsidence are not related. A statistical analysis by Bromley et al. (2015) finds a weak correlation between subsidence averaged across 16 indicative benchmark and net mass extraction ($R^2 = 0.4$). Results are that for every 1 Mt/year increase in extraction there would be an additional 1 mm/year of subsidence across those 16 benchmarks.

Enthalpy

Enthalpy (H) is the thermodynamic potential of the fluids being extracted from the geothermal system. It consists of the internal energy of the system (U) plus the product of the pressure (p) and volume of the system (V), ($H = U + pV$). MRP undertakes discharge enthalpy monitoring at the surface of their seven production wells that contribute to KGL. Because enthalpy is monitored at the surface, unlike pressure, it does not correspond to any depth, although all of MRP's production is from Greywacke Basement. Changes in discharge enthalpy can be correlated to changes in subsurface temperature, localised boiling, or feedzone contributions (John Clark pers. comm., 2014). Enthalpy can therefore be changed by (1) heating or cooling of the reservoir, (2) by adding or taking away matter, this is production and injection or natural inflows of cold meteoric waters, (3) a change in the pressure of the system, or (4) a change in the volume of the system. All of these factors influence each other making it difficult to identify the reason for a change in enthalpy, instead it can be put down to combination of all four factors. The enthalpy across all seven wells shows a gradual decreasing trend since monitoring began in mid-2008 (Fig. 3.15).

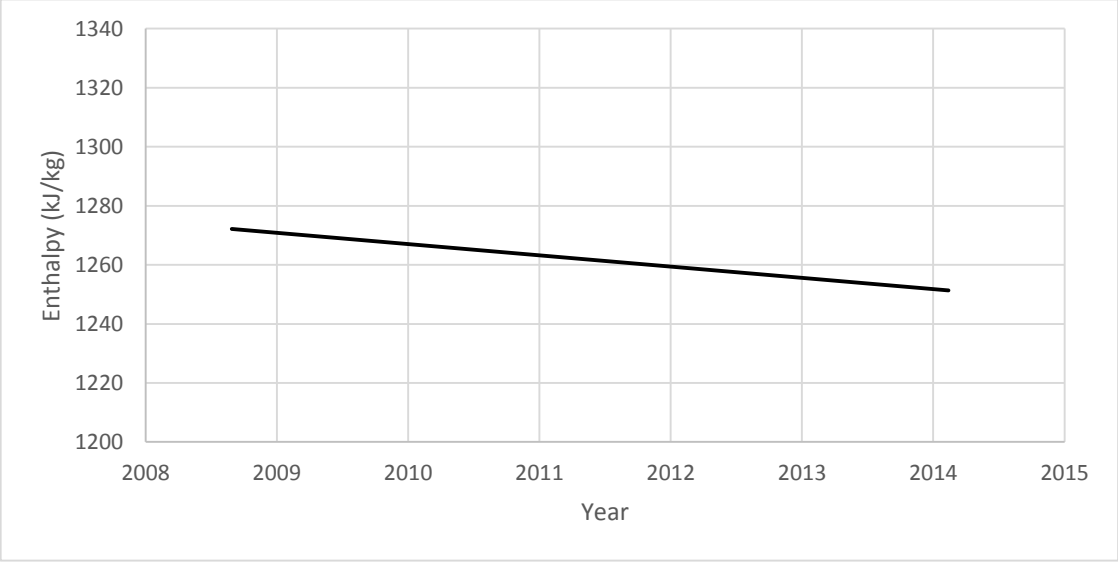

Figure 3.15: Linear trendline of the average enthalpy across the seven KGF wells. Moving average removed due to commercial sensitivity.

3.7 Conclusions

Following the spatial analysis of subsidence and comparison with monitoring datasets, conclusions can be drawn about the subsidence occurring at KGF and suggestions can be made regarding the presence of Bowls B and D south of KGL, and the lack of an anomaly across the mill site.

- The 1987 Edgecumbe earthquake caused an average of 225 mm of subsidence across the field, the largest recorded subsidence at KGF to date. This showed that the Whakatane Graben is actively subsiding.
- The reference benchmark for KGF surveys is located outside of the field wide subsidence bowl, but is affected by regional subsidence. Measured ground deformation at KGF is therefore independent of the regional subsidence occurring because of the TVZ and Whakatane Graben structures.
- Field wide subsidence is driven by deep reservoir processes, this bowl has low to no potential to be disruptive due to its low tilt across such a large area.
- Localised subsidence features or anomalies are the results of shallow processes, of the two present within the developed area of KGF (Bowls B and D), neither has an effect on the mill site. These features have been present since the earliest levelling surveys conducted in the 1970s.
- Average rates of subsidence at KGF are steadily increasing due to the broadening of the field wide bowl.
- The main subsidence related concern at KGF is subsidence across the mill site and the effect on mill operations. While subsidence rates increase, tilt rates remain within the 1 mm/30 m/year threshold of NST paper machines (John Clark pers. comm., 2014) and the 2 mm/100 m/year of CHH machinery (Derrick Hope, pers. comm., 2014).
- When compared with monitored parameters at KGF subsidence appears unrelated to production, injection, net loss, and loosely related to pressure drawdown and enthalpy. It is widely accepted that these parameters can effect subsidence but impossible to directly correlate them at KGF over such large datasets.

4 Modelling of Cover Sequences

The ability to visualise the subsurface of a geothermal field is vital to comprehensively understand the stratigraphic relationships of the area. The use of implicit and dynamic 3D modelling software allows geologically complex areas to be graphically represented, interpreted, and communicated; these data can then be used to assist in decision making utilising the most up to date information available. Two models for KGF currently exist which are used to enable reservoir engineers and field managers to operate the field for maximum efficiency. Both models include all aspects of the geothermal field and are utilised in parallel model development for the field; MVS software platform (CTECH, 2014) maintained by Mighty River Power Ltd. (MRP), and a Leapfrog Geothermal (ARANZ Geo Ltd., 2014a) model published in Milicich et al. (2013a) and Milicich et al. (2014).

Milicich et al. (2014) developed a 3-D interpretive model for the Kawerau Geothermal Field (KGF) to support exploration by constraining borehole targeting, and reducing drilling risk and cost. The model provided insights regarding the geological framework, controls on permeability, cover sequences and basement stratigraphic correlations, and the evolution of the geothermal system assisted by age data (Milicich et al., 2013b). Using the well logs from Milicich (2013b) and drilling data (dip and azimuth) from MRP a three-dimensional model of the shallow cover sequences is developed here. The aim of the model is to identify whether the presence of the subsidence anomalies (Bowls B and D) can be accounted for within well logs and if the geologic conditions below the mill site have the potential to cause a subsidence anomaly.

Leapfrog Geo is a dynamic 3D geological modelling program developed by ARANZ Geo. in Christchurch, New Zealand and is the leading geological mining software around the world (ARANZ Geo Ltd., 2014b). Leapfrog Geo allows dynamic modelling of the cover sequences of KGF where information can be updated at any step through the workflow. Workflow methods are set out documenting the steps taken and data used to build the model. The model is then analysed and interpretations made based on the results. Electronic Appendix 1 contains the data used to build the model, a video showing the model being built, and the model in Leapfrog Viewer.

4.1 Workflow Methods

The following steps are taken to build a model of the cover sequences at Kawerau:

1) Constraining the boundaries of the model

The model focuses on the central area of KGF where benchmarks and wells are spatially dense to ensure the best correlation between ground deformation measurements and geological information. The model measures 4.4 by 3.5 km and is constrained vertically by a digital elevation model (DEM) at the surface and at -750 m below relative level (RL) to include the shallow units of interest and model the units which are realistically causing the subsidence anomalies.

2) Importing data

Data imported into the model includes the KGF well logs (Milicich, 2013b), dip and azimuth data from the drilling of KGF wells provided by MRP, surface geology (Leonard et al., 2010) (see Fig. 1.8), cumulative subsidence contours from 2010-2013 drawn in ArcMap (see Fig. 3.3), a digital elevation model (https://koordinates.com/layer/3730-06-tauranga-15m-dem-nzsosdem-v10/), and Bay of Plenty 0.25m Rural Aerial Photos (https://data.linz.govt.nz/search/?q=bay%20of%20plenty) (Fig. 4.1).

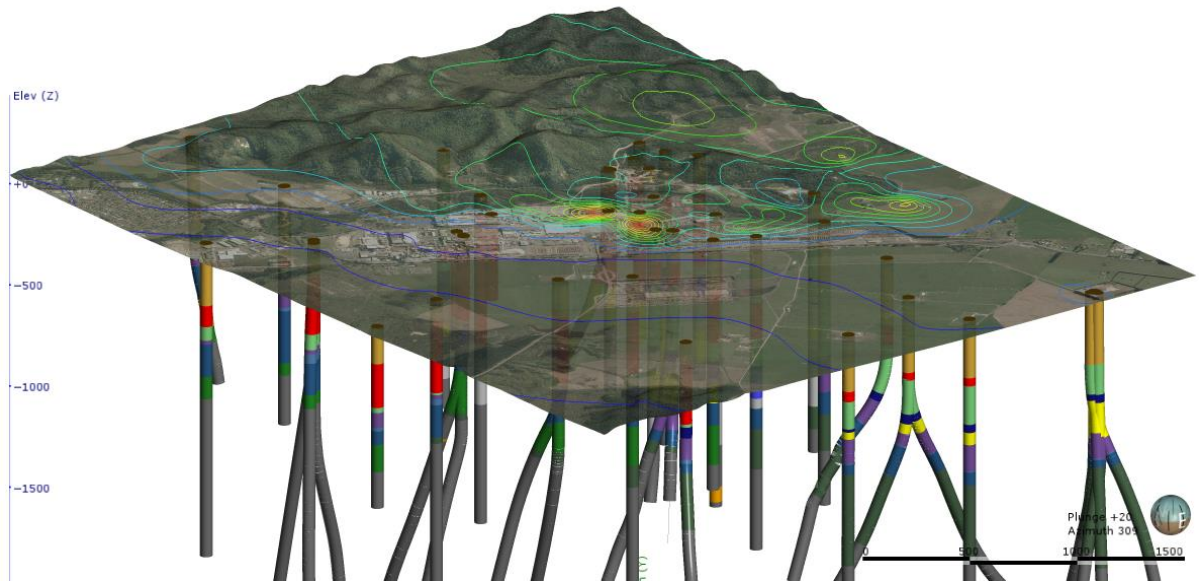

Figure 4.1: Imported data displayed in Leapfrog Geo within model boundaries. Data includes: DEM, 2010-2013 cumulative subsidence, aerial photos, and well logs.

3) Building the geological surfaces

To create the three-dimensional model, surfaces of the geological units must first be created. This involves a two dimensional surface being placed through all the upper and lower contact points of each deposit in each borehole where the unit occurs (Fig 4.2). Each lithology is then constrained by the units above and below, the surface geology bound by the topography from a DEM, and the basement material limited by the specified depth to complete the block model. Intrusions are created separately to deposits; with the software told which units are deposited temporally before and after an intrusive event. This is done by ignoring younger lithologies which ensures correct interactions between intrusions and deposits. The 2D surfaces are then transformed into a three-dimensional model by filling the gaps between the 2D surfaces with 3D blocks and specifying the interactions between all formations by setting the stratigraphic order using the stratigraphy from drilling logs and age data from Milicich et al. (2013b).

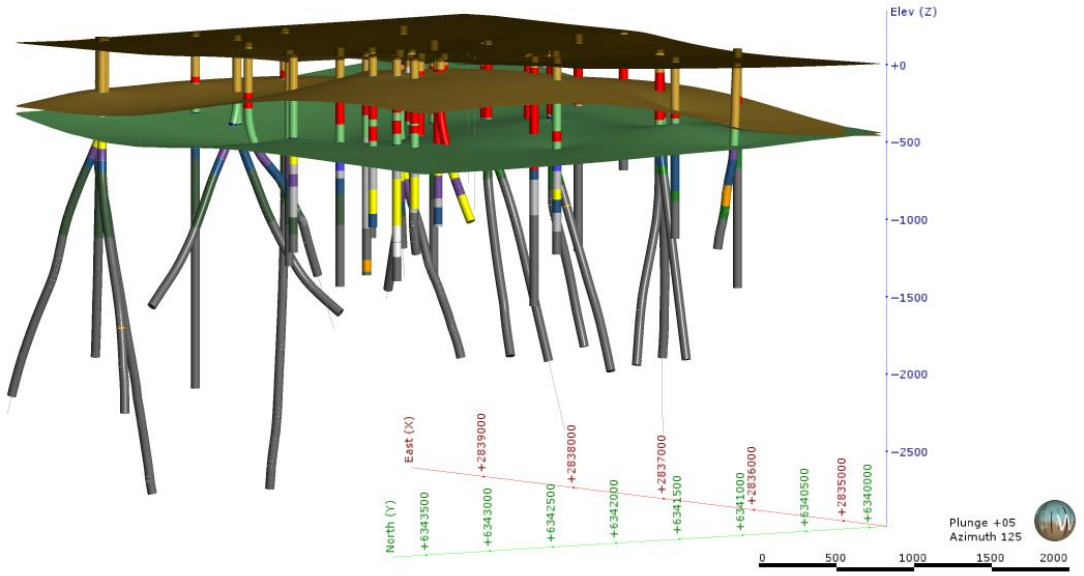

Figure 4.2: Two dimensional surfaces placed through contacts in well logs used to build the model.

4) Intrusions

When an intrusion is defined in Leapfrog Geo the software infers the space occupied by the intrusion based on borehole data. When a large area has not been drilled but the surrounding area has been, the software assumes there is no intrusion present in this space despite the surrounding area being occupied by intrusive material. To remediate this a trend is placed through the intrusion, which effectively links multiple parts of the intrusion to produce a single intrusive body and gives the intrusion a more geologically realistic shape. The result of this is a smooth spatially correct intrusive body (Fig. 4.3).

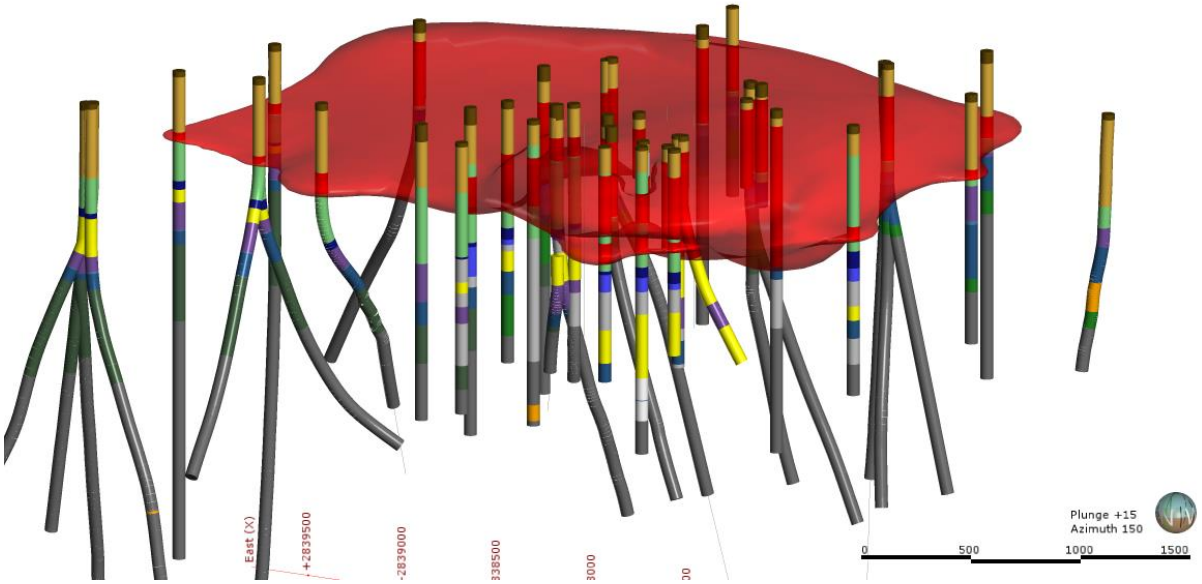

Figure 4.3: Extrusive Caxton Formation at KGF displayed in Leapfrog Geo from borehole data.

5) Incorporating surface geology

Because the Leapfrog model is initially based on well logs, formations that are undrilled are not included in the model, making the model incorrect. This occurs where surface geology differs to the well logs e.g. the presence of undrilled rhyolite domes west of KGF. To correct this the QMAP (Leonard et al., 2010 (see Fig. 1.8)) is imported as a shapefile, draped over the topography and units manually drawn into the model. This is done with the Onepu rhyolite domes west of KGF, Rotoiti Formation ignimbrites north of the Onepu domes, and the industrial fill below Bowl C.

4.2 Cover Sequences Model

The geology represented in the model is fully described in Chapter 1 and summarised in Table 4.1. For the purpose of analysing the cover sequences and their contribution to subsidence at Kawerau the model is limited to -750 mRL. This removes the need to model the more complicated lithologies at depth which have been offset by faulting; Milicich et al. (2014) includes a complete Leapfrog Geothermal model of KGF and shows the complexity of faulting at depth (see Fig. 1.7). The model presented here includes four units present in the KGF boreholes (Recent Alluvium, Matahina ignimbrite, Tahuna Formation, and the extrusive Caxton Formation) and three units drawn into the model from the surface geology QMAP (Onepu Formation, Rotoiti Formation, and Industrial fill). Descriptions of the seven units present are summarised in Table 4.1.

Formation	Description
Recent Alluvium	Pumiceous silts, sands and gravels interspersed with clay lenses and peat deposits.
Matahina ignimbrite	Partly welded grey-brown ignimbrite and vitric tuff (pl, qz, px).
Tahuna Formation	Crystal rich, fine sandstone, siltstone, muddy lithic breccia, and unwelded pumice-rhyolite lapilli tuff.
Caxton Formation	Buried domes of spherulitic and banded rhyolite (corroded and fractured qz and pl).
Onepu Formation	Two surficial domes of rhyodacite (pl, qz, px, hbl, bt)
Rotoiti Formation	Non-welded rhyolite ignimbrite usually with moderate to high crystal content.
Industrial Fill	Anthropogenic mill waste.

Table 4-1: Summary of the stratigraphic units modelled at KGF. Descriptions from Milicich et al. (2014) and Leonard et al. (2010). Pl – Plagioclase, Qz – Quartz, Px – Pyroxene, Hbl – Hornblende, Bt – Biotite.

Subsidence anomalies (Fig. 4.4) are considered to be due to anomalous geological conditions at depth; for example Bowl C is explained by the compaction of industrial mill waste and the now extinct thermal feature to the north-east of Bowl C which is the approximate location of the Onepu thermal area (see Fig. 1.8) (Allis, 1997). To investigate potential geological anomalies in the units at KGF four cross-sections; three W-E and one S-N are placed through the model (Fig. 4.4): 1) through subsidence bowls B and D (Fig. 4.5); 2) through the north area of the mill site ~500 m south of the bowls B and D (Fig. 4.6); 3) through the south area of the mill site ~1 km south of bowls B and D (Fig. 4.7); and 4) parallel with SH34 through the mill site and bowl C (Fig. 4.8).

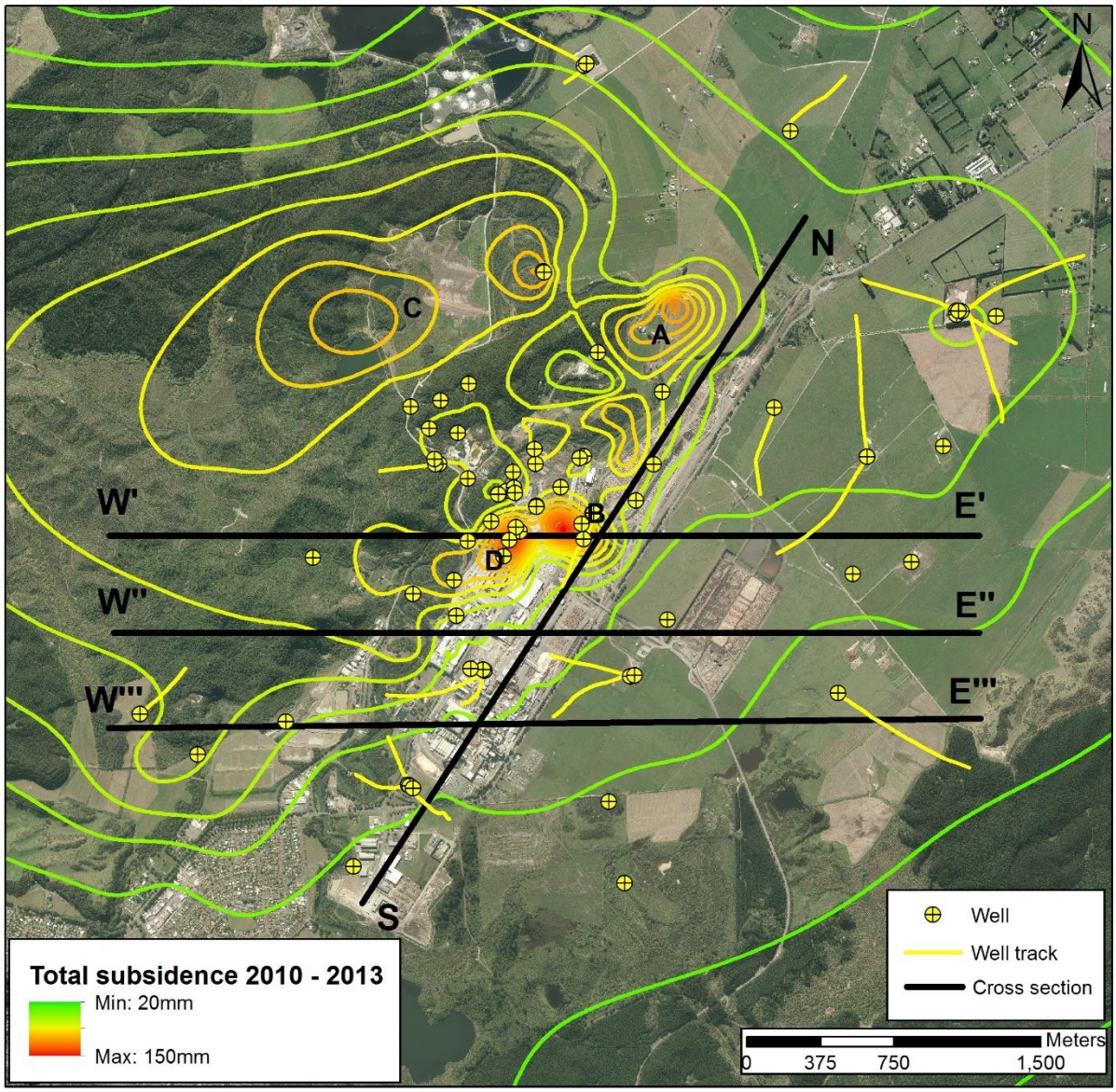

Figure 4.4: Map showing location of cross sections, wells used to complete cover sequences model and total subsidence from 2010-2013 (10 mm contour spacing) showing the location of subsidence anomalies.

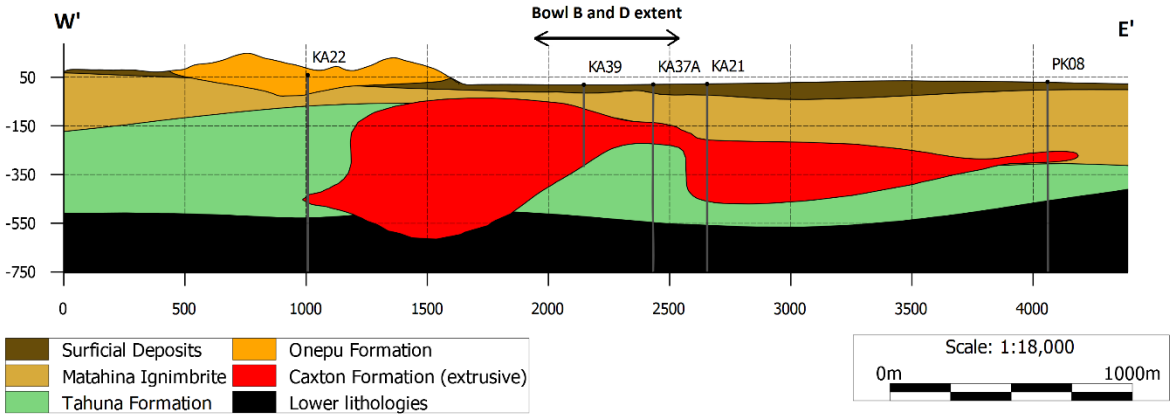

Figure 4.5: West to East cross section through subsidence Bowls B and D.

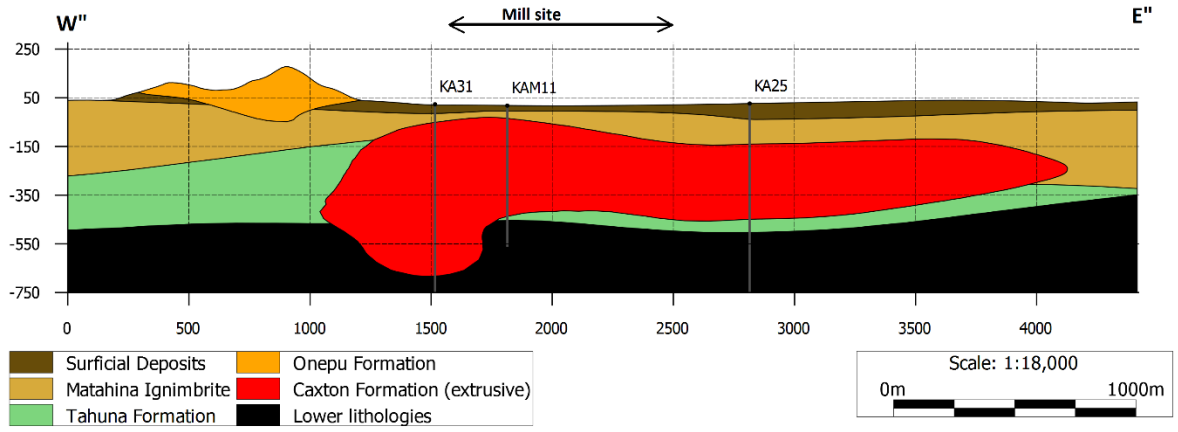

Figure 4.6: West to East cross section through northern area of the Tasman Mill site ~500 m south of Fig. 4.5.

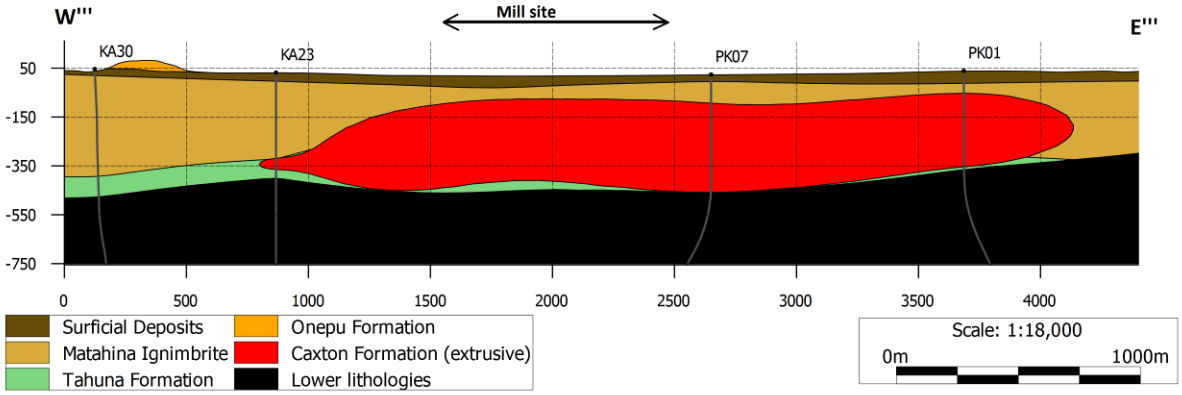

Figure 4.7: West to East cross section through southern area of the Tasman Mill site ~1000m south of Fig. 4.5.

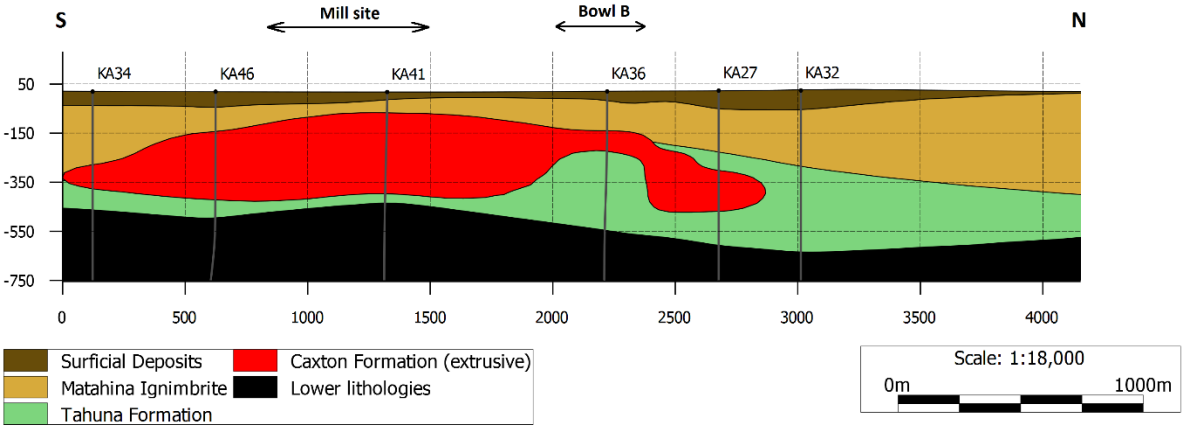

Figure 4.8: South to North cross section through the Tasman Mill site and subsidence Bowl B.

The cross section through Bowls B and D (Fig. 4.5) shows that below the extent of the bowls is an anomalous thickness of Tahuna Formation. The four wells imprinted on the section are KA39, KA37A, KA21, and PK08 and are located 125 m, 0 m, 156 m, and 113 m from the section respectively, the close spacing of the wells to the cross section shows that the section is drawn with a high degree of certainty.

The cross sections through the mill site (Fig 4.6, 4.7 & 4.8) and isopach map (Fig. 4.9) show that the Caxton Formation is of uniform thickness beneath the mill site with the exception of a potential source area near KA31 where it is thicker. Below the mill site the Tahuna Formation is thin compared to below Bowls B and D (Fig 4.6, 4.7 & 4.8). The S-N cross section through the mill site and Bowl B shows the difference in thicknesses of Caxton and Tahuna Formation between the mill site and subsidence anomalies (Fig. 4.8) and a slice through the three-dimensional model shows the thickness of Tahuna Formation beneath Bowls B and D (Fig. 4.10).

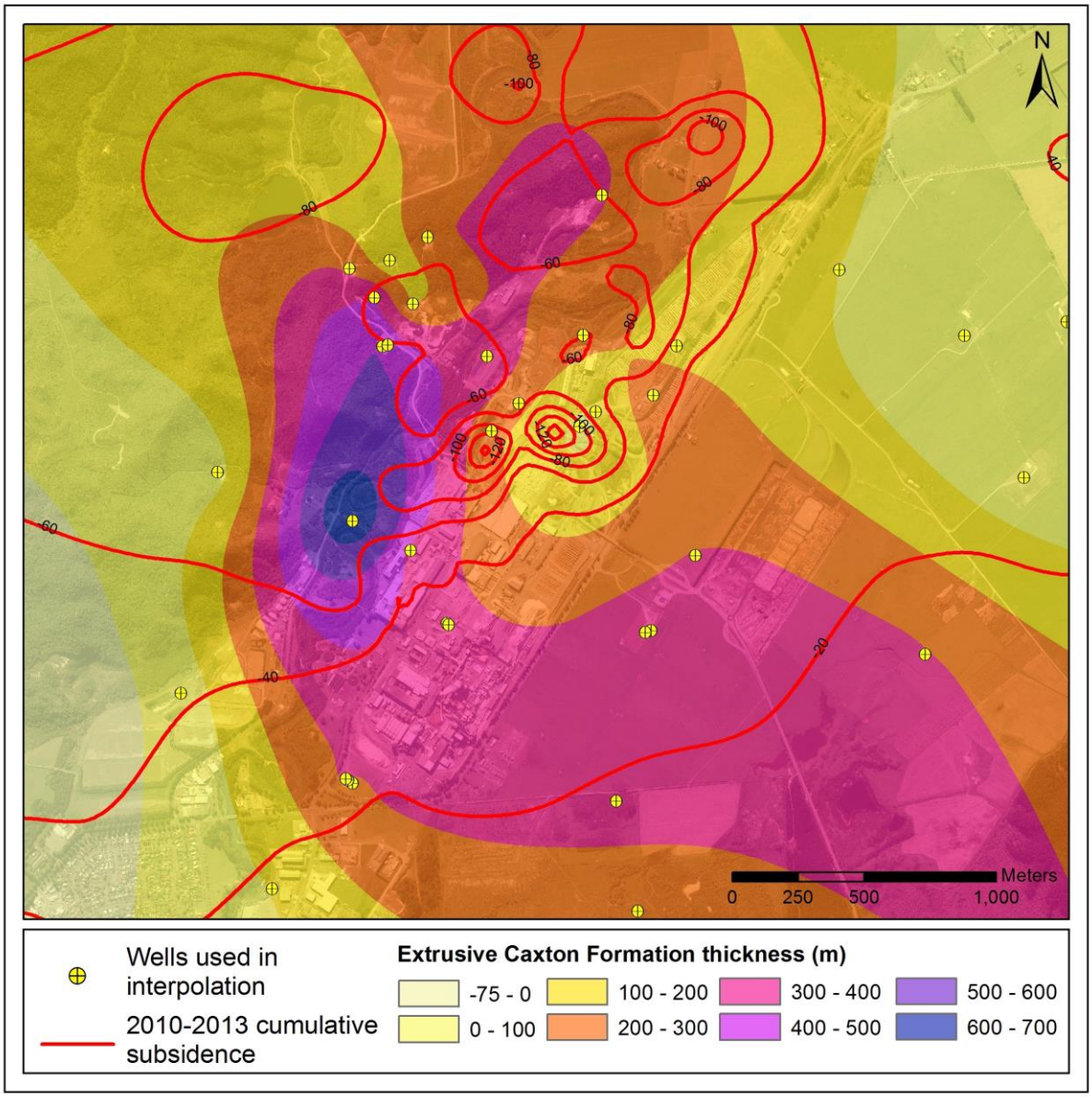

Figure 4.9: Isopach map showing the thickness of the extrusive Caxton Formation across KGF. Created in ArcMap using Milicich (2013) well logs.

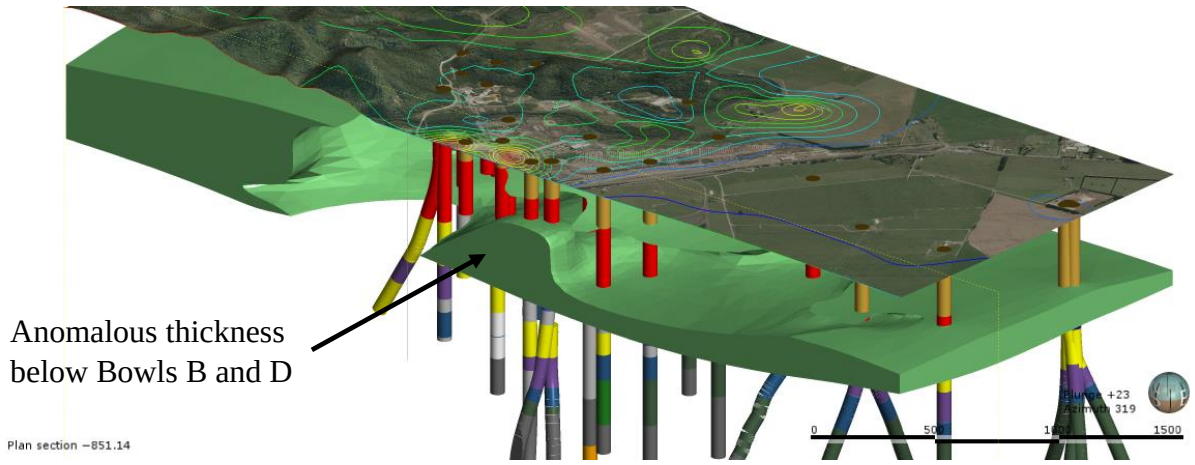

Figure 4.10: West to East slice through the Tahuna Formation showing he anomalous thickness of the formation below Bowls B and D

The relative level isopach map of the Matahina ignimbrite (Fig. 4.11) shows evidence for paleochannels into which the Recent alluvium has been deposited. With the Recent alluvium being relatively flat across KGF at the surface this means that the paleochannels in the Matahina ignimbrite have greater thicknesses of Recent alluvium filling them relative to the rest of the KGF. Approximately below Bowls B and D is a paleochannel where the relative level is lower than the surrounding area. A proposed mechanism for the presence of Bowls B and D is that the paleochannel has channelled the deposition of Recent alluvium resulting in a deposit of weak, unconsolidated alluvium at this location. A larger paleochannel is present east of the Tasman Mill site and does not exhibit subsidence features at the surface. This could be because the channel is large enough to not result in weak, unconsolidated material being deposited within it. The points from which this channel has been drawn are however widely spaced, with more points east of Kawerau Geothermal Ltd. power station (KGL) and Tasman Mill the channel could become better defined.

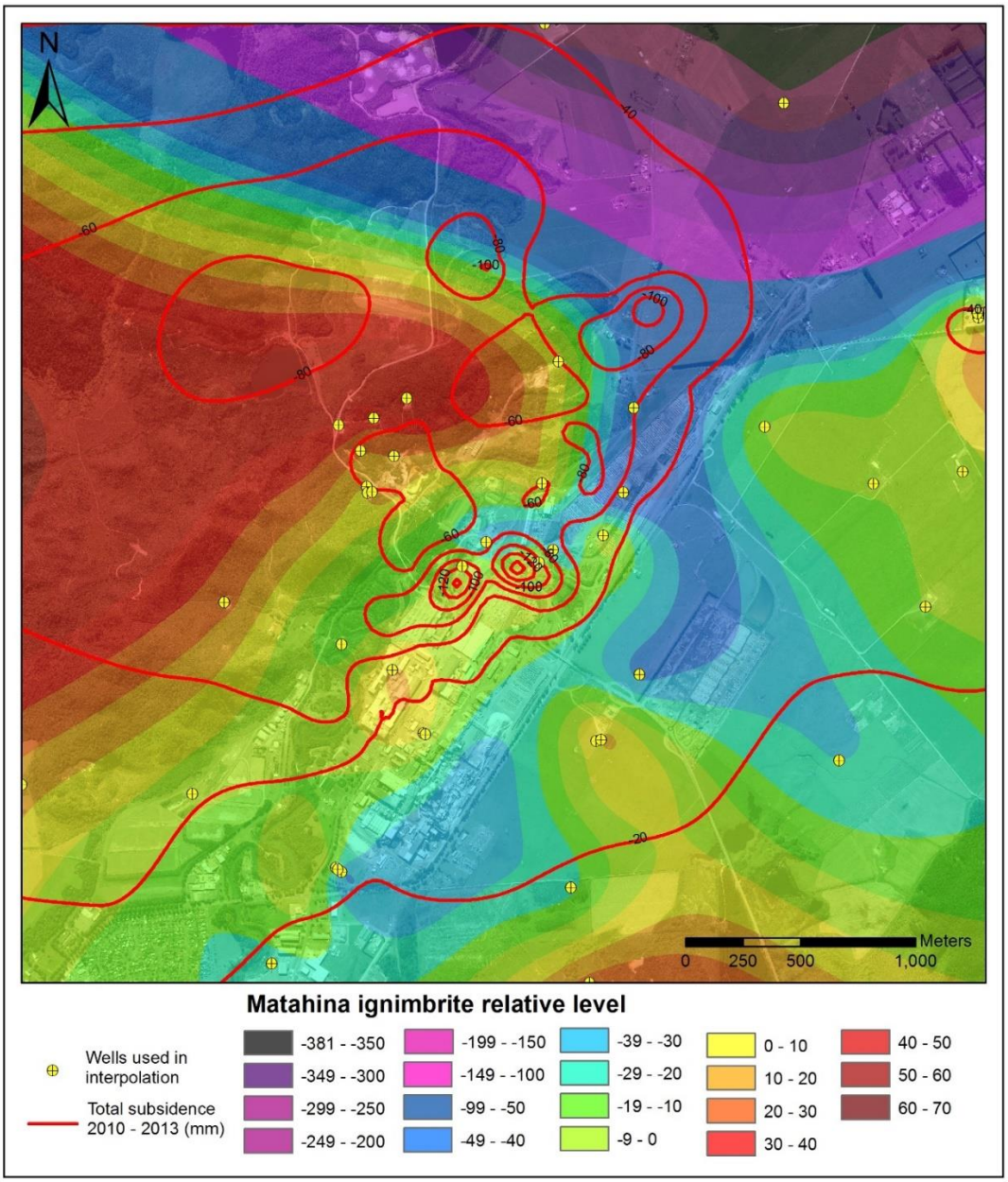

Figure 4.11: Relative level of Matahina ignimbrite across KGF with 2010-2013 cumulative subsidence to show location of subsidence features (relative level isopach shapefile from John Clark, pers. comm., 2014).

4.2.1 Geological Interpretation

Following the deposition of the Tahuna Formation (0.44 Ma) the Caxton Formation (0.36 Ma) was extruded from around the location of KA31 (Figs. 4.6 & 4.9). The Caxton Formation was extruded across the Tahuna Formation and filled channels where the Tahuna Formation had been eroded, probably by the Tarawera River; the western end of Figure 4.6 and northern end of Figure 4.8 show how thick the Tahuna Formation may have been before erosion occurred. In some wells on the spatial edge of the Caxton Formation the Tahuna and Caxton formations are interlayered, where the Tahuna Formation is present above and below the Caxton Formation e.g. KA27, (Figs. 4.8 & 4.12). This indicates that the extrusive member of the

Caxton Formation has either replaced the Tahuna Formation at this location or there has been some Tahuna Formation deposition following the extrusion of Caxton Formation, where processes from a paleo-channel of the Tarawera River in combination with faulting have created a large (>200 m deep) valley into which the Caxton Formation has flowed. Dating of the Tahuna Formation was completed on sample of a tuff from three wells (Milicich et al., 2013b). The tuff in all three wells is located towards the base of the Tahuna Formation indicating deposition of the Tahuna Formation occurred after the 0.44 Ma age provided by the tuff.

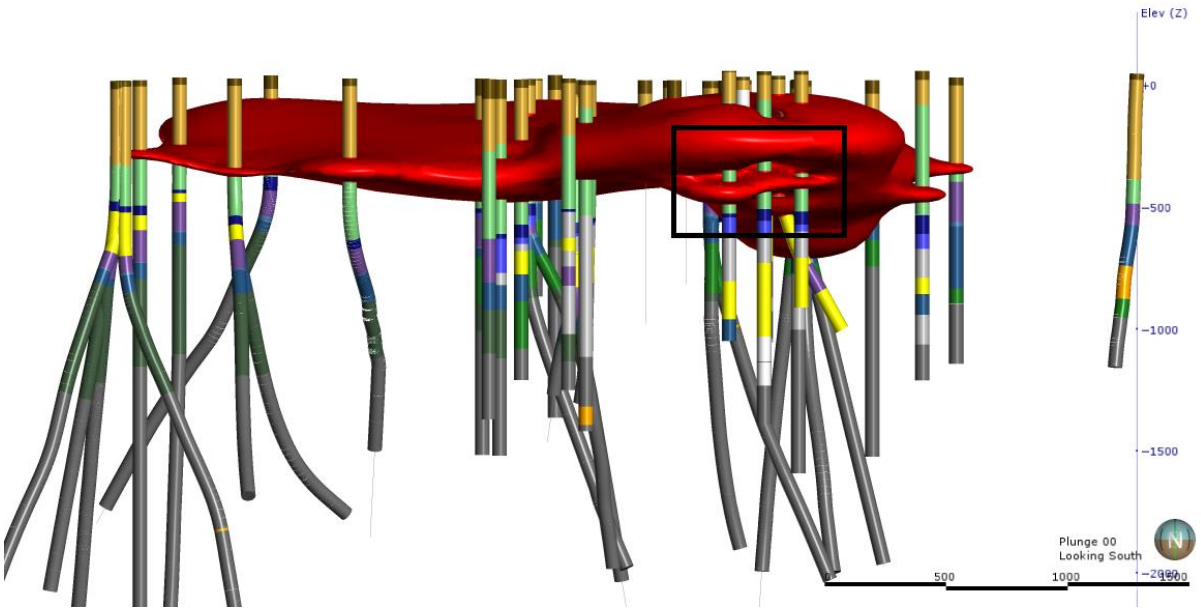

Figure 4.12: Interlayering of the Caxton and Tahuna formation at the north end of the extrusion.

Cross sections of the model through the mill site (Figs. 4.6, 4.7 and 4.8) show that the geology beneath the mill site is highly uniform. The lack of a subsidence anomaly can be explained by the uniform geology, it also shows that the geological conditions for an anomaly to form in the future do not exist. The model is well constrained through the mill site with the presence of KA46, KA47 and KA52 at the south end of the mill, and KA41 and KA42 in the north.

4.2.2 Proposed Mechanisms of Subsidence Anomalies

From the Leapfrog Geo modelling mechanisms for subsidence Bowls B and D can be proposed. The key mechanism being proposed here is that the anomalous thickness of Tahuna Formation below the bowls is more compressible than the overlying Caxton Formation The lack of a subsidence anomaly across the mill site where the Caxton Formation is three times thicker than below Bowl B (KA41 vs. KA36) provides further support to this mechanism. To test this samples of the Caxton and Tahuna formation are obtained from KGF and their compressive properties analysed.

Other possible mechanisms that may be causing or contributing to Bowls B and D are:

- Effective stress changes at within a shallow aquifer due to the aquifer pressures being drawn down (Bromley and Currie, 2003). However shallow pressure measurements from KA14 located <100m south of the centre of Bowl D do not support this (see Figs. 3.11 & 3.12).
- Localised hydrothermal alteration of the cover sequences to clay. Due to the locations and depths of KGF wells there is no evidence for this, KA36 and KA40 are closest to the centres of Bowls B and D respectively and are not noted to support this. KA37, KA39, and KA47 on the edges of Bowls B and D also have no evidence to support this. The presence of a subsidence anomaly near the Onepu thermal area by GDL1 and GDL2 (see Figs. 1.8 & 4.13) raises the possibility that this could also be occurring beneath Bowls B and D where a historical thermal feature has ceased activity.
- Paleochannels in the Matahina ignimbrite channelling the deposition of the Recent alluvium resulting in weak material beneath Bowls B and D (Fig. 4.11). This mechanism is proposed in Bromley et al. (2015) and evidence of the paleochannels is provided here but requires samples of Recent alluvium from Bowls B and D to be compared with that across the rest of KGF to confirm.
- The presence of a cavern that is steadily collapsing. No evidence exists to support this hypothesis, however it cannot be dismissed until the subsidence anomalies are drilled. If a cavern was to be intersected there would be a noticeable increase in the rate of penetration coinciding with the decrease in the relative level of the drill bit.
- The presence of brecciation of the Caxton and Tahuna formations that potentially hosts high amounts of compressible clay. This mechanism is analysed is the following section.

4.2.3 Brecciation

A brecciated section consists of coarse (usually >2 mm) fragmented rock consisting of angular clasts of one or more lithologies (Milicich, 2013b), and can occur by multiple mechanisms. In a geothermal field brecciation can occur as a result of hydrothermal eruptions, auto-brecciation resulting from lava flows, and possibly historical debris flows (John Clark, pers. comm., 2014). Brecciation of the Caxton and Tahuna formations could have occurred following or resulting from the extrusion of the Caxton Formation (0.36 Ma) which was then buried by the deposition of Matahina ignimbrite (0.32 Ma). A proposed mechanism is therefore that brecciation results in weaker formations that are contributing to the subsidence anomalies.

Brecciation of the Caxton and Tahuna formations is identified in 17 KGF wells at a range of depths (Table 4.2) but the mechanism(s) producing the brecciation are currently unknown. No brecciation is identified in the Matahina ignimbrite or Recent alluvium (Milicich, 2013b). The location of the wells which exhibit brecciated Tahuna and Caxton formations is spread across KGF, however there is a cluster around Bowls B and D and the numerous small subsidence features around the centre of the field wide subsidence feature (Fig. 4.13). Interestingly the wells showing brecciation in the north-east of the field are also surrounded by a small subsidence feature despite being injection wells.

To discover the extent of brecciation in Tahuna and Caxton formations the brecciated sections are incorporated into the Leapfrog Geo model. Because of the relative thickness compared with other units across KGF, the spacing of the wells across the subsidence anomalies, and not knowing the mechanisms for brecciation no correlation is able to be made.

Comparing the brecciation depths in KA36 and KA40 which are near the centre of Bowls B and D respectively; KA36 has 100 m of brecciation occurring from 354 to 454 mCHF in the Tahuna Formation, and KA40 has just 15 m of brecciation occurring from 75 to 90 mCHF in the Caxton Formation. It is interpreted that if the brecciation in both wells is resulted from a hydrothermal eruption, and the same event, that KA36 and Bowl B are closer to the eruption centre, while KA40 is towards the edge of the eruptions range. This explains the difference in depths of brecciation between the two wells with the distal well showing shallower brecciation because of the crater shape left by the eruption. An alternative is that two separate brecciation events form the material for the source of Bowls B and D. KAM1 and KA14, south of KA40 but within Bowl D had no cuttings available for logging to determine whether brecciation extends beyond KA40, this also applies to KAM5 south of KA36 within Bowl C. Until further investigation is completed into the mechanisms of brecciation at KGF this remains an untested hypothesis.

Well	Formation	Depth (mCHF)		Thickness (m)
		From	To	
KA17	Caxton	218	242	24
	Caxton	248	297	49
KA21	Caxton	247	260	13
KA24	Caxton	94	224	130
KA27	Tahuna	494	534	40
KA28	Tahuna	515	555	40
KA30	Tahuna	464	534	70
KA32	Tahuna	535	595	60
	Tahuna	625	655	30
KA34	Caxton	304	314	10
	Caxton	344	354	10
KA35	Caxton	94	224	130
KA36	Tahuna	354	454	100
KA37	Tahuna	404	474	70
KA38	Caxton	285	355	70
KA40	Caxton	75	90	15
KA43	Tahuna	350	405	55
KA44	Tahuna	350	400	50
KA47	Tahuna	410	580	170
KA50	Tahuna	345	415	70

Table 4-2: Occurrences of brecciated material in Kawerau wells (from Milicich, 2013b).

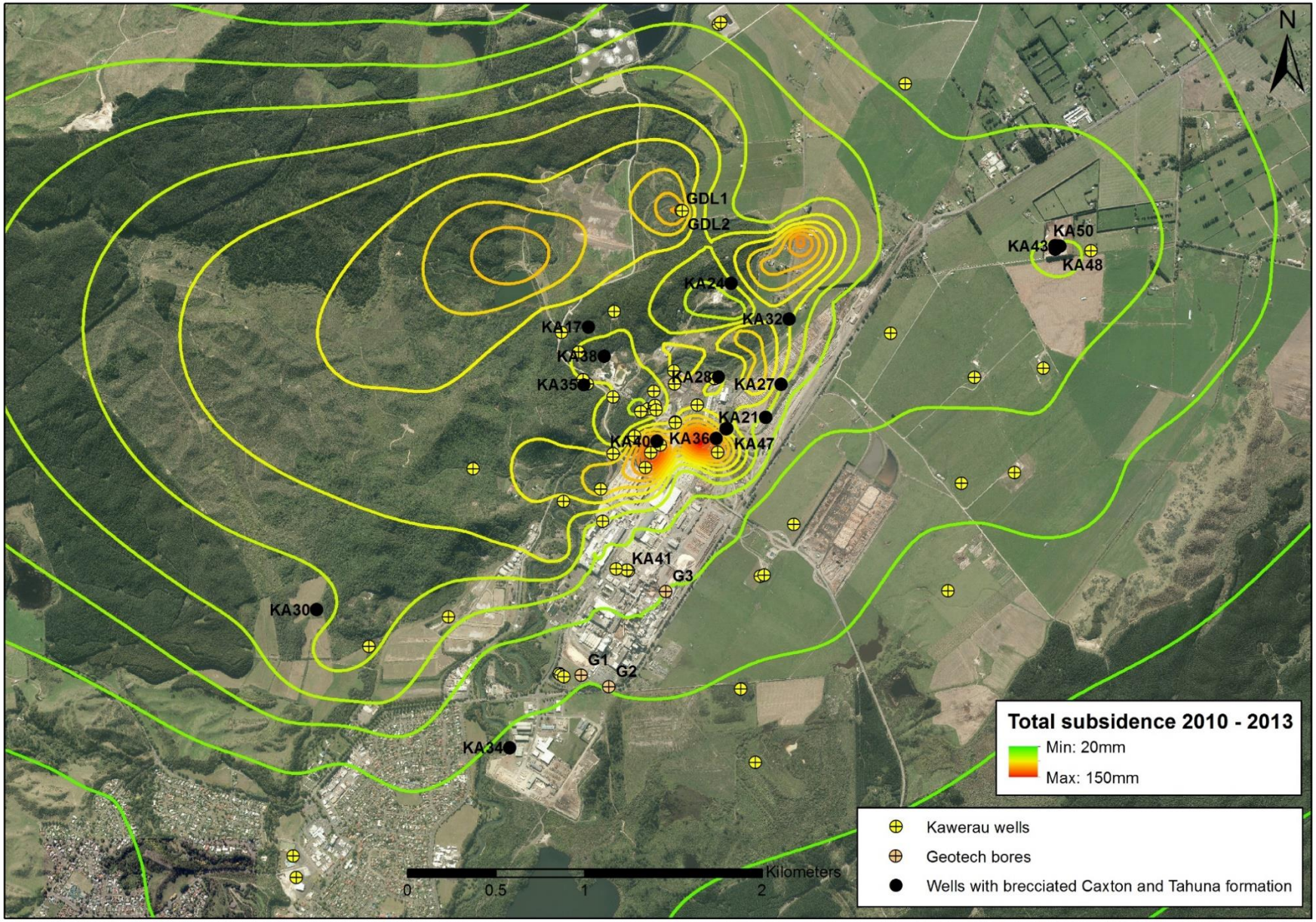

Figure 4.13: Locations of wells with brecciated Tahuna and Caxton formations shown in Table 4.2.

4.3 Geotechnical Investigation

In 2005 three shallow geotechnical bores (G1, G2, and G3) were drilled on the boundaries of Carter Holt Harvey's (CHH) mill site by Sinclair Knight Merz (SKM), and along with KA41 used to assess the potential for subsidence to affect the CHH mill site (Fig. 4.13). This was completed because CHH were concerned that increased production associated with the commissioning of the KGL power station would affect the Tasman Kawerau Mill site (SKM, 2005). The three shallow bores were drilled to 90 m, 115.5 m, and 120 m respectively and include loggings of the recent alluvium and top section of the Matahina ignimbrite.

The SKM report suggests that a rhyolite dome in the northwest of CHH Tasman Mill would decrease the likelihood of differential subsidence across the mill site. In 2005 the extent of the rhyolite dome (extrusive Caxton Formation) was unknown, work by Milicich et al. (2013a) and in this thesis confirms the extent of the Caxton Formation below the mill site. It is spatially large enough and thick enough with little geological variation to prevent significant differential subsidence (Figs. 4.6, 4.7, 4.8 & 4.9).

Results of the geotechnical drilling are as follows:

Formation	**Depth encountered below existing ground level (m)**			
Borehole	G1	G2	G3	KA41
Fill and Top soil	-(2)	0.0 – 0.4	0.0 – 0.4	Not logged
Recent alluvium	0.0 – 69.0	0.4 – 69.7	0.4 – 81.0	0.0 – 65.0
Matahina ignimbrite	69.0 – 90.0	69.7 – 115.5(1)	-(2)	65.0 – 70.0
Caxton Formation (extrusive)	-(2)	-(2)	81.0 – 120(1)	70.0 – 420.0
Water table (prior to drilling)	11.5	>12(2)	>12(2)	Not recorded
Notes	EOB at 90.0 m	EOB at 115.5 m	EOB at 120 m	Geothermal well

Table 4-3: Summary of condition encountered during geotechnical investigation carries out by SKM (2005). (1) = Base of formation not encountered, (2) = Not encountered, EOB = End of Borehole.

To further the analysis of SKM (2005) detailed engineering geology logs of G1, G2, and G3 are extracted from the report, and imported into Leapfrog Geo. The analysis however resulted in unsuccessful modelling because the detailed logs produced units that are too thin to be correlated across the mill site between boreholes spaced 95 – 610 m apart. The conclusion from

this is that differences in grainsize within the Recent alluvium below the mill site are thin, extremely localised lenses of sediment or clay, and too small to contribute to differential subsidence across the mill site. The heterogeneity of the recent alluvium therefore makes the identification of sub-units meaningless in the context of subsidence at KGF with current available data. Conclusions of the SKM (2005) report are that the upper 70 to 80 m of Recent alluvium consisted of loose to medium density sand derived from ignimbrite, rhyolite, and pumice deposited by Tarawera and Rangitaiki Rivers and that significant differential subsidence from compaction of the alluvium is considered unlikely.

4.4 Conclusions

Modelling of the cover sequences at KGF has provided reasonable answers for the subsidence anomalies south of the power station. Of the five mechanisms proposed one can be tested with current material available, the other three may be better characterised should core-drilling be completed into the centre of the anomalies. Conclusions of this chapter are as follows:

- There is anomalous thickness of Tahuna Formation below Bowls B and D that has not been eroded and filled with Caxton Formation like the surrounding area. It is proposed that the Tahuna Formation is more compressible than the Caxton Formation which has resulted in Bowls B and D. Testing of the Tahuna and Caxton formations will prove or disprove this hypothesis.
- Four other mechanisms for Bowls B and D that could be evaluated through new drilling into the centre of the bowls are: 1) effective stress changes below the bowls related to pressure changes in a shallow aquifer, 2) the presence of clay within the shallow formations below the bowls, whether hydrothermal in origin or depositional, 3) the channelling of weak material Recent alluvium by paleochannels in the Matahina ignimbrite, and 4) the presence of a cavern or caverns that are steadily collapsing. Of the four proposed mechanisms that cannot be tested, based on the data presented, the second and third mechanisms are the most likely, based on a lack of evidence for mechanisms one and four being responsible.
- The geological conditions for the proposed mechanisms of the subsidence anomalies at KGF existed before production began in 1956.
- The brecciation of Caxton and Tahuna formations is widespread throughout KGF wells at a range of depths. Due to the spatial density of wells and variation in depths, modelling of the brecciation was unsuccessful.

- The geotechnical investigation completed by SKM in 2005 concluded that conditions required for a subsidence anomaly to develop across the mill site are not present. Later modelling and investigations by Milicich et al. (2014) and in this thesis have come to the same conclusion.
- Drilling of the subsidence anomalies may provide support for some suggested mechanisms.

5 Properties of the Shallow Cover Sequences

Following the spatial analysis of subsidence and modelling of the cover sequences at Kawerau Geothermal Field (KGF) two subsidence anomalies are identified (Bowls B and D) and mechanisms for their presence proposed. One of the mechanisms is that the anomalous thickness of Tahuna Formation below the bowls is more compressible than the overlying Caxton Formation. From this it is also inferred that the Tasman Mill site is not at risk from the development of a subsidence anomaly because there are no anomalous thicknesses of a formation beneath it.

To test this proposed mechanism, samples of the Tahuna and Caxton formations are selected from KGF and their compressibility compared. To aid in the analysis thin section analysis and X-Ray diffraction (XRD) are carried out on the Tahuna and Caxton samples. Samples of the Recent alluvium from below the mill site described in the Sinclair Knight Merz (SKM, 2005) engineering geology logs as having a clay component have XRD and Laser sizing completed on them to identify the type and percentage of clay present and whether there is enough present to contribute to subsidence.

From this an interpretation is made on whether the anomalous thickness of Tahuna Formation present below Bowls B and D is the primary mechanism for their presence. Conclusions are also made about the clay layers present within the Recent alluvium and whether they have the potential to cause subsidence below the mill site.

5.1 Methods

5.1.1 Sample Description

The samples used in this study are sourced from Kawerau production wells, monitoring wells, and geotechnical investigation boreholes (Fig. 5.1 & Table 5.1). The geotechnical bores and monitoring wells (G2 and KAM11) are drilled vertically (90° dip), and KA37A, a production well near KGL, is drilled slightly off vertical (88-89° dip) in the well track of KA37 until 850 mCHF where significant deviation is utilized to reach the target zone. Samples obtained vary in diameter and length due to drill bit sizes, well purpose, and conditions encountered. KA37 and G2 are cored at ~50 mm diameter and KAM11 cored to ~80 mm diameter with sample lengths between 140 and 250 mm.

The cores have been described by SKM (2005) (G2), GNS Science (KAM11) and Milicich (2013b) (KA37). SKM completed a geotechnical investigation into subsidence below the mill

site in 2005 which included the drilling and logging of three boreholes to a maximum of 120 m below ground level (BGL) (SKM, 2005). GNS Science logged KAM11 during drilling and produced engineering geological logs for the well (Kilgour, 2008; Read & Kilgour, 2009). Milicich (2013b) re-logged all KGF wells as part of a PhD thesis at Victoria University, Wellington. All samples were stored in the Kawerau core shed where they have dried out over time, the youngest of the samples (KAM11) was in storage since late 2008.

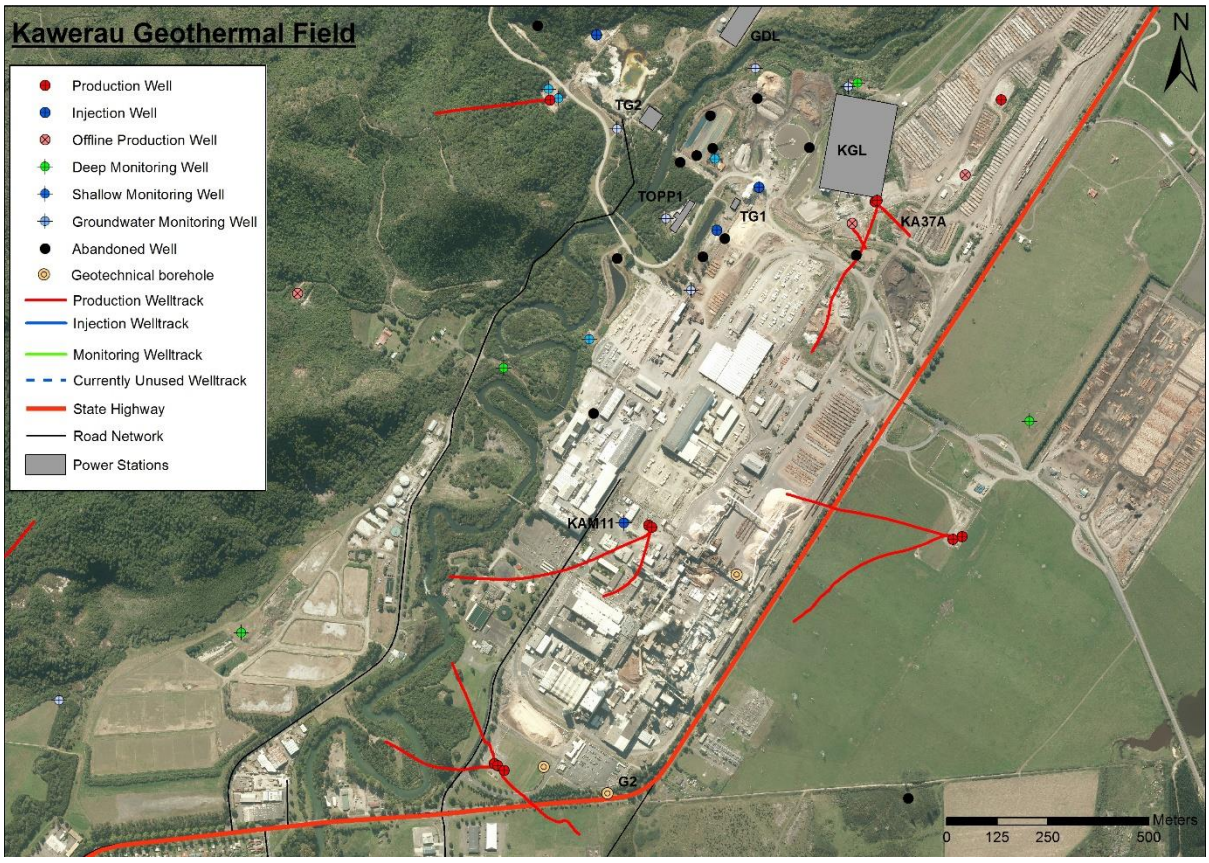

Figure 5.1: Tasman mill site and nearby geothermal wells, including source wells and geotechnical bores for samples used in testing.

Well	Depth of sample (m BGL)	Well Type	Formation	Drilled
G2	50 – 50.5	Geotechnical bore	Recent alluvium	17 November, 2005
KAM11	203.5 – 203.8	Shallow monitoring	Caxton	June-July, 2008
KAM11	424.4	Shallow monitoring	Tahuna	June-July, 2008
KA37	474.2	Production	Tahuna	November, 1999

Table 5-1: Summary of wells and depths of samples used for this study.

5.1.2 Physical Properties

The physical properties of the samples are the controlling factors on their behaviour at depth and whether they contribute to subsidence at Kawerau; it is therefore vital to record the properties of each sample before testing. This includes density and effective porosity measured using two methods.

Effective porosity is the void space of the material able to be filled with a fluid. In a geothermal system the greater the effective pore space within a formation the more it will be able to be compressed if effective stress increases. To measure porosity the procedure recommended by the International Society for Rock Mechanics (ISRM) (Ulusay & Hudson, 2007) is followed with one exception; samples are dried at 55 °C until no weight change is recorded over three successive measurements to avoid the alteration of clays which occurs at 60 °C (Moritz, 1995); ISRM 1974-2006 recommends drying at 105 ± 3 °C for 24 hours. The two methods from ISRM used to find the porosity and density are:

1) Saturation and calliper techniques.
2) Saturation and buoyancy techniques.

The first method is intended for use on samples with a uniform geometry, the second is used on rock samples with lumps or aggregate of irregular geometry but may also be applied to samples of regular geometry.

Method 1 uses the following equations:

Pore volume (Equation 1)	$V_V = \frac{\mathrm{M_{sat}} - \mathrm{M_s}}{\rho_\mathrm{w}}$
Porosity (Equation 2)	$n = \frac{100V_v}{V}\%$
Dry density of rock (Equation 3)	$\rho_d = \frac{M_s}{V}$

Method 2 uses equations (2) and (3) from method 1 along with the following:

Bulk volume (Equation 4)	$\mathrm{V} = \frac{\mathrm{M_{sat}} - \mathrm{M_s}}{\rho_\mathrm{w}}$

The procedures for both methods are similar and can be completed at the same time:

1) Calliper measurements for method 1 are made to determine the volume and the samples are saturated in a vacuum for 24 hours.
2) The samples are removed from the vacuum, transferred to an underwater basket and saturated-submerged mass (M_{sub}) is determined from the difference between the saturated-submerged mass of basket plus sample and that of the basket alone.
3) The samples surface is dried and its saturated-surface-dry mass (M_{sat}) is determined.
4) The sample is oven-dried and its mass is determined to give grain mass (M_s).
5) Using equations 1 – 4 the properties are determined (Tables 5.2 – 5.5).

5.1.3 Thin Section Analysis

Thin sections of Caxton and Tahuna formation samples (2 x KAM11 Caxton (1 flow-banded and 1 brecciated), 1 x KAM11 Tahuna, 1 x KA37 Tahuna) were made at UC and the petrography assessed. Thin section mineralogy of Tahuna and Caxton formations has been completed by Milicich et al. (2013a) and Wyering et al. (2014) on different samples and these are used to cross check petrographic interpretations made here. Browne (1979), Macdonald & Muffler (1972), and Wood et al. (2001) have also completed thin section analyses of KGF material but at greater depths than required for this analysis. Results of the thin section analysis include a summary table (Table 5.7) of mineral percentages for each thin section along with a description of petrography.

5.1.4 X-Ray Diffraction (XRD) and Laser sizing

X-Ray Diffraction (XRD) is a technique used to identify the structure of a crystal and is commonly used for the identification of clays. It is a useful analysis for KGF samples because of the potential presence of shrinking and swelling clays in the Recent Alluvium, particularly beneath the mill site. Swelling clays in the presence of water have exchangeable cations which hydrate, forcing clay layers apart (Anderson et al., 2010); in a geothermal field with changing groundwater levels dehydration of a shrinking clay could potentially result in subsidence at the surface. Clays are classified by their structure and studies of swelling clays are most focussed on those clays with a 2:1 smectite ratio due to their high swelling potential (Grim, 1968). XRD is carried out on three formations; Recent alluvium from G2, and Tahuna and Caxton formations from KAM11.

To extract the clay particles required for XRD from Recent alluvium samples the samples are saturated with deionised water to separate the sample into individual grains, wet sieved to

separate the sediments <63 µm (smallest sieve size possible), oven dried at 50 °C to remove all moisture, and sealed in plastic tubes.

Samples of Tahuna and Caxton formations are taken from KAM11, a monitoring well within the mill site; based on Milicich (2013b) the samples from KAM11 are similar to the lithologies beneath Bowls B and D. To prepare the samples for XRD they are mechanically crushed using a mortar and pestle before being wet sieved separating the particles <63 µm, oven dried at 50 °C and sealed in plastic tubes.

Despite sieving the Recent alluvium samples to <63 µm they may contain grainsizes larger than clay; which is classified by NZGS (2005) as being <2 µm. Laser sizing is therefore carried out on un-sieved samples from G2 to find the grainsize percentages in the samples. This is completed at UC using a Micromeritics Saturn Digisizer 2 5205. A small amount of sample (~1 cm^3) is submerged in sodium hexametaphosphate $(NaPO_3)_6$ and mixed using a magnetic stirrer. Once the sample is sufficiently mixed and no layering is occurring a small amount is extracted from the centre of water column while mixing is still occurring to ensure a distributed grainsize and placed in the digisizer for analysis.

5.1.5 Compressibility

The most common test to find the compressibility of rock is a triaxial (K_0) test as used in Bromley et al. (2010). Due to the age, condition and amount of suitable material available from KGF over-coring the samples to complete triaxial testing risked destroying the samples. The failed recovery of over-cored samples would result in no data without more samples available. The decision was therefore made to develop a testing procedure that could compare the compressibility of Caxton and Tahuna formations whilst reducing the likelihood of destroying the samples during preparation.

The developed procedure needed to be able to load the samples in a controlled manner where the amount of load on the sample is known throughout the test. To do this the soils shear box at UC is used. The shear box has a loading lever with a known lever ratio of 1:10 that could place load on a sample. To control the load on the samples a platen of a known area and mass is placed on top of the sample onto which the load is applied (Fig. 5.2). Because of the dimensions of the samples chosen from KGF the decision is made to cut the cores into 30 mm thick sections ensuring samples are of approximately the same dimensions. To add confinement to the sample as it would experience at depth a resin is used, which has compressive and tensile strengths greater than that of the sample, preventing the sample from failing (Table 5.2). To

measure the amount strain occurring along the sample length during loading a Silvat gauge is used. The Silvat gauge records the change in height of the sample at two second intervals from which strains are calculated using the physical properties measurements.

Stress	Failure strain	Density
Tensile	50 – 60 MPa	1.1 – 1.5 g/cm^3
Compressive	90 – 100 MPa	

Table 5-2: Properties of the Nuplex Electrical Industry, K146 Epoxy system resin used.

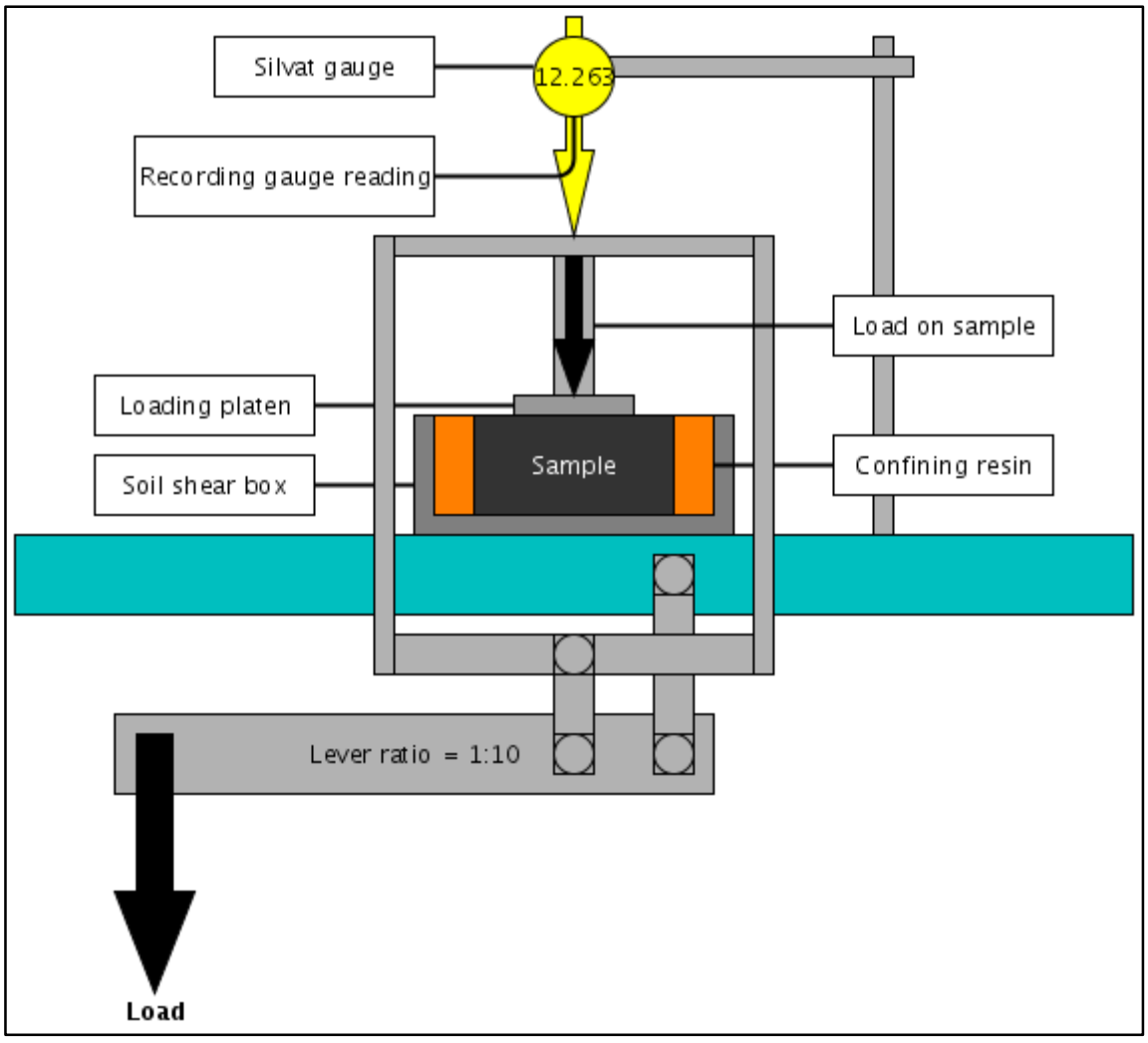

Figure 5.2: Schematic of the soils shear box loading machine used to test the compressibility of samples at University of Canterbury.

Using the above methods variable sized loading platens and different loading cycles are applied to find the best loading-unloading methodology to compare the two samples. In total five tests are completed on each sample: 1) dry single load-unload test with 82 mm diameter loading platen, 2) dry single load-unload test with 53 mm diameter loading platen, 3) repeat of test two, 4) dry cyclic load-unload with 53 mm platen for four cycles, and 5) saturated cyclic load-unload

with 53 mm platen for five cycles. A single loading-unloading cycle consists of loading 5 kg plates on the lever at 30 second intervals until 50 kg total is on the lever (500 kg or 2.22 MPa (53 mm platen) on sample) and then unloading the plates at 30 second intervals. When completing cyclic loading (Tests 4 and 5) the lever is loaded and then unloaded until one 5 kg plate remain before being reloaded, this is to avoid recording any play in the machine. During the saturated tests the samples are open top and bottom and water is able to be squeezed from the sample due to the vertical stress applied as a function of the effective porosity and permeability of the sample.

Test 1, with the 83 mm diameter platen, produced nearly identical results from both Caxton and Tahuna samples. The interpretation is that the resin is the primary controlling factor on the amount of strain the sample sustained. By using a smaller platen in all subsequent tests the sample properties became the controlling factor rather than the confining resin. Test 2 is repeated as Test 3 due to a failure of the recording software which caused data to be lost during the Tahuna Formation sample test. Cyclic testing is performed to determine whether the samples exhibited plastic or elastic behaviour during repeated loading and unloading. Saturated cyclic testing is performed to determine the behaviour of the samples when the pore space is filled; the effective porosity and permeability of the material becomes a factor during this test. Here the dry and saturated tests of each sample are compared and the two samples are compared against each other in both dry and saturated states.

Raw data from the Silvat gauge is recorded in millimetres (to three decimal places) of deformation versus time, which must then be processed to a stress-strain graph. To do this the zero is reset to after the first 5 kg plate is loaded onto the sample due to play in the machine, the lowest Silvat gauge reading at each load (220 KPa intervals) extracted from the raw data, and subtracted from the zero value providing total deformation at each load interval (*C*). The following equations are used to produce a stress-strain graph:

$Stress\ (MPa) = \frac{\left(\frac{m * a}{A}\right)}{1000000}$	$Strain\ (\%) = \left(\frac{-C}{H}\right) * 100$
(Equation 5)	(Equation 6)
Where:	
m = mass on lever a = acceleration A = area of loading platen	C = corrected compression of sample H = height of sample

The slopes of the stress-strain graphs are then used to manually determine the Young's Modulus of the samples during loading and unloading. Young's modulus is the ratio of compressive stress to the resulting strain and allows us to compare the elastic properties of the two formations. Young's Modulus is calculated using the below equation:

$E = \frac{\Delta\sigma_a}{\Delta\varepsilon_a}$ (Equation 7)	Where: E = Young's modulus (MPa) $\Delta\sigma_a$ = Change in axial stress $\Delta\varepsilon_a$ = Change in axial strain

Due to the limited amount of material available to be sampled only one sample of Caxton Formation is able to be cut, this is tested alongside a sample of Tahuna Formation of similar dimensions. Both samples are loaded and unloaded multiple times with each sample loaded under the same conditions as the other and samples given equal time between tests to recover any elastic strain.

5.2 Results

Results from all methods are presented here in their processed form. Initial details of samples and raw XRD, laser sizing, and compressibility data and graphs are located in Electronic Appendix 2.

5.1.1 Physical Properties

Length (mm)	29.39	**Saturated weight (g)**	292.3
Diameter (mm)	84.02	**Sample depth (mCHF)**	426.4
Radius (mm)	42.01	**Pore volume (m^3)**	0.0000590
Bulk volume (m^3)	0.000162945	**Porosity (%)**	36.208
Bulk volume (cm^3)	162.945365668	**Dry density (kg/m^3)**	1431.77
Submerged weight (g)	136.08	**Saturated density (kg/m^3)**	1793.85
Dry weight (g)	233.3		

Table 5-3: Tahuna Formation – Sample 11A: Porosity and Density using Saturation and Vernier callipers.

Saturated density (kg/m^3)	1793.85	**Pore volume (cc)**	59
Bulk volume (m^3)	0.00015622	**Porosity (%)**	37.767
Bulk volume (cm^3)	156.22	**Dry density (kg/m^3)**	1493.41
Pore volume (m^3)	5.9E-05		
Porosity difference between two methods (%)	4.42	**Density difference between two methods (%)**	4.20

Table 5-4: Tahuna Formation – Sample 11A: Porosity and Density using Saturation and Buoyancy.

Length (mm)	31.17	**Saturated weight (g)**	358.0
Diameter	82.13	**Sample depth (mCHF)**	203.8
Radius	41.07	**Pore volume (m^3)**	0.0000186
Bulk volume (m^3)	0.000165144	**Porosity (%)**	11.263
Bulk volume (cm^3)	165.144441957	**Dry density (kg/m^3)**	2055.17
Submerged weight (g)	198.64	**Saturated density (kg/m^3)**	2167.80
Dry weight (g)	339.4		

Table 5-5: Caxton Formation – Sample 11E: Porosity and Density using Saturation and Vernier callipers.

Saturated density (kg/m^3)	2167.80	**Pore volume (cc)**	18.6
Bulk volume (m^3)	0.00015936	**Porosity (%)**	11.672
Bulk volume (cm^3)	159.36	**Dry density (kg/m^3)**	2129.77
Pore volume (m^3)	1.9E-05		
Porosity difference between two methods (%)	3.540	**Density difference between two methods (%)**	3.398

Table 5-6: Caxton Formation – Sample 11E: Porosity and Density using Saturation and Buoyancy.

Key results from the physical properties testing are that the Caxton Formation is 1.43 times denser when dry than the Tahuna Formation, and the Tahuna Formation has 3 times more effective porosity than the Caxton Formation. The two methods for measuring the properties had <5 % difference between their results but due to the irregular geometry of the samples the saturation and buoyancy method results are used for calculations.

5.2.1 Thin Section Analysis

Thin sections are cut from the Tahuna and Caxton samples and are described here. Table 5.7 summarises the mineral percentages present in each sample.

Tahuna Formation: Sample 11A

Based on GNS 2008/305LR (Kilgour, 2008; Read & Kilgour, 2009), Milicich (2013b), and from nearby KA41 and KA42 well logs Sample 11A is a cream to white, non-welded ignimbrite layer within the Tahuna Formation (Fig. 5.3). The sample is highly altered moderately crystalline ignimbrite with large (~2 mm) feldspars, small (0.5 mm) quartz and few larger (~2 mm) fractured quartz. Other identifiable minerals include biotite and secondary calcite, many of which are embayed with unidentifiable alteration products. Identifiable minerals are mostly primary with some identifiable secondary minerals, most secondary materials are unidentifiable.

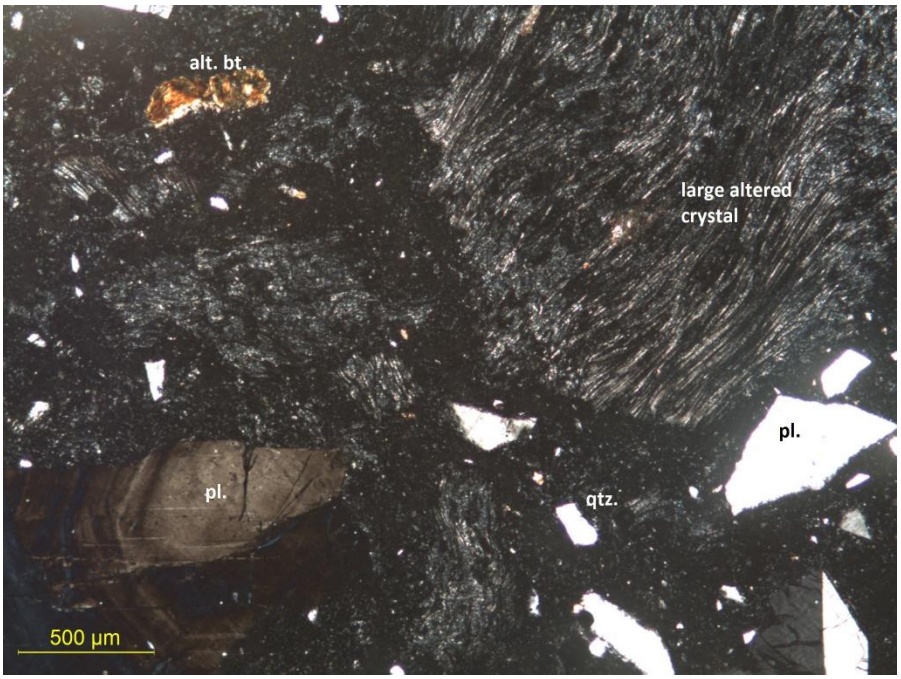

Figure 5.3: Cross polarised photomicrograph of Sample 11A showing altered biotite (bt.), quartz (qtz.), plagioclase (pl.) and one large indistinguishable crystal.

Tahuna Formation: Sample 37A

Sample 37A (Fig. 5.4) is from KA37 located on the eastern edge of Bowl C. The sample is from the top of the vitric tuff unit of the Tahuna Formation which is present from 474 – 534 mCHF (Milicich, 2013b). The sample is fresh and moderately crystalline with a structure-less fractured glassy groundmass. Fractures are filled with an isotropic filling with small (40 times magnification required) calcite and biotite, some larger (~0.5 mm) secondary calcite is also

present. The majority of minerals present are euhedral quartz approximately 0.5 – 1 mm in size with a few larger (~2 mm) quartz.

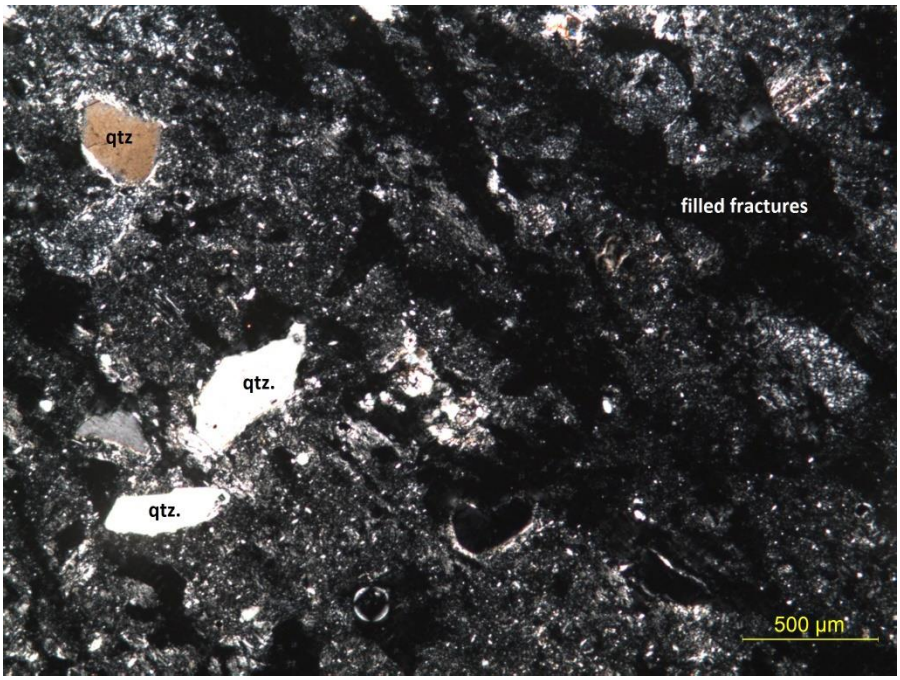

Figure 5.4: Cross polarised photomicrograph of Sample 37A displaying fractures filled with an isotropic material (most likely clay) and relatively large quartz minerals (qtz.).

Caxton Formation: Sample 11C (brecciated sample)

Sample 11C (Fig. 5.5) comes from the monitoring well KAM11 located in the mill site, it is a purple-grey, brecciated, flow banded rhyolite with light iron oxidation on the outside of the core. Due to the brecciated nature of the sample the thin section is slightly thicker than normal, producing anomalously high birefringence in quartz. Brecciation has produced a higher percentage of clay when compared to Sample 11E. The sample is crystal poor with small (<1 mm) embayed quartz and plagioclase. The groundmass is brecciated and scattered with small plagioclase.

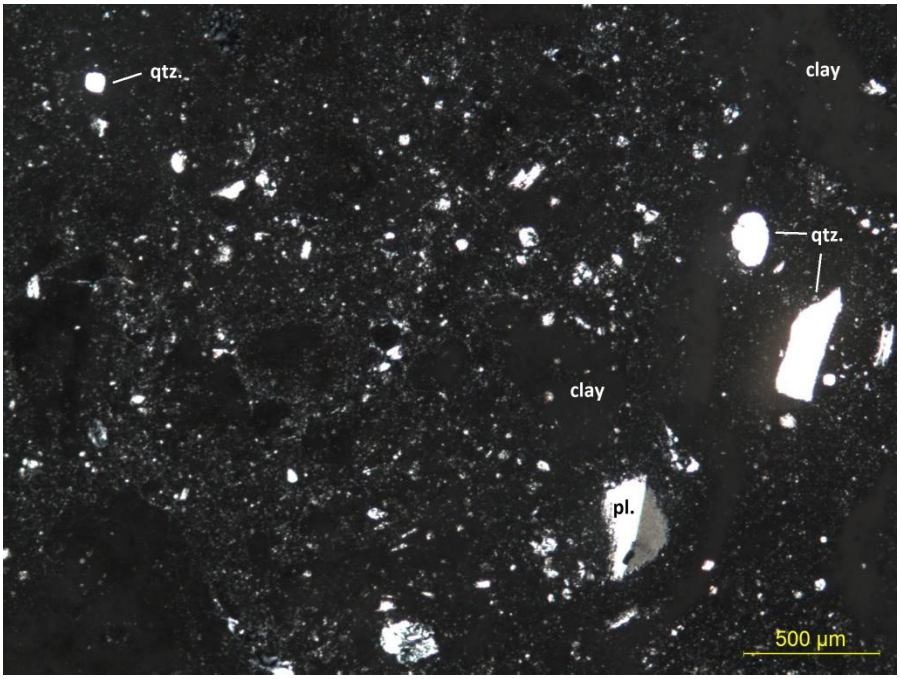

Figure 5.5: Cross polarised photomicrograph of Sample 11C showing embayed quartz (qtz.) and plagioclase (pl.) with some mineral altered to clay.

Caxton Formation: Sample 11E (flow-banded sample)

Sample 11E (Fig. 5.6) comes from the monitoring well KAM11 located in the mill site, it is a purple-grey flow banded rhyolite with heavy iron oxidation on the outside of the core and is from the crystal-poor member of the Caxton extrusive (Milicich, 2013b). The groundmass is devitrified and scattered with very small (<0.5 mm) plagioclase with minor small (<2 mm long) fractured embayed quartz and plagioclase ± biotite ± amphibole.

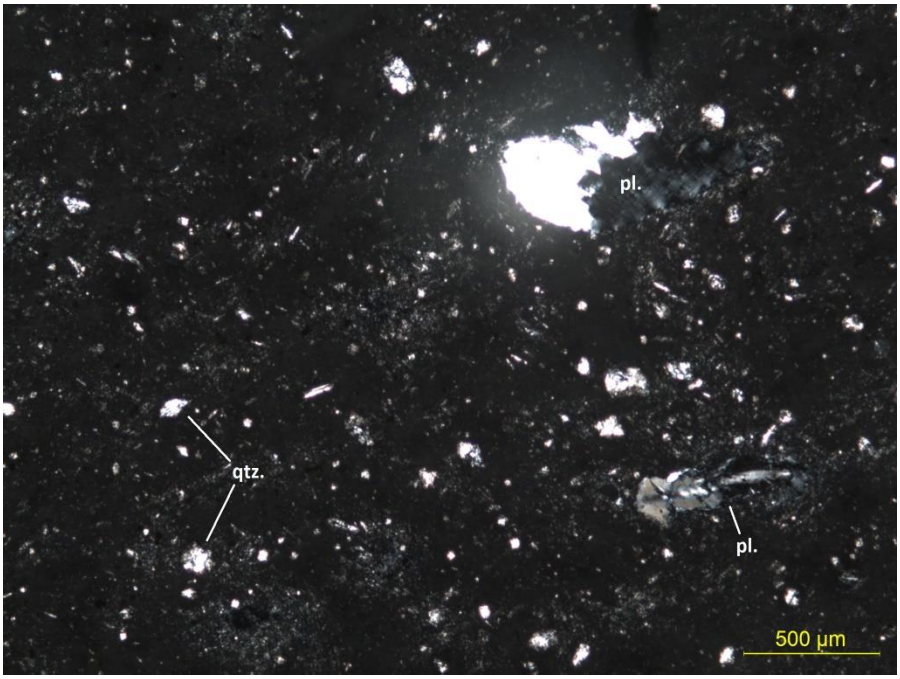

Figure 5.6: Cross polarised photomicrograph of Sample 11E displaying devitrified groundmass with quartz (qtz.) and plagioclase (pl.).

Sample	Alteration/Groundmass	Quartz	Feldspar	Biotite	Amphibole	Calcite
11A	70	10	15	2	-	3
37A	85	12	-	1	-	2
11C	87	5	5	1	2	-
11E	80	5	10	3	2	-

Table 5-7: Summary of mineral percentages from thin section analysis.

5.2.2 X-Ray Diffraction (XRD)

Logging of the geotechnical bores revealed the primary grainsize of Recent alluvium is sand which is interspersed with gravel, silt, and clay. Samples are taken from borehole G2 which has the most variance in grainsize and most material available. The thickest sections of clay and silt are <2 m thick with the majority <0.5 m thick across all three boreholes. Modelling of the Recent alluvium based on geotechnical bore logs shows that the main grainsize is sand and that other grainsizes within the alluvium are not wide spread; they are thin localised lenses that would have little effect on surface deformation. Silts and clays make up 3% of the core logged as Recent alluvium across the three boreholes, with none present in G3.

XRD results (Table 5.8) show that the shallow cover sequences will have little effect on surface deformation; quartz, albite, and kaolinite have little potential to swell or shrink in changing groundwater conditions (Bronswijk, 1988). Quartz is a primary mineral, extremely abundant and likely from the materials original source area, albite is a primary feldspar mineral, and also

likely from the original source area of the Recent alluvium. Kaolinite is formed by the decomposition of other aluminosilicates, especially feldspars by either weathering and/or hydrothermal activity in acidic, low temperature, low pressure environment (King, 2009). In the surficial deposits at KGF it is likely formed by weathering processes during transportation with a low amount a hydrothermal alteration. Kaolinite is a low shrink and swell mineral with high temperatures required for dehydration to occur (Grim, 1962).

Sample	Borehole	Depth (m)	Quartz (%)	Albite (%)	Kaolinite (%)
G2D1	G2	50	60	30	10
G2D2	G2	50.14	65	35	trace
G2E1	G2	50.32	65	35	trace
G2E2	G2	50.5	60	40	trace

Table 5-8: XRD results from shallow geotechnical boreholes within the mill site.

XRD results from the Tahuna and Caxton formations (Table 5.9) shows a small amount of the shrinking-swelling smectite group. KAM11 samples consist of cristobalite and albite in all three samples and montmorillonite in the shallow Tahuna Formation sample (11A). Cristobalite is a high temperature form of quartz and has the same chemical formula but a different crystal structure (Allaby, 2008), and is potentially associated with the extrusive Caxton Formation. Albite is a plagioclase feldspar mineral and is the sodium end member of tectosilicate minerals that can be found in sedimentary formations but also formed by hydrothermal activity. Montmorillonite is a very soft phyllosilicate member of the smectite group, and therefore a shrinking-swelling clay. It results from the decomposition of volcanic ashes in marine basins or at a later stage of hydrothermal alteration (Ferris, 2005; Steiner, 1968). This leads to the interpretation that following the deposition of the Tahuna Formation KGF was below sea level, which is consistent with members of the Tahuna Formation including shallow marine sediments and shells (Milicich et al., 2013b). The ten percent detected within Sample 11A, even in a thicker formation such as that below Bowls B and D, is unlikely to be responsible for the formation of the bowls.

Sample 37A from KA37 on the north-east edge of Bowl C, is a relatively fresh, unaltered tuff from the bottom of the Tahuna Formation. XRD resulted in primarily quartz with a low percentage of illite. Quartz as previously discussed is extremely abundant and a primary mineral indicating low alteration. Illite is a group name for non-expanding, clay sized, micaceous minerals and is formed by the weathering decomposition or hydrothermal alteration

of muscovite or feldspar (Allaby, 2008). Therefore the fresh tuff does not possess a mineralogy associated with compressible material that could contribute to a subsidence anomaly.

Sample	Well	Formation	Depth (mCHF)	Cristobalite	Albite	Montmorillonite	Quartz	Illite
11A	KAM11	Tahuna	426.4	60	30	10	-	-
11C	KAM11	Caxton	203.5	60	40	-	-	-
11E	KAM11	Caxton	203.8	65	35	-	-	-
37A	KA37	Tahuna	474.2	-	-	-	85	15

Table 5-9: XRD results from Tahuna and Caxton formations in wells KAM11 and KA37.

5.2.3 Laser Sizing

Because of the presence of larger grainsizes within the Recent alluvium laser sizing is carried out on un-sieved samples from the same section of core XRD is completed on to ascertain the percentages of grainsize present within the samples.

Tables 5.10 and 5.11 show that clay makes up a very small percentage of the samples overall percentage. In the logs completed by SKM (2005) at the time of drilling samples G2D and G2E are two of the few samples described as having clay present. Conclusions of this are that the Recent alluvium will not behave in a plastic manner, and is unlikely to behave in a manner causing subsidence below the mill site.

Sample	Borehole	Grainsize	Size (µm)	Percentage (%)
G2D	G2	Clay	<2	4.00
		Silt	2 – 6	6.97
		Fine Sand	6 – 200	85.77
		Medium Sand	200 – 2000	3.27
	Total			100

Table 5-10: Laser sizing results from sample G2D.

Sample	Borehole	Grainsize	Size (µm)	Percentage (%)
G2E	G2	Clay	<2	5.13
		Silt	2 – 6	9.63
		Fine Sand	6 – 200	83.23
		Medium Sand	200 – 2000	2.00
	Total			100

Table 5-11: Laser sizing summary from sample G2E.

5.2.4 Compressibility

Results of the cyclic loading of both dry and saturated Tahuna and Caxton formation sample are presented and compared here. Cyclic loading best represents the behaviour of the sample in changing pressures likely experienced in-situ.

Tahuna Formation: Dry cyclic versus Saturated cyclic

The Tahuna Formation sample has an effective porosity of 38%. Dry cyclic loading is carried out first, followed by saturated testing following 24 hours submerged in deionised water in a vacuum.

Dry cyclic loading resulted in a relatively high amount of plastic deformation at the conclusion of the first cycle (Fig. 5.7 and Table 5.12). The following three cycles display mostly elastic behaviour with a minimal amount of plastic deformation between each cycle. Two Young's moduli are calculated for the dry sample during the linear period of deformation, one during loading and one during unloading. Unloading Young's Modulus is found to be 1.54 times that of the loading Young's Modulus. (Fig. 5.7).

The saturated material behaved more rigidly when initially loaded than the dry sample, indicated by a smaller hysteresis (Fig. 5.7 and Table 5.13). When loaded the saturated sample exhibited a linear stress-strain relationship through all four cycles. In comparison during unloading the sample behaved in a plastic manner initially, with the elastic recovery of strain occurring when the effective stress is below 0.75 MPa. When the Young's Modulus is compared between the dry and saturated samples it is 3.33 times less during saturated loading and 2.0 times less during saturated unloading indicating more elastic behaviour when saturated.

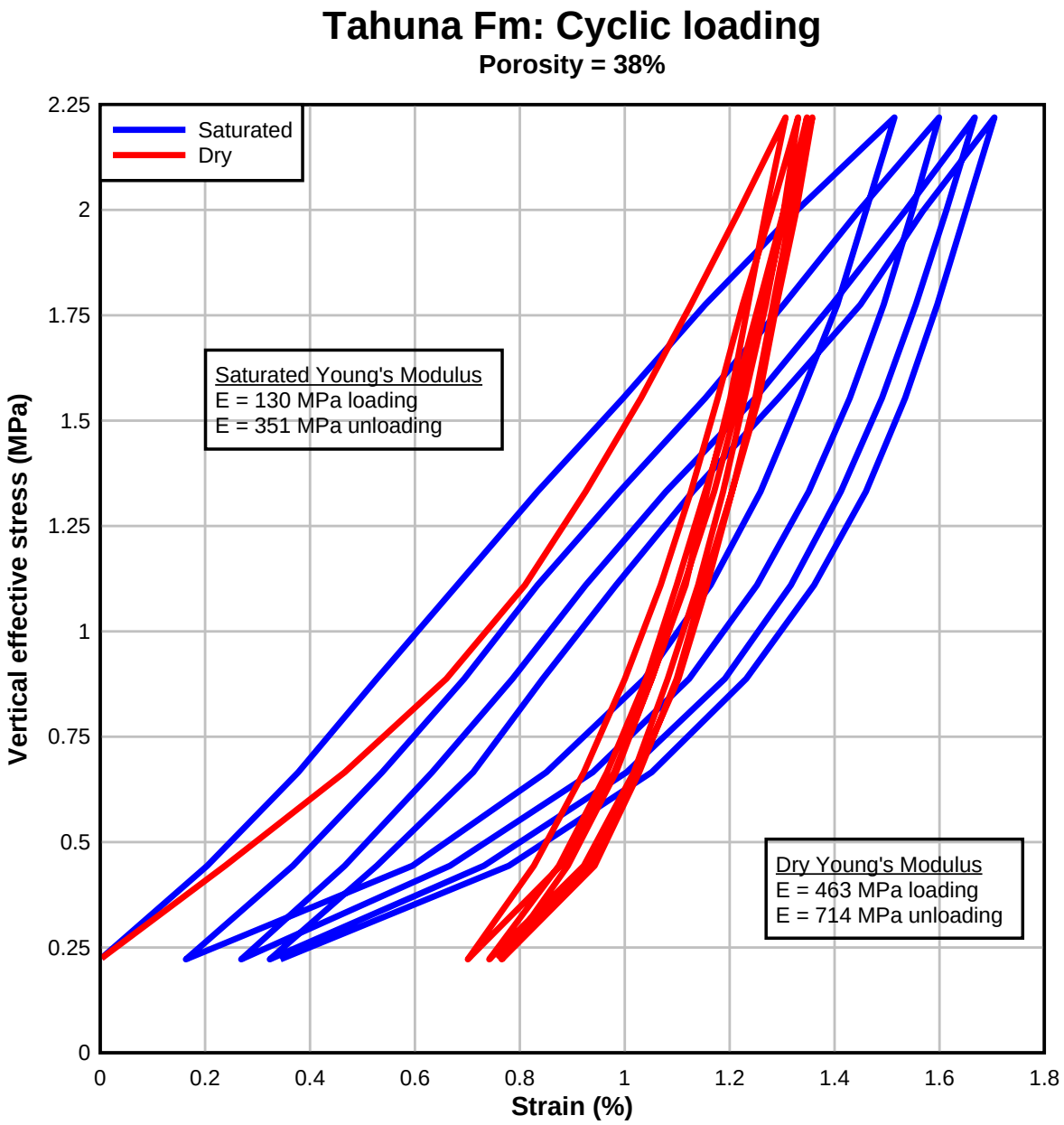

Figure 5.7: Stress-strain graph showing the deformation of the Tahuna Formation sample under cyclic loading when oven dry and saturated.

Tahuna: Dry	**Strain under 0.22 MPa**	**Strain under 2.22 MPa**
Cycle 1	0 %	1.31 %
Cycle 2	0.70 %	1.33 %
Cycle 3	0.74 %	1.34 %
Cycle 4	0.77 %	1.36 %
End Cycle 4	0.76 %	

Table 5-12: Simplified results of cyclic loading on dry Tahuna Formation sample.

Tahuna: Saturated	Strain under 0.22 MPa	Strain under 2.22 MPa
Cycle 1	0 %	1.51 %
Cycle 2	0.16 %	1.60 %
Cycle 3	0.27 %	1.67 %
Cycle 4	0.32 %	1.70 %
End Cycle 4	0.34 %	

Table 5-13: Simplified results of cyclic loading on saturated Tahuna Formation sample.

Caxton Formation: Dry cyclic versus Saturated cyclic

The Caxton Formation sample from KAM11 has a much lower effective porosity of 12% compared to the Tahuna Formation sample. Like the Tahuna Formation sample the Caxton Formation sample is loaded when dry first followed by saturated testing after 24 hours submerged in deionised water in a vacuum.

Results for the dry test are similar to the Tahuna Formation test with a large amount of plastic deformation occurring during the first cycle and mostly elastic deformation occurring during each cycle thereafter (Fig. 5.8 and Table 5.14). Dry Young's Moduli for the Caxton sample is similar to the dry Tahuna Formation sample during loading and slightly higher during unloading.

The saturated sample deformed in a linear manner until ~1.75 MPa at which point a higher percentage of strain occurred proportional to stress applied. The saturated sample deformed less than the dry sample but has lower Young's Moduli values indicating more plastic behaviour when saturated once the initial plastic deformation of the first dry cycle is overcome. Overall the saturated sample undergoes less strain than the dry sample and is more elastic, indicated by the lower Young's Moduli and smaller hysteresis.

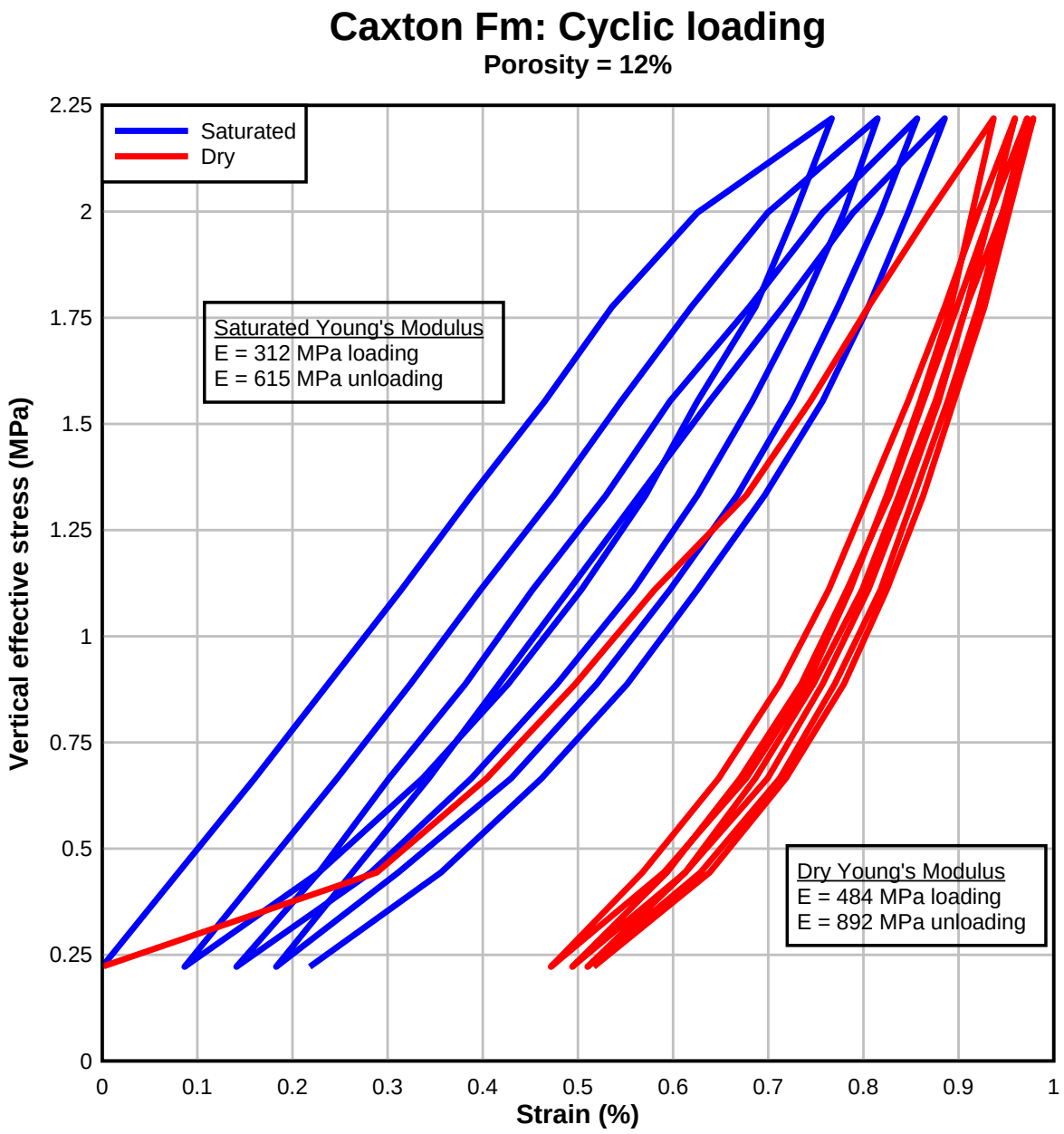

Figure 5.8: Stress-strain graph showing the deformation of the Tahuna Formation sample under cyclic loading when oven dry and saturated.

Caxton: Dry	**Strain under 0.22 MPa**	**Strain under 2.22 MPa**
Cycle 1	0 %	0.94 %
Cycle 2	0.47 %	0.96 %
Cycle 3	0.49 %	0.97 %
Cycle 4	0.51 %	0.98 %
End Cycle 4	0.52 %	

Table 5-14: Simplified results of cyclic loading on dry Caxton Formation sample.

Caxton: Saturated	Strain under 0.22 MPa	Strain under 2.22 MPa
Cycle 1	0 %	0.76 %
Cycle 2	0.09 %	0.81 %
Cycle 3	0.14 %	0.86 %
Cycle 4	0.18 %	0.89 %
End Cycle 4	0.21 %	

Table 5-15: Simplified results of cyclic loading on saturated Caxton Formation sample.

Dry Tahuna Formation versus Dry Caxton Formation

The dry Tahuna and Caxton samples behaved in very similar ways when compared, except for the initially higher amount of plastic deformation that occurred in the Tahuna Formation sample (Fig. 5.9). Following the plastic behaviour of the first cycle both samples behave elastically with a very small amount of plastic deformation in the next three cycles. The Young's Moduli of the two samples is relatively similar; the Tahuna sample has lower Young's Moduli, particularly during the unloading segment of the cycles. This indicates more elastic deformation occurring within the Tahuna Formation sample. Both samples show the majority of deformation is plastic and therefore permanent.

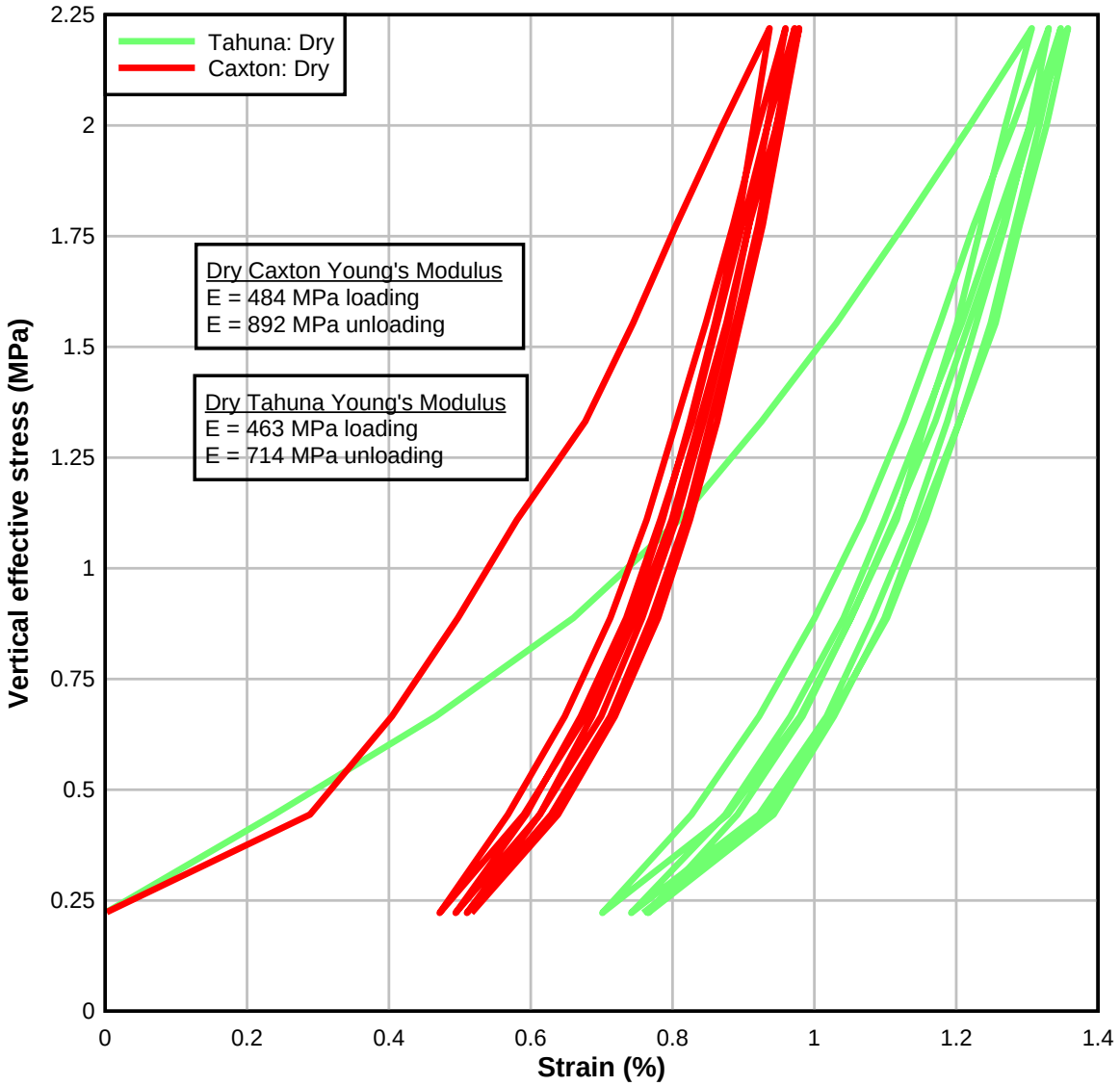

Figure 5.9: Stress-strain graph showing the deformation of the dry Caxton sample vs. the dry Tahuna Formation sample.

Saturated Tahuna Formation versus Saturated Caxton Formation

Comparing the saturated Tahuna and Caxton samples (Fig. 5.10) a similar relationship as the comparison of the dry samples is evident; the Caxton Formation deforms less than the Tahuna Formation but is less elastic. The deformation occurring in both samples is mostly elastic, exhibited by the small hystereses in both plots. A comparison of both plots shows that the Tahuna Formation is approximately twice as soft as the Caxton Formation while the Young's Moduli show that the Tahuna Formation is approximately twice as elastic as the Caxton Formation.

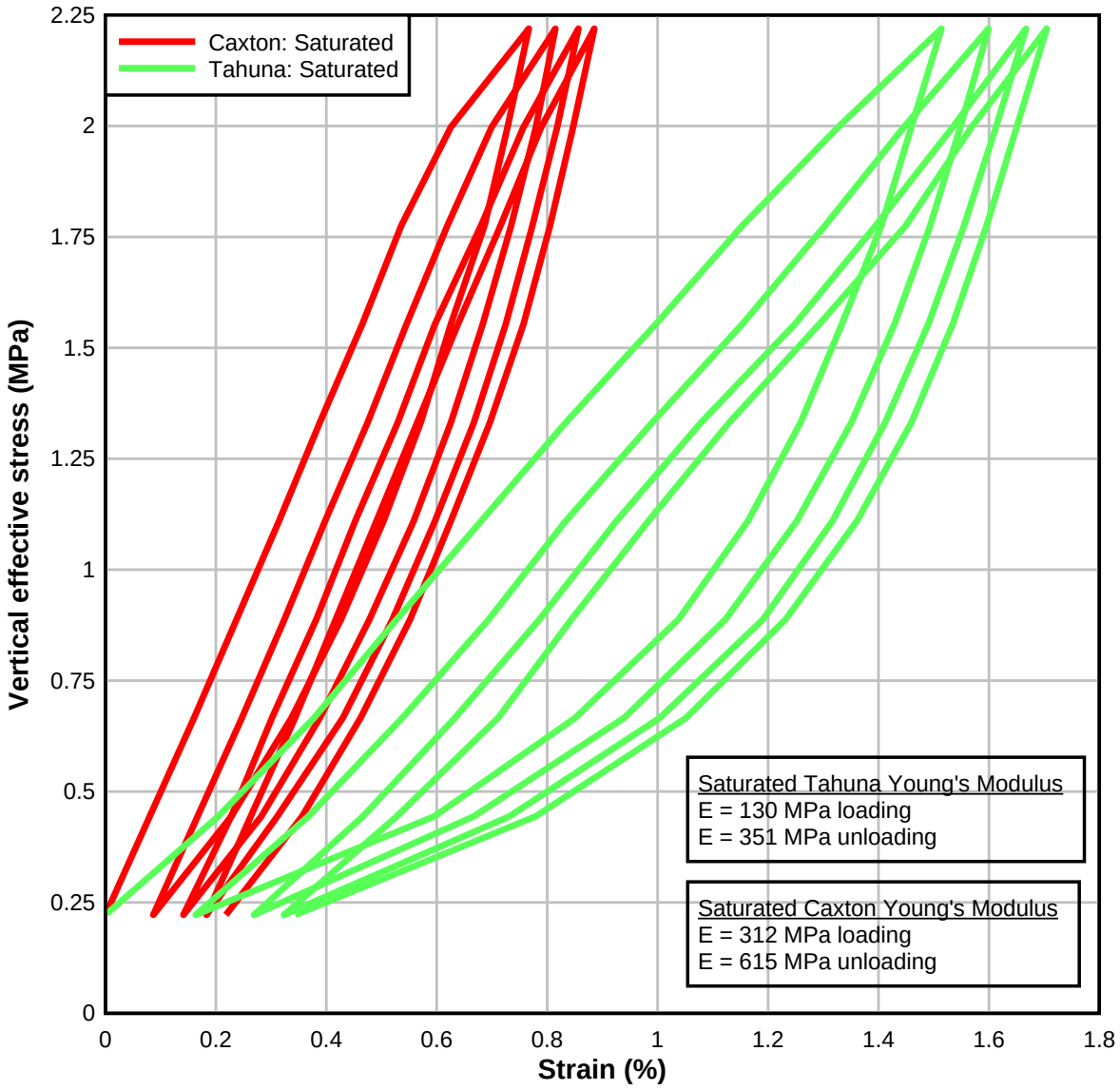

Figure 5.10: Stress-strain graph showing the deformation of the saturated Caxton sample vs. the saturated Tahuna Formation sample.

5.3 Conclusions

Techniques used here to analyse all samples are chosen for their ability to reveal properties of the samples that could contribute to subsidence. Techniques included petrography, X-Ray diffraction, grainsize analysis and compressibility.

- X-Ray diffraction is completed on samples of Recent alluvium, Tahuna Formation, and Caxton Formation to detect the presence of clay minerals, such as smectite, that exhibit shrinking and swelling behaviour when hydrated and dehydrated. XRD results show that clay minerals are a minority in all samples and swelling clay minerals are an extreme minority where present.

- Grainsize analysis of the Recent alluvium samples from beneath the mill site is completed on samples described as having a clay component in their grainsize make up. Based on the NZGS classification for clay 4 – 5% of the samples consisted of clay particles. This is interpreted to be too low to contribute to subsidence across the mill site.
- A new method is developed to test the compressibility of weak rocks and used on the Tahuna and Caxton samples from KGF. The method produced stress-strain relationships from cyclic loading for each formation when both dry and saturated. Results found that the Tahuna Formation is more compressible and elastic than the Caxton Formation.
- The low Young's moduli calculated for the samples are likely a factor of the testing method. Further testing of other soft rocks in the same method will help to further constrain the methodology and allow the comparison of different materials.

6 Hazard Analysis of Kawerau Geothermal Field

6.1 Introduction

Kawerau Geothermal Field (KGF) is located in an area of active volcanism and fault activity. Because of this there are numerous natural events with the potential to impact it including; earthquake, volcanic, flooding, and subsidence. The first three will most likely be catastrophic events causing sudden, large amounts of damage, while subsidence is an ongoing, low magnitude occurrence that can steadily cause damage. Subsidence can be monitored, planned for, and mitigated whereas the other three may not occur during the lifetime of installed infrastructure or some operations. Here historic occurrences of each hazard around KGF are documented and their potential to impact KGF in the future discussed and analysed.

6.2 Earthquake

Numerous faults are present around KGF, but none have surface ruptures through the field (Bignall & Milicich, 2012). Nearby faults include the Onepu Fault, Rotoitipaku Fault Zone, Te Teko Fault, and Edgecumbe Fault (Fig. 6.1); there are also numerous faults further afield that have the potential to rupture and affect KGF. A summary of all nearby faults, their relative location, and reoccurrence interval is provided (Table 6.1). Shallow micro-seismicity (<M2.5) is also likely induced by geothermal operations (e.g. Allis, 1982b); associated with stress changes within the reservoir micro-seismicity does not have an effect on the surrounding area or KGF operations and likely occurs unnoticed except by monitoring equipment. Over the past 10 years the Kawerau area has averaged ~50 micro-seismic events per. year. (Geonet, 2015).

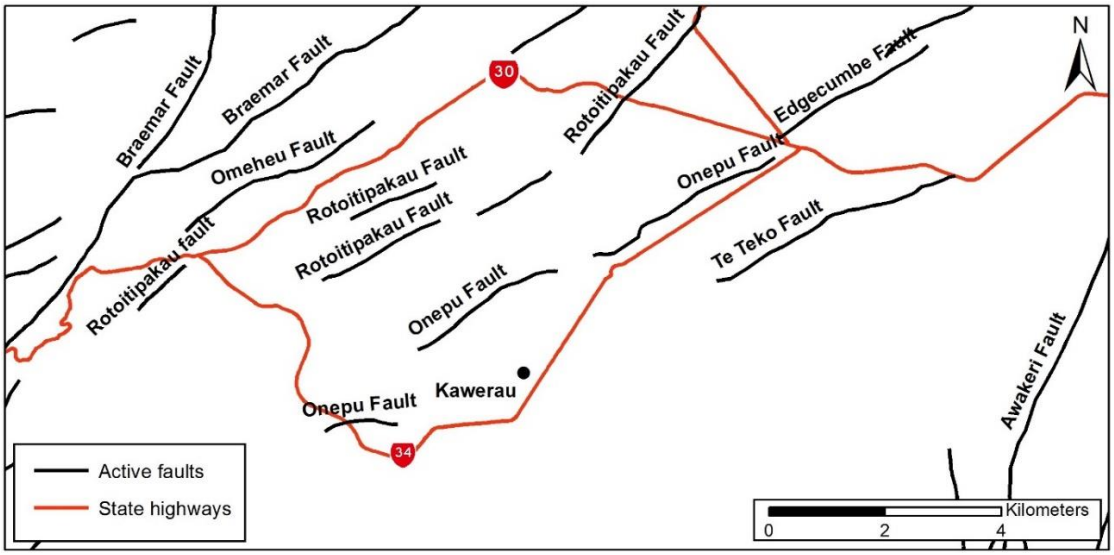

Figure 6.1: Active faults near KGF (Leonard et al., 2010).

Fault	Reoccurrence interval (year)	Relative location to KGF
Onepu	2000 – 3000	1.5km West
Edgecumbe	<2000	6km Northeast
Rotoitipaku	Unknown	3.1km West
Te Teko	2000 – 3500	3.7km Northeast
Waiohau	2000 – 3500	7.5km East
Awakeri	Unknown	8.8km East
Braemar	<2000	6.3km Northeast

Table 6-1: Faults near KGF, their reoccurrence interval and location relative to KGF (GeoNet, 2014).

6.2.1 1987 Edgecumbe Earthquake

The Edgecumbe Earthquake occurred on 2 March, 1987 and measured M_L 6.3 at a depth of 8 km with an epicentre ~21 km northeast of KGF (Anderson & Webb, 1989). The epicentre was located within the main regional structure of the Whakatane Graben where the northeast-striking rift of the Taupo Volcanic Zone intersects the north-south trending North Island Shear Belt (Nairn and Beanland, 1989). The earthquake was associated with renewed rupture along the Edgecumbe, Onepu, and Rotoitipaku faults which have evidence of previous ruptures that was unrecognised until this event, and four new ruptures along the Awaiti, Otakiri, Te Teko, and Omeheu faults. All ruptures were across the Rangitaiki Plains and were mostly downthrown to the northwest (Beanland et al., 1989). The fault ruptures ranged in length at the surface from 0.5 – 7 km. The maximum displacement occurred along the Edgecumbe faults with maximum vertical (2.5 m) and extensional displacements (1.8 m) occurring in the middle of the fault rupture (Beanland et al., 1989). Surface rupture near KGF was limited to the Rotoitipaku and Onepu faults which cross the north and western margins of the field, no ground rupture occurred within the mill complex or across the rest of the field.

Damage to the Tasman Pulp and Paper Mill was widespread with almost every building damaged but the mechanical aspect of operations fared well considering the aggressive chemicals used and dynamic forces of machinery being amplified by the earthquake. Mechanical damage ranged from misalignments of machinery to failure requiring the replacement of key components. Toxic chemicals were not an issue following the earthquake, but carbon dioxide was isolated by operators before a serious problem resulted. The conclusion from the earthquakes effects on Tasman Mill was that the design parameters on most processes were sufficient to safeguard the plant from seismic events (Hodge & Macfarlane, 1988). Improvements have since been made to many structures providing greater protection against future seismic events (e.g. Beca Group, 2011).

A benchmark levelling survey was carried out in April, 1987, following the earthquake, to assess the vertical deformation caused at KGF, 173 benchmarks were included in the survey (see Table 3.1) and an average of 226.1 mm of subsidence was recorded across the field. The earthquake was also accompanied with ~1 m of horizontal extension across the Whakatane Graben, far exceeding rates from geodetic surveys from 1929 – 1976 which show a spreading rate of ~7 – 8 mm/year (Nairn and Beanland, 1989).

KGF experienced MMI (Modified Mercalli Intensity scale) level 9 shaking during the Edgecumbe earthquake, located on the southern tip of MMI 9 isoseismal line (Berryman & Beanland, 1989; Dowrick & Rhoades, 1993). Kawerau has a mean reoccurrence interval of c. 200 years for MMI 9 shaking, with M6 – 6.5 earthquakes occurring at least once every 100 years within the Whakatane Graben in events similar to the Edgecumbe earthquake (Berryman & Beanland, 1989).

6.3 Volcanic

Volcanic hazards include both the direct and indirect effects of volcanic activity. Direct effects include eruptions and explosions, lava, and pyroclastic flows or falls. Indirect effects include break-out floods which is included in the flooding section.

Only one geothermal power station has been affected by a volcanic eruption, the Amatitlán geothermal plant in the May 2010 Pacaya volcano eruption in Guatemala (Wardman et al., 2012a). The eruption required the plant to be shut for three weeks for cleaning of the estimated 20 cm of mostly lapilli-sized tephra. Flashover also caused issues for distribution lines. The issue of flashover from deposits of volcanic ash on HV transmission lines is documented in Wardman et al. (2012b) and the effect of volcanic ash on wider infrastructure is discussed in Wilson et al. (2012).

Putauaki

Putauaki (Mt. Edgecumbe) is a dacite-andesite cone on the southern boundary of KGF. The main cone is ~5000 years old (Bignall & Milicich, 2012), with the youngest eruption dated at 2400 years before present (BP) (Carroll et al., 1997). Putauaki is considered to be active or potentially active but there has been no activity since 1850 years BP (Carroll et al., 1997). No Putauaki material has been located in KGF drillholes indicating that Putauaki is not a particularly violent volcano, although the nearby Tarawera River could have eroded material from the geologic history at Kawerau. The hazard posed by Putauaki has been assessed and it

is indicated that future events are likely, however the eruption history of the volcano is too short to accurately predict future behaviour (Nairn, 1995). Future eruptions would most likely be similar to past events involving irregular ash falls having a small effect on the area. A worst case scenario would involve lava and/or pyroclastic flows causing widespread damage to the Kawerau area (Bignall & Milicich, 2012). In eruption scenarios developed for the area (Fig 6.2), Nairn (2002) described the south-east area of KGF as being at risk from the effects of a Putauaki eruption, most likely ash fall and pyroclastic flows.

Okataina Volcanic Centre (OVC)

OVC has erupted large amounts of material, including the Matahina ignimbrite which underlies an area of 2000 km^2 and ranges in thickness from 5 – 200 m (Bailey & Carr, 1994). OVC is located south-west of KGF and encompasses most of the area between KGF and Rotorua. Between 400,000 and 50,000 years BP there have been five or six large eruptions from OVC which removed 500 km^3 of magma and formed an 18 x 25 km caldera (Nairn, 1993). A series of eight smaller eruptions from 50,000 – 21,000 years BP covered the same area in thinner layers of ash and pumice, and reshaped the caldera. Over the last 21,000 years 11 eruptive episodes from OVC have been identified involving between 0.5 and 17 km^3 of magma with quiescence periods of 700 – 3000 years between these events; the most recent of which was the eruption of Mt. Tarawera in 1886 (Nairn, 1993). A summary of OVC eruptive episodes is provided in Table 6.2.

Eruptive Episode	Age (ka)	Quiescence (years)	Lava Volume (km^3)	Pumice Volume (km^3)
Tarawera	AD 1886	700	-	2
Kaharoa	0.7	2700	2.5	5
Rotokawau	3.4	1500	-	0.7
Whakatane	5	2500	9	10
Mamaku	7.5	1500	15	6
Rotoma	9	2000	2	13
Waiohau	11	2500	4	15
Rotorua	13.5	1500	1	7
Rerewhakaaitu	15	3000	2	6
Okareka	18	3000	5	6
Te Rere	21	3000	10	5

Table 6-2: Sequence of OVC eruptions and volumes (from Nairn, 2002).

A map (Fig 6.2) and scenarios have been developed for OVC with expected hazards from an OVC eruption including ash fall, pyroclastic flows, lava flows, hydrothermal eruptions, volcanic gases, lahars, floods and volcanic earthquakes (Nairn, 2002). The hazards expected from OVC are often compared with those experienced during and after the 1991 Pinatubo eruptions in the Philippines (Hodgson & Nairn, 2004; Hodgson & Nairn, 2005).

The hazard map for OVC and the surrounding area shows the locations of the Haroharo and Tarawera vents that form OVC and the area that will be completely devastated in a typical eruption by one or more of the hazards listed above. Because of the position of KGF on the east bank of the Tarawera River it is at risk of post eruption flooding and lahars, as is the rest of the Rangitaiki Plains (Fig. 6.2).

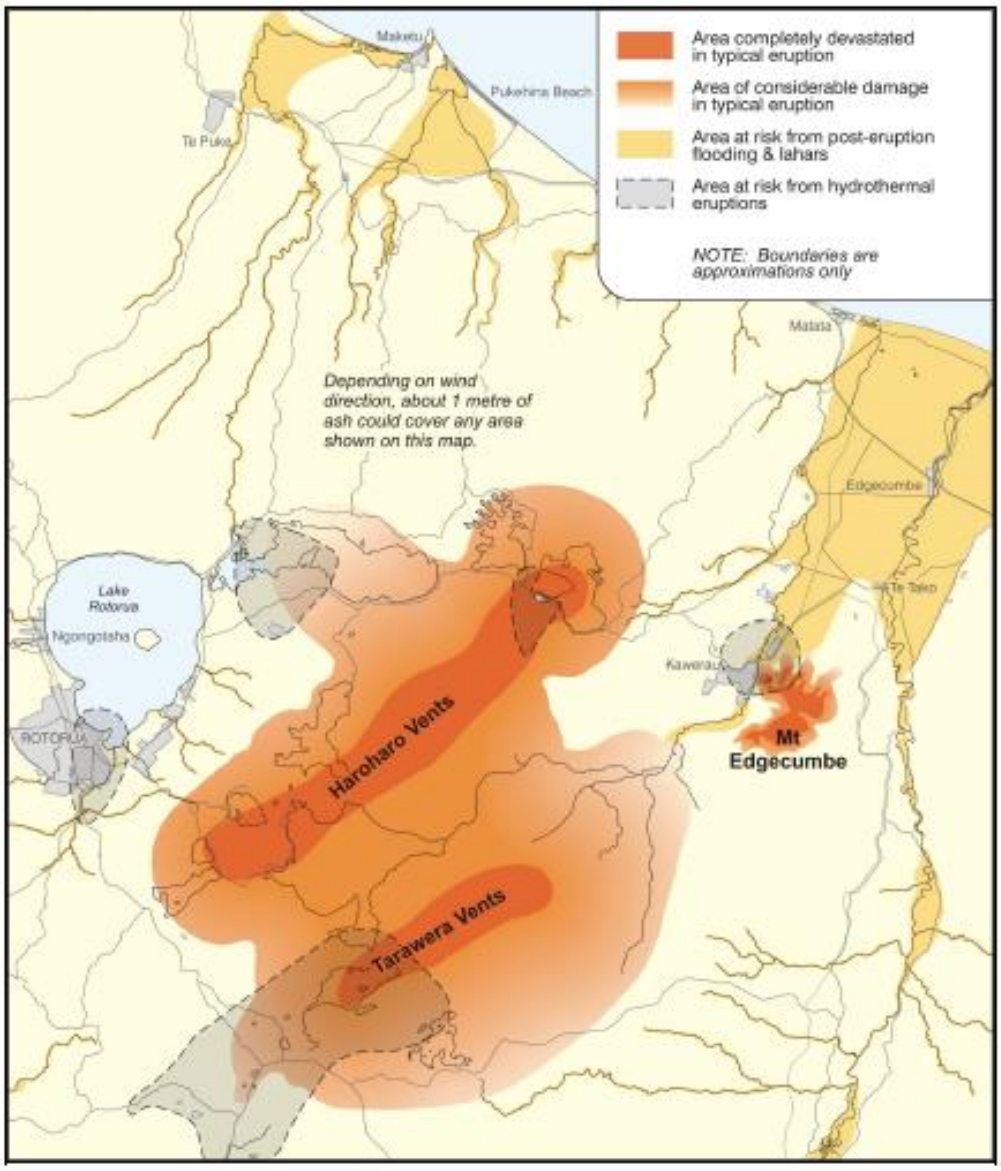

Figure 6.2: Volcanic hazard map of the OVC and surrounding area (from Nairn, 2002).

Hydrothermal eruptions

Hydrothermal eruptions have been mapped at KGF on the south-eastern margin of the field (Nairn & Wiradiradja, 1980). Deposits are dated at 9,000 and 14,000 years BP and indicate an excavation depth of at least 152 m BGL based on the lithology of the clasts present. Seven other hydrothermal eruption centres have been inferred by Christensen (1987). The occurrence of a hydrothermal eruptions could coincide with an increase in the activity of Putauaki (Bignall & Milicich, 2012) and the whole field is considered to have the potential for hydrothermal eruptions (Nairn, 2002) (Fig. 6.2). The identification of the mechanisms of brecciation in KGF well logs (Milicich, 2013b) (see section 4.2.3) would aid in further constraining the probability of a hydrothermal eruption at Kawerau.

Lava flows

Identified lava flows in the stratigraphy at KGF include the Kawerau Andesite, Caxton Formation, and Onepu Formation. Little is known about the Kawerau Andesite due to its depth and age, but the shallow Caxton Formation and surficial Onepu Formation are well documented. From modelling it is known that the Caxton Formation is extruded from multiple vents with the main one around KA31 (see Fig. 4.9), and that it forms a layer below most of KGF. The Onepu Formation forms two domes directly west of the Tasman Mill site with elevations of 186 and 189 mASL (see Fig 1.8) and is identified as an intrusive body in the Torlesse greywacke. The domes are inferred to have been extruded from two separate vents.

A lava flow occurring at KGF would likely destroy all infrastructure in its path with little mitigation possible. However the movement of magma through the crust is often associated with clusters of earthquake at increasingly shallow depths so there would be some warning of an event (Sparks, 2003).

Pyroclastic flows

Nearly all OVC eruptions have been associated with pyroclastic flows near their vents. Pyroclastic flows are the most destructive manifestation of volcanic activity, most of the deaths from the 1886 Tarawera eruption were caused by pyroclastic base surges (Nairn, 1993). Pyroclastic flows are deposited as ignimbrites, which are present in the KGF well logs at four intervals consisting of the Matahina ignimbrite, Karaponga Formation, Raepehu Formation, and Te Teko Formation (Leonard et al., 2010; Milicich et al., 2013b; Wilson et al., 1995b). All four deposits show that large, distal volcanism has the potential to impact KGF, however based on the interval of ignimbrite deposition at KGF (0.2 – 0.5 Ma (Milicich et al., 2013b)), events are extremely sporadic. The nearby Putauaki is also considered to have the potential of generating a pyroclastic flow in a worst case scenario (Nairn, 2002; Bignall & Milicich, 2012), however there is no evidence in the KGF well logs of pyroclastic flows from Putauaki in the past (Milicich et al., 2013). But there have been some block and ash flows associated with the formation of Putauaki.

Overall Volcanogenic Hazard

The potential damage resulting from a volcanogenic event is high, KGL power station cost NZ$300 million to commission and there are five other power stations present with at least one more having recently gained resource consent. CHH Tasman was also recently sold along with

four other pulp and paper related companies for NZ$1.037 billion (Read, 2014). On top of base values is also the lost revenue an event would result in. Volcanogenic events occur sporadically through history, while none have occurred since the development of KGF the possibility of an event is ever present, the probability of a large eruption from the nearby OVC is approximately 1/20 (5%) in any 100 year period (Nairn, 1993).

6.4 Flooding

With the Tarawera River less than 500 m from all major infrastructure at KGF and the known flooding history of the Rangitaiki Plains associated with the deposition of the Recent alluvium (Hodgson & Nairn, 2004), there is a risk of flooding impacting KGF. As it passes the Tasman Mill site and KGL power station the Tarawera River is well constrained in its current course; based on LiDAR data its banks are >6 m higher than the average river level (Figs. 6.3 and 6.4). A review of the flood carrying capacity of the Tarawera River was completed in 2005, however the analysis was completed below SH30 (5 km north of KGF) (Arts, 2005). Hydraulic modelling of the Rangitaiki Plains was also completed in 2011 but analysis of the Tarawera River also started north of Kawerau, peak flood depths in the area were low, ranging between 0.05 and 0.3 m for a 1/100 year event taking into account climate change to 2080 (Wallace, 2011). Continuous flow records for the river date back to 1955, maximum flow was record in 1962 at 92.4 m^3/s and the 100 year return period flow is estimated at 100.22 m^3/s (Arts, 2005). Figure 6.4 shows the path of the Tarawera River past the Tasman Mill site and KGL power station, combining the 6 – 7 m of free board in the banks alongside the Tasman Mill complex, and estimated 100 year flood flow, the mill site and KGL should not be inundated in a 100 year flood event. There is also no documented event of flooding from the maximum flow recorded in 1962. A 100 year flood interval was chosen as the maximum level of analysis due to the combination of available information in Arts (2005) and Wallace (2011), and their analysis. The possibility of an event larger than the 100 year flood is a possibility however any analysis regarding this is yet to be undertaken.

Historic flooding events which resulted in the deposition of the Recent alluvium of the past 60,000 years have all been as a result of outbreak floods following the catastrophic failure of a volcanogenic dam blocking Lake Tarawera. Evidence for flooding is recorded in the exposed Tarawera River valley at ~8 ka, ~0.7 ka (AD 1315), and AD 1904 indicating a low return interval for this type of event. Landslide dams within the Tarawera Gorge also have the potential to block the Tarawera River and fail causing an outbreak flood. The slopes of the

Tarawera Gorge are well vegetated and dotted with small slope failure scars, particularly around the Tarawera Falls, none of which are large enough to sufficiently block the 150 m wide gorge base to form a landslide dam.

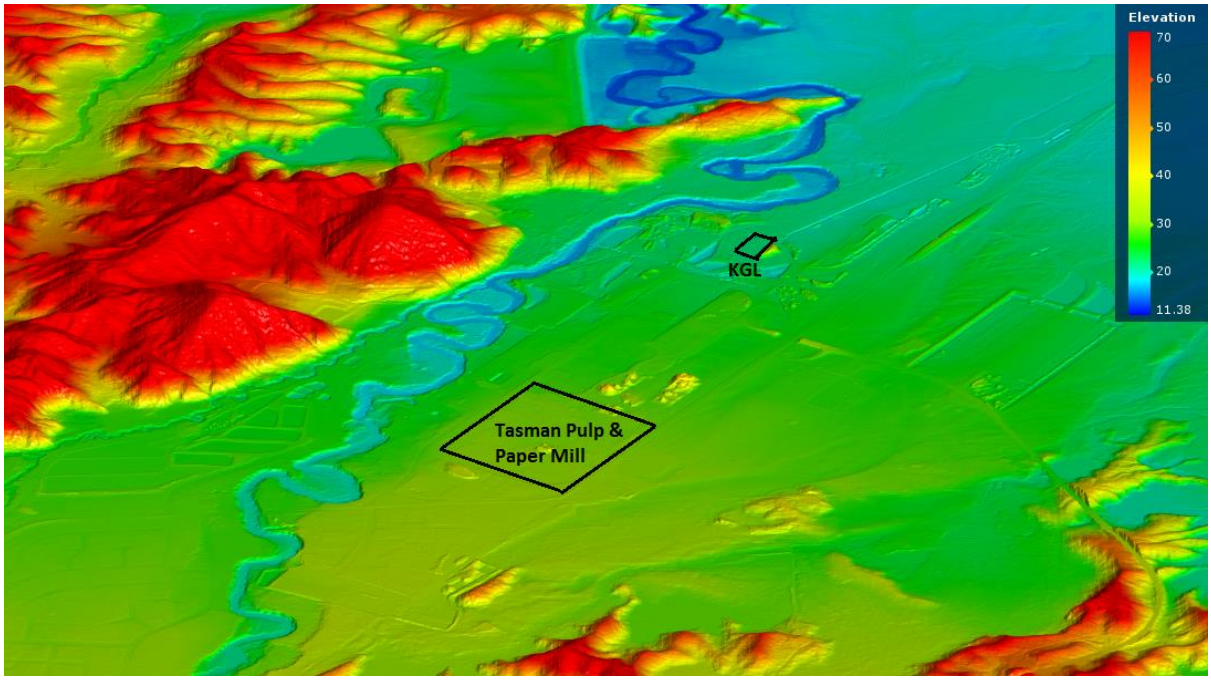

Figure 6.3: LiDAR in Leapfrog Geo showing the confinement of the Tarawera River with nearby Tasman Mill site and KGL power station (LiDAR source: BOPRC, 2014).

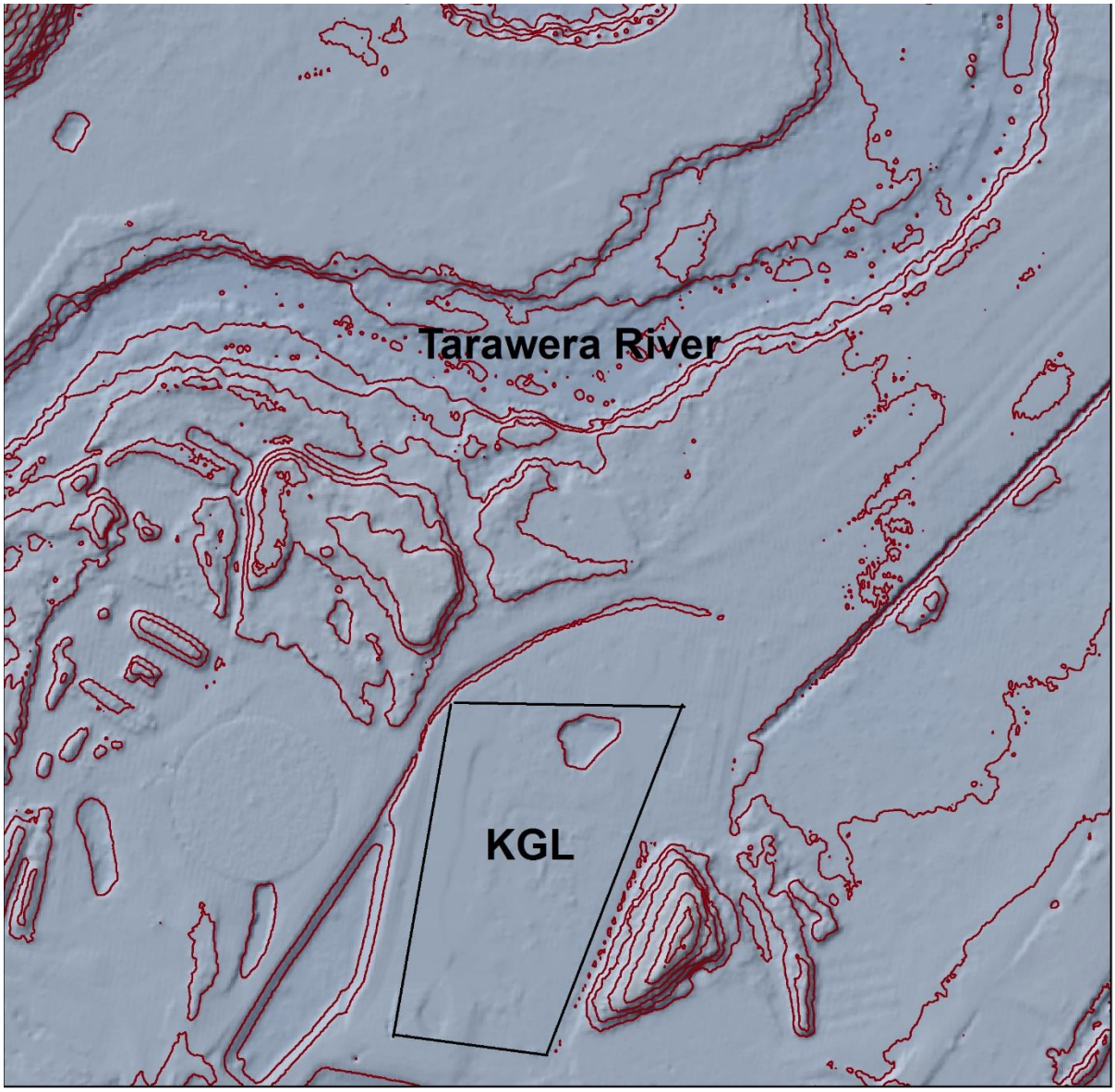

Figure 6.4: 1 m digital elevation model derived from BOPRC, 2014 LiDAR with 2 m elevation contours from near KGL power station showing the banks of the Tarawera River are >6m above the river bed on both sides.

6.5 Tsunami

Despite being more than 20 km from the coast line the majority of KGF is less than 30 m above sea level. Power (2013) defines the maximum tsunami amplitude for a 500 year return period at Whakatane (28 km northeast of Kawerau) to be ~4.7 m within the 50th percentile and for a 2,500 year return period to be ~6.7 m within the 50th percentile. Paleotsunami deposits litter the New Zealand coastline and even the shores of Lake Taupo, but none have been large enough to travel as far inland as KGF (Power, 2013). Based on the assumption that wave height is roughly equal to wave run-up elevation a tsunami travelling across the Rangitaiki Plain to KGF is considered improbable (Power, 2013).

6.6 Subsidence

Subsidence as a hazard to KGF differs to the other three examined here because it does not occur as a catastrophic event, instead occurring steadily over time. Subsidence itself does not cause damage to structures and infrastructure, but it is the amount of differential subsidence or ground tilt that is associated with the subsidence that causes damage. Differential subsidence is the difference in ground deformation between two points and is expressed in millimetres/metres/year. Differential subsidence differs across the field and depends on the type of subsidence feature affecting the area, for example subsidence anomalies typically have higher differential subsidence than field wide subsidence.

Structures vulnerable to differential subsidence at KGF, include all Tasman Mill site buildings and the five KGF power stations (Fig. 6.5). There are three subsidence anomalies with differential subsidence values high enough to cause damage to structures, one is ~1 km north of KGL, the other two are directly south of KGL. Differential subsidence tilt rates in Bowl B, south of KGL, averaged 5.7 mm/30 m/year across four tilt triangles, the method used to calculate tilt (Abele & Currie, 2013). Tilt across the Tasman Mill site is calculated annually using benchmarks across the NST paper machines (see Table 3.3), the current long term average from 2009 – 2013 is 0.45 mm/30 m/year, well within the mill site tolerances for differential subsidence which are approximately 1 mm/30 m/year (John Clark, pers. comm., 2014). Analysis of sensitive mill machinery on the CHH site show that tilt across these structures is mostly within the tolerance of 2 mm/100 m/year (Derrick Hope, pers. comm., 2014)

A map created from the 2010 – 2013 accumulated subsidence contours show the areas where subsidence features have the potential to effect structures and infrastructure (Figs. 6.5 & 6.6). High risk areas are those around the three high tilt anomalies, Bowls A, B, and D and is defined by the -90 mm contour around Bowls B and D, and the -80 mm contour around Bowl A. Of the three power stations on the edge only KGF has reported damage to the cooling towers which is being monitored.

The high-moderate area forms a 100 m buffer around the high risk areas and encompasses the edges of Bowls A, B and D and also includes Bowl C where it is defined by the -70 mm contour. It should be noted that the high-moderate area around Bowls B and D is where the highest ground tension is likely to be occurring anywhere across KGF resulting in the highest amount of damage. The moderate risk area encompasses all of the above area and is defined by the -40

mm contour. Ground tilt values in this area are typically low, however there are some higher values particularly around the five power stations shown by the close spacing of the contour lines (Fig. 6.5). A low subsidence hazard covers the rest of the field wide subsidence bowl and is defined by the -20 mm contour. This area has been shown to be subsiding slowly with low tilt rates which have a low potential to damage structures over time. The majority of the mill site falls into this area, with the exception of the SCA plant. The area covered by each relative subsidence hazard is shown in Table 6.3.

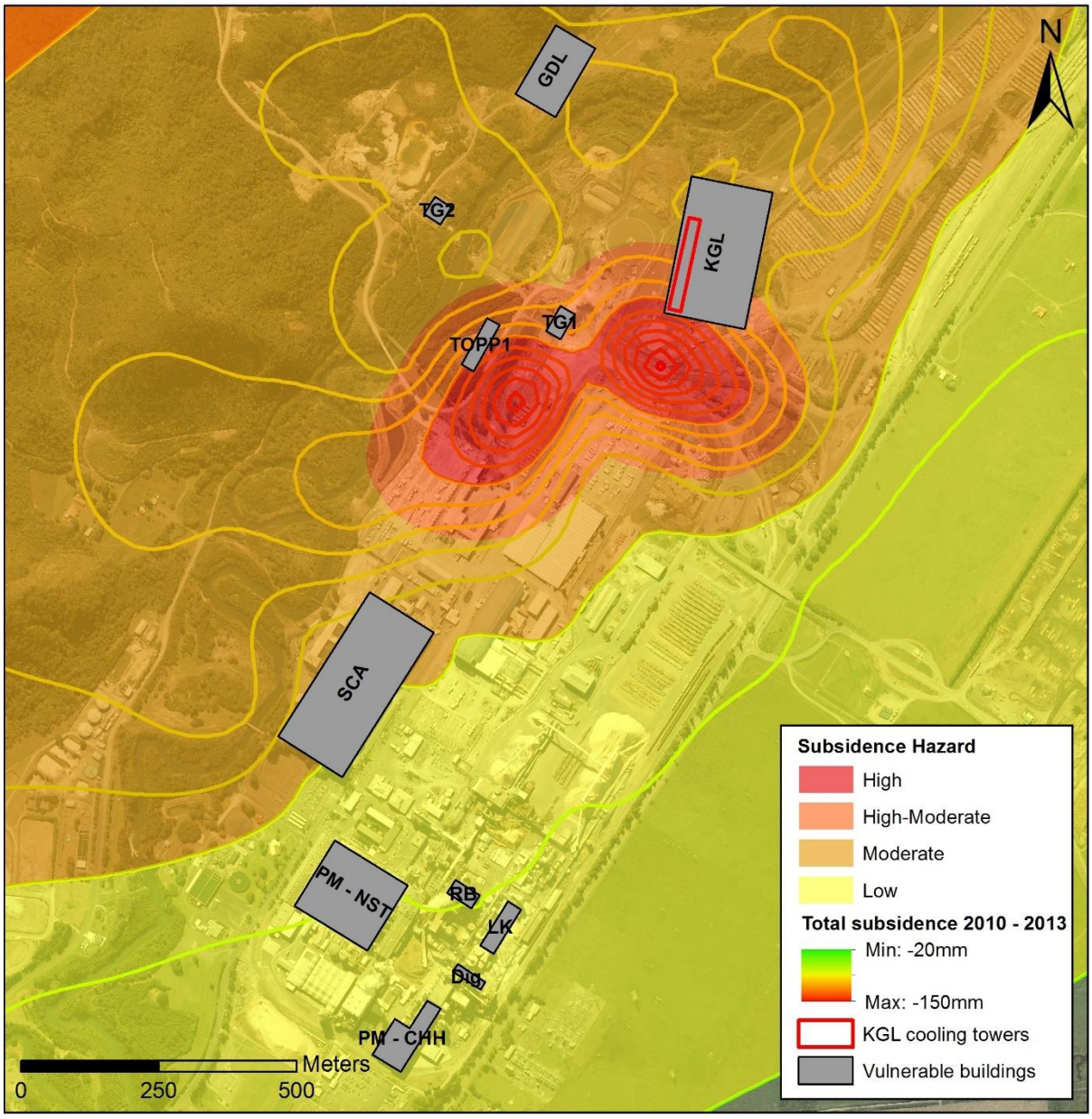

Figure 6.5: Close up of the perceived subsidence hazard to the Tasman Mill site and KGF power station.

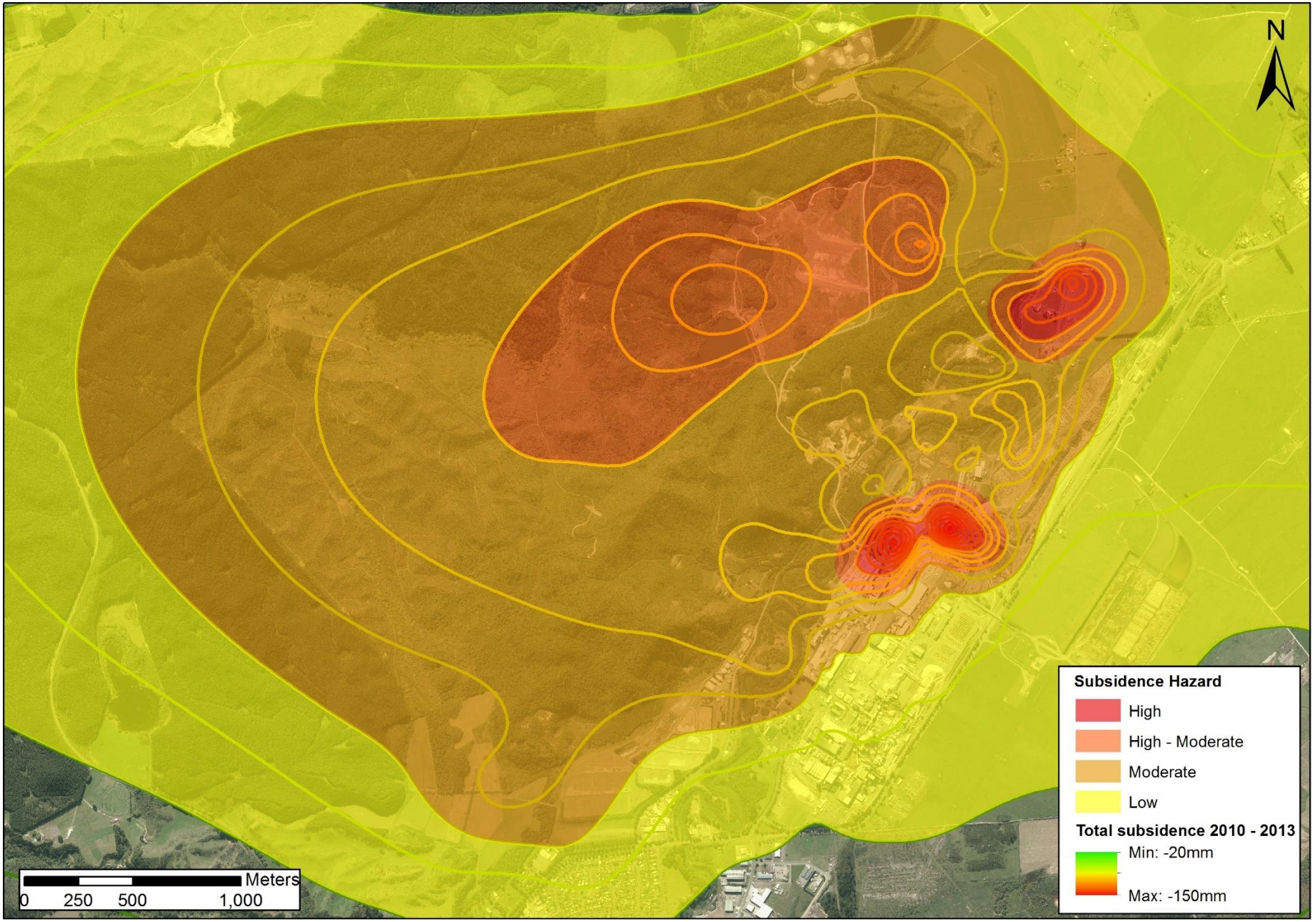

Figure 6.6: Relative perceived hazard to KGF from subsidence.

Subsidence Hazard	Area (km^2)
High	0.20
High-Moderate	2.05
Moderate	10.44
Low	16.55

Table 6-3: Area of each subsidence hazard shown in Figure 6.6.

6.7 Probabilistic Hazard Analysis

Using reoccurrence intervals of the range of events to have impacted KGF in the past a probabilistic hazard analysis of each event impacting KGF in the future can be completed (Table 6.4). For example a 1 in 100 year flood has annual probability of 1%. Many of these events occur outside of 100 year return intervals and therefore have annual probabilities of <1%.

Event	Reoccurrence Interval (years)	Last event	Annual probability	Source
OVC eruption	2000	AD1886	<1%	Nairn (1993; 2002)
Putauaki eruption	Unknown – last active 1850 years BP	~AD185	<1%	Bignall & Milicich, (2012); Carroll et al., (1997)
Local earthquake >M 6	100	AD1987	1%	Berryman & Beanland (1989)
Flood – volcanogenic	700	AD1904	<1%	Hodgson & Nairn (2005)
≥100 year flood	100	Never	≤1%	Arts (2005); Wallace (2011)
Hydrothermal eruption	>5000	9000 years BP	<1%	Nairn & Wiradiradja (1980)

Table 6-4: Probabilistic hazard analysis of events impacting KGF.

6.8 Conclusions

From this analysis it is clear that natural hazards have a low probability of impacting KGF, however the risk present is higher for some events due to the large amount of infrastructure, associated investment in the area, and annual turnover associated with Tasman Mill and KGL

power station. There are three types of events that would be potentially catastrophic at KGF depending on their magnitude, these are: 1) earthquake, 2) volcanic hazards including eruptions, hydrothermal explosions, and lava flows, and 3) flooding from the nearby Tarawera River. The fourth hazard is subsidence which is ongoing and related to geothermal operations but monitored and mitigated sufficiently so that it will not impact the operations of KGF users.

7 Discussion and Management of subsidence at Kawerau

7.1 Interpretation and Implications of Key Results

Analysis of subsidence at KGF completed here can be considered from three parameters: 1) Spatial analysis of subsidence using the benchmark network, which includes the analysis of monitoring datasets, 2) Modelling of cover sequences, and 3) Properties of shallow cover sequences. Each section directly influences the analysis carried out in the subsequent section while analysis of the first parameter incorporates current knowledge on subsidence and its causes from other geothermal fields in New Zealand as well as overseas.

The following consists of a discussion on: the management of subsidence Bowls B and D with the affected infrastructure highlighted and mitigation methods outlined whether current or required in the future; management of the subsidence occurring across the Tasman Mill site with tilt rates across mill machinery highlighted and the effect of subsidence on operations analysed; potential mechanisms for the field wide subsidence occurring; future subsidence considered based on current trends, and finally considerations for further development of KGF.

7.1.1 Spatial Analysis of Subsidence

Spatial analysis of the benchmark network reveals two types of subsidence features at KGF; a broad field wide subsidence bowl and four subsidence anomalies which are superimposed on the field wide bowl. The two types of subsidence features are considered to be driven by mechanisms which are largely separate from each other due to their differing scales. To support interpretations made on the potential mechanisms for subsidence other datasets were analysed and compared with subsidence. From the spatial analysis recent trends in subsidence at KGF were analysed and reasons for them proposed. A site specific analysis of the subsidence occurring across the Tasman Mill site was completed because of the sensitivity of machinery on the site and concerns from the operating companies regarding subsidence across the mill site.

Due to its size, 17 km^2 based on the -10 mm contour in the most recent survey, the field wide bowl is interpreted as being driven by deep reservoir processes, most likely a combination of thermal contraction, shown by the decreasing trend in enthalpy and small decrease in temperature, and compaction of the reservoir due to the small amount of pressure drawdown occurring. Field wide subsidence is a

common occurrence in geothermal, oil, and gas fields around the world and is managed by re-injecting fluids into the reservoir to maintain pressure and sound management to maintain temperatures.

The analysis of subsidence from 2007 – 2013 reveals recent trends in subsidence. The main trend is the continued increase in size of the field wide subsidence bowl. In the analysis completed here this is shown by the movement of the -5, -10, and -15 mm contours east across the mill site and aided by Energy Surveys reports which calculated the area covered by the -10 mm contour (see Table 3.2). It should be noted that in Energy Survey's reports each survey consists of more benchmarks than the previous one in the analysis, potentially making it a measure of effect. An increase in size of the field wide bowl is evident in Energy Survey's calculations when the KGL power station was commissioned because of the associated increase in production. The broadening of the field wide bowl has no effect on the operations at KGF due to the extremely low ground tilt occurring across it.

The four subsidence anomalies at KGF have been termed Bowls A – D by Energy Surveys Ltd. and MRP. Bowl A is located in farm land ~1 km north of KGL power station, Bowl B is directly south of the power station, Bowl C is 1.5 km west of the power station near Lake Rotoitipaku, and Bowl D is directly west of Bowl C (see Fig 3.3). The mechanism for Bowl C is likely to be a combination of the compression of mill waste deposited on the site and thermal contraction due to the downflow of meteoric water associated with historic Rotoitipaku thermal features, but the mechanisms of the other three bowls are currently unknown. The importance of knowing the bowl mechanisms is so that if required mitigation can be undertaken to slow the rate of subsidence.

Trends in the subsidence anomalies show that Bowl A and B fluctuate in their intensity between annual surveys. This could be because of the role the invasion of meteoric waters, potentially related to rainfall, has in the formation of the bowls. The intensity of Bowls B and D could not be correlated with other analysed datasets here. In the 2009 – 2010 survey both Bowls A and B had their highest subsidence rates analysed here, the following year rates in both bowls decreased by 15 – 20 mm/year. The installation of a weather station at KGF would aid in confirming this. The other trend is the development of Bowl D. Bowl D is obviously present from the 2010 – 2011 survey and its rate of subsidence intensifying each year, potentially indicating a different mechanism to that driving the other anomalies. However the proximity of Bowls B and D suggests that Bowl D could be driven by similar processes as Bowl B.

Identified trends in the anomalies have little effect on operations at KGF because of their current spatial location; continued re-levelling of the benchmarks will be sufficient to track their development and alleviate concerns.

Differential tilt occurring in the mill site is shown to be within the tolerances of machinery. Average differential tilt across the NST paper machines is 0.45 mm/30 m/year (Tolerance: 1 mm/30 m/year) and tilts across the CHH site are shown to be within their tolerance of 2 mm/100 m/year. This means that with the continued annual re-levelling of benchmarks operations in the mill site can continue, knowing that current monitoring with an extending benchmark network is sufficient and that subsidence is not an issue.

Other datasets analysed to support mechanisms proposed for the subsidence at KGF are pressure drawdown, enthalpy, and production and injection. Pressure drawdown was demonstrated to be occurring in the deep greywacke reservoir with ~5 bar since 2008 but not in the shallow well (KA14) near Bowl D. Enthalpy has a decreasing trend across the field but because of the parameters used to calculate enthalpy it is difficult to pinpoint the reason for the decrease. Finally production and injection was shown to have a weak correlation ($R^2 = 0.4$) when correlated with subsidence at 16 benchmarks in a statistical analysis by Bromley et al. (2015) but field wide trends displayed here could not be correlated.

Analysis has also shown that peak subsidence rates at KGF of 60 mm/year are low in comparison with other geothermal fields that experienced nearly 500 mm/year of peak subsidence. This has resulted in costly investigation and remediation to control these features. With sound management KGF and Tasman Mill site will be able to be operated with minimal effect from subsidence and therefore avoid potential costs of investigation and remediation.

7.1.2 Modelling of Cover Sequences

Modelling of the shallow cover sequences is completed to discover whether there is an anomalous thickness of a geological unit present that is responsible for the presence of Bowls B and D. The lower constraint on the model of -750 m below relative level is chosen because based on the size of Bowls B and D it is not believed that the source for the bowl could be below the first four formations that occupy the stratigraphy to this depth.

The model revealed an anomalous thickness of Tahuna Formation below Bowl C from 244 – 564 mCHF (KA36) that is stratigraphically beneath the extrusive Caxton Formation, which where present is located at these depths beneath the majority of KGF. An analysis of the

extrusive member of the Caxton Formation confirmed that the formation is relatively thin below the bowls and thick across the mill site. Recent alluvium and Matahina ignimbrite which are above the Caxton and Tahuna formations do not display any clear anomalies in thickness in the Leapfrog Geo model. From this the hypothesis that the Tahuna Formation is more compressible that the Caxton Formation was developed as a potential mechanism for the presence of Bowls B and D.

An analysis in the relative level of the Matahina ignimbrite was undertaken to locate paleochannels in the surface that could have channelled the deposition weaker sediments in the overlying Recent alluvium. This found a large channel east of the Tasman Mill site that has no subsidence anomalies present above it, and the tongue of a channel which extends approximately below Bowls B and D. The proposed mechanism from this was that the channel below could have channelled weaker Recent alluvium material into the area below Bowls B and D.

From all the analysis completed other proposed mechanisms including; the presence of brecciation within the Tahuna and Caxton formations below Bowls B and D, localised hydrothermal alteration of the cover sequences to highly compressible clay, and the presence of a steadily collapsing cavern beneath the bowls.

Analysis of the spatial distribution of brecciation in the Tahuna and Caxton formations showed that 17 wells with it a varying depth, with a cluster near Bowls B and D. However because the mechanisms of brecciation are unknown correlation is currently not possible. Along with the other two proposed mechanisms mentioned here further investigation is required to prove or disprove these mechanisms

Modelling of engineering geological logs from beneath the mill site was completed unsuccessfully. The conclusion of this was that the differences in grainsize in the Recent alluvium below the mill site were thin, extremely localised, and that the heterogeneity of the Recent alluvium across the mill site makes the identification of subunits meaningless. The conclusion of this is that the Recent alluvium does not have the potential to subsidence anomalously beneath the mill site. Furthermore the mill site does not have the geological conditions present to have a subsidence anomaly develop in the future.

7.1.3 Properties of Cover Sequences

Based on the development of the hypothesis that the anomalous thickness of Tahuna Formation below Bowls B and D is responsible for the bowls, samples of Caxton and Tahuna formations were collected from KGF and tested for their relative compressibility and physical properties. The samples had XRD performed on them; results found 10% montmorillonite, a very soft phyllosilicate member of the smectite group of clays, in the Tahuna Formation sample. The 10% shrink-swell clay is interpreted as not being enough to cause a subsidence anomaly but it could be a contributing factor to the Tahuna Formation being more compressible than the overlying Caxton Formation.

Tahuna and Caxton compressibility results show that when saturated the Tahuna Formation is twice as compressible as the Caxton Formation (0.8% vs. 1.6% strain) when under the same amount of stress. Cyclic stress-strain graphs show that early plastic deformation transitions to elastic deformation as loading and unloading cycles are completed, this is shown by the decreasing amount of strain between start and end points of each cycle. Samples tested here displayed similar stress-strain curves to Heap & Faulkner (2008) and Heap et al. (2009) but with much smaller stresses. Deformation is interpreted as being the compression of clays present in the sample, explaining why the Tahuna Formation sample experiences twice the amount strain of the Caxton Formation sample due to its high alteration. Deformation could also be occurring due the closing of micro-cracks which formed when the samples were initially cored due to the release of lithostatic stresses on the samples. Because of the low stresses exhibited on the samples during testing the vast majority of the deformation is likely that from the compression of clays within the sample. Comparing the relative compressibility values of the Caxton and Tahuna formations with other subsidence studies it is clear that the Tahuna Formation is not compressible enough to be entirely responsible for the subsidence bowls. The possibility that it is contributing to the bowls cannot be dismissed and more investigation is required to identify the mechanisms forming the bowls.

Samples of the Recent alluvium from geotechnical boreholes in the Tasman Mill site were also taken and their properties analysed examining the potential for them to contribute to subsidence. Samples included those described as having a clay component in the engineering geology logs; these samples had XRD and laser sizing completed on them to identify whether shrink-swell clay minerals are present as these could contribute to ground deformation in changing ground water conditions, and to analyse the percentage of clay grains present. XRD found trace to 10% kaolinite in the samples; laser sizing found that ~5% of the samples

grainsize is classifiable as clay. Both sets of results are interpreted to show that the Recent alluvium does not contribute to subsidence across the mill site. The possibility of the Recent alluvium contributing to subsidence elsewhere at KGF, as proposed in paleochannels, cannot be dismissed without further investigation.

7.2 Management of Subsidence Bowls B and D

Spatial analysis of the benchmark network at KGF completed in Chapter 3 revealed two subsidence anomalies south of Kawerau Geothermal Ltd. (KGL) power station, termed Bowls B and D, and revealed that the features have been present since the first benchmark re-levelling survey in 1972. Subsidence anomalies have the potential to affect the infrastructure required to operate the geothermal field because high differential tilt resulting from the anomalies can cause cracking of pipes, and disturbance to structures (Bruno, 1992; Bloomer & Currie, 2001). High differential tilt is identified by the close spacing of subsidence contours, the closer the contours, the greater the tilt, and is associated with subsidence anomalies. Placing a cross section through the subsidence contours shows the relatively higher tilt of an anomaly compared to the field wide subsidence bowl (Fig. 7.1). Combined with high ground tilt the edges of a subsidence anomaly have a high amount of ground tension occurring which has the potential to cause cracking of foundations on the surface.

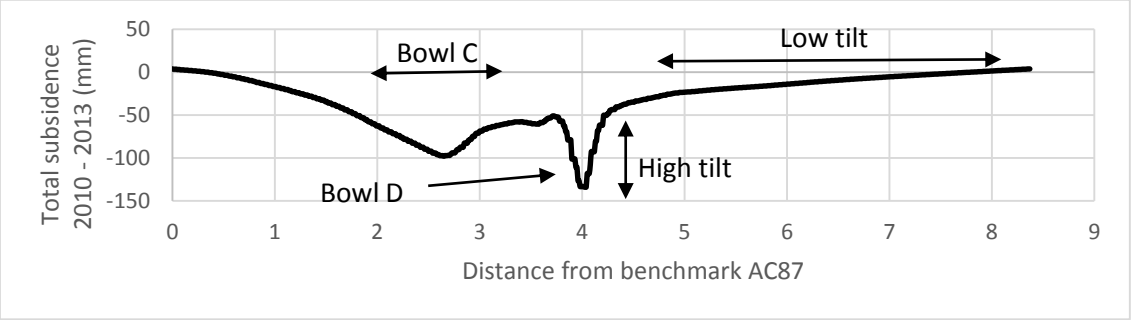

Figure 7.1: Northwest – Southeast cross section of KGF subsidence from benchmark AC87 to H663.

Infrastructure located within, or near to, Bowl's B and D includes: KGL, TOPP1, and TG1 power stations, associated geothermal piping, and gravel access roads. KGL is on the northern edge of Bowl B and is operated by MRP, TOPP1 is owned by Norske Skog Tasman and is located on the north-west edge of Bowl D, TG1 (recently decommissioned) is operated by Nova Energy is located on the north edge of Bowl D and west edge of Bowl B. Geothermal piping which services the power stations is located through the centre of both anomalies and

the east edge of Bowl B. Gravel access roads are located through Bowl B and along the edge of Bowl D (Fig. 7.2).

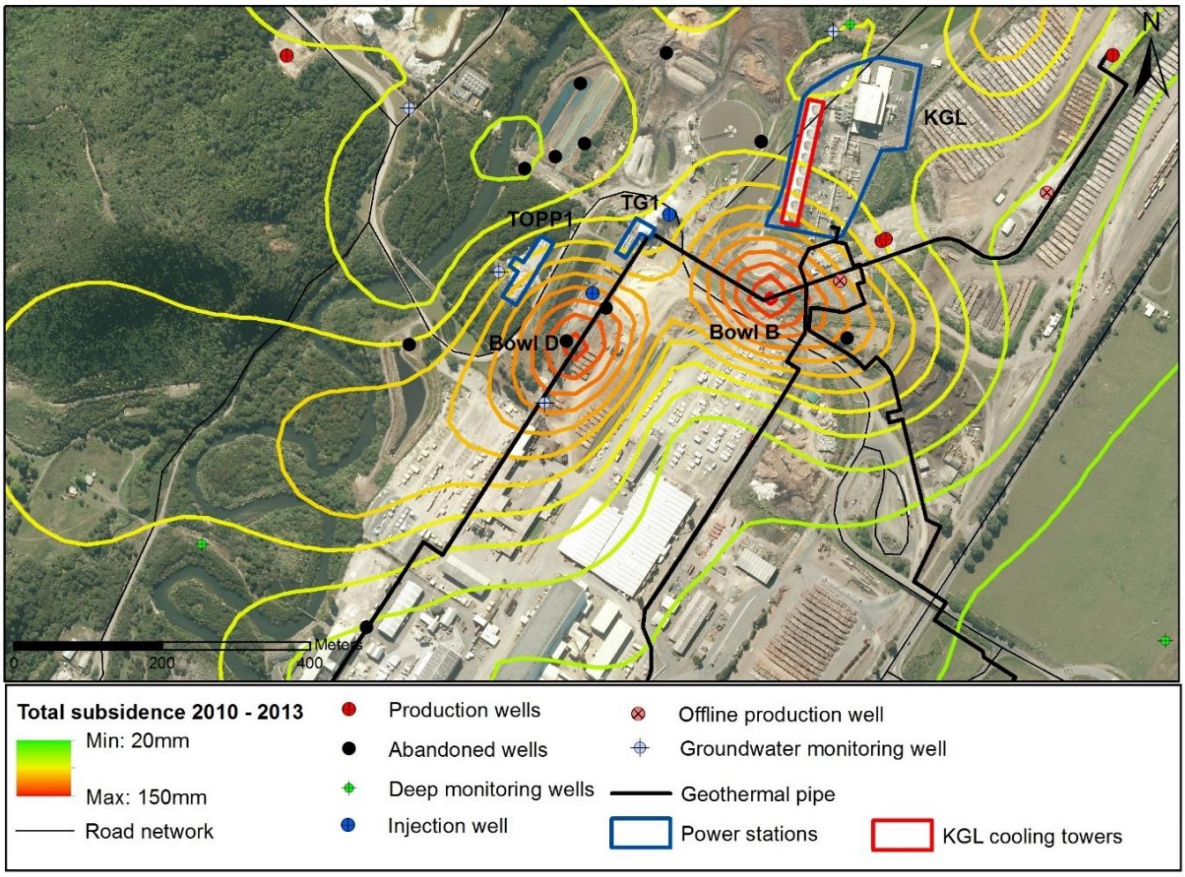

Figure 7.2: Subsidence Bowls B and D with nearby geothermal related infrastructure and the road network.

The 106 MW KGL power station was commissioned in July 2008 and provides power to the national grid. Located north of the Bowl B, on a historic airfield, the power station's cooling towers are on the edge of Bowl B. Because of the ground tension occurring beneath the cooling tower cracks have been observed in the sealing material between joints of the tower walls (low concrete wall (Fig. 7.3)). To monitor this 29 pairs of pins have been placed the length of the wall in construction joins (~5.5 m spacing) and measurement of the distance between the pins with a digital micrometer is undertaken to track the spreading occurring along the wall (Abele & Marcel, 2013).

Figure 7.3: North-west corner of the KGL cooling towers, looking south along the west wall towards Bowl B.

The two smaller power stations, TOPP1 and TG1 (Fig. 7.2), both have smaller footprints (~2900 m^2 and ~350 m^2 respectively) than the cooling towers, because of this the ground tension occurring on the edge of the anomalies has less effect on these structures. The orientation of TOPP1 and TG1 is also a factor on the effect of ground tension. TOPP1 and the KGL cooling towers have approximately the same footprint (2900 m^2 and 3500 m^2) but because TOPP1 is orientated approximately parallel with the subsidence contours and the cooling towers are perpendicular to the contours the cooling towers cross a greater number of contours and experience a higher amount of ground tilt. If the cooling towers were oriented west to east, instead of north to south, in approximately the same location it is unlikely the tension cracking would have as large an effect. Based on the 2012-2013 benchmark re-levelling survey the KGL cooling towers are intersected by the -25, -30, and -35 mm contours with the contours becoming tighter spaced the closer they are to the centre of the bowl. TOPP1 is situated between the -30 and -35 mm contours, and TG1 between the -25 and -30 mm contours. To maintain the structural integrity of the cooling towers they may need to be adjusted in the future and/or have cracks filled to keep the base and concrete wall water tight.

The tensile strength of the geothermal pipes and the amount of strain on the pipe due to tilt are controls on whether it will fail due to a subsidence feature. Geothermal pipes have a minimum lifespan of 25 years, after which the metallurgy is tested and monitoring occurs while operations continue, but this is discounting external stresses on the pipes. Pipes are already placed under high amounts of strain due to the hot, pressurised fluids they transmit causing expansion and contraction. The stresses placed on them due to ground deformation is mitigated with adjustment of the pipe supports. Ground deformation is therefore unlikely to cause catastrophic failure, but if it did shutting off the well providing the fluid would alleviate fluid being released until a permanent solution (replacement) could occur (John Clark pers. comm., 2014).

Gravel access roads around KGF have been mapped and are shown in Figure 7.2. One of these roads, which is unnamed, runs west off SH34, south of KGL, through Bowl B and around the western edge of Bowl D, and across the Tarawera River. The subsidence anomalies have had no direct effect on the road and are unlikely to do so in the future.

Other effects subsidence can have on a geothermal field's infrastructure include flooding. The path of the meandering Tarawera River is well confined due to the steep banks (see Fig 6.4) and the centre of Bowl D (the nearest to the river) is approximately 225 m from the bank of the Tarawera River. At current subsidence rates and due to the spatial location of the bowl it will not have an effect on the path of the Tarawera River in the foreseeable future. On the northern edge of Bowl B and west of KGL is a shallow clarifying pond. If the base and walls of the storage pond are damaged by differential tilt the contents of the pond would slowly leak; rates of discharge would depend on the amount of damage but given the slow rate of ground deformation the contents of the pond would not leak at rate which would cause flooding before damage could be repaired. As previously stated the cooling towers structure is affected by the differential tilt of Bowl B, the wall which has joins opening due to this contains water from the cooling towers and if broken by differential tilt could leak across the KGL site, but due to the slow rate of subsidence any damaged joins could be resealed before significant leaking occurred. The ponding of rainfall within the subsidence anomalies could also be an issue if they become deep enough relative to the surrounding area, Mackenzie (2011) presented evidence for this occurring in the past. During heavy rainfall events if ponding became an issue pumping of the ponding into the Tarawera River or away from KGL would be an option.

To better manage and mitigate Bowls B and D greater understanding of their mechanisms is required. Methods used at other geothermal fields to achieve this include Geertsma modelling of subsidence features to provide insight and geotechnical investigations with associated laboratory testing of material to identify the mechanisms.

A Geertsma approach uses a model that assumes a buried cylindrical body of compressing material with a depth and radius that are adjusted to optimise the fit to observed surface deformation data along a radial profile. The data consists of vertical or horizontal changes but is best constrained with both (Bromley et al., 2010). Data for the model comes from benchmark levelling surveys but must have a high spatial density with benchmarks (Chris Bromley, pers. comm., 2014). The result of the model is that the source depth of the anomaly is found. To do this with Bowls B and D at KGF new benchmarks would need to be installed through the anomalies, although the analysis has been completed with current benchmark measurements with differing results (John Clark, pers. comm., 2014). With geothermal pipes already passing through the centre of the bowls the pipe supports could have benchmarks installed with more placed in between to increase the density (Fig. 7.4).

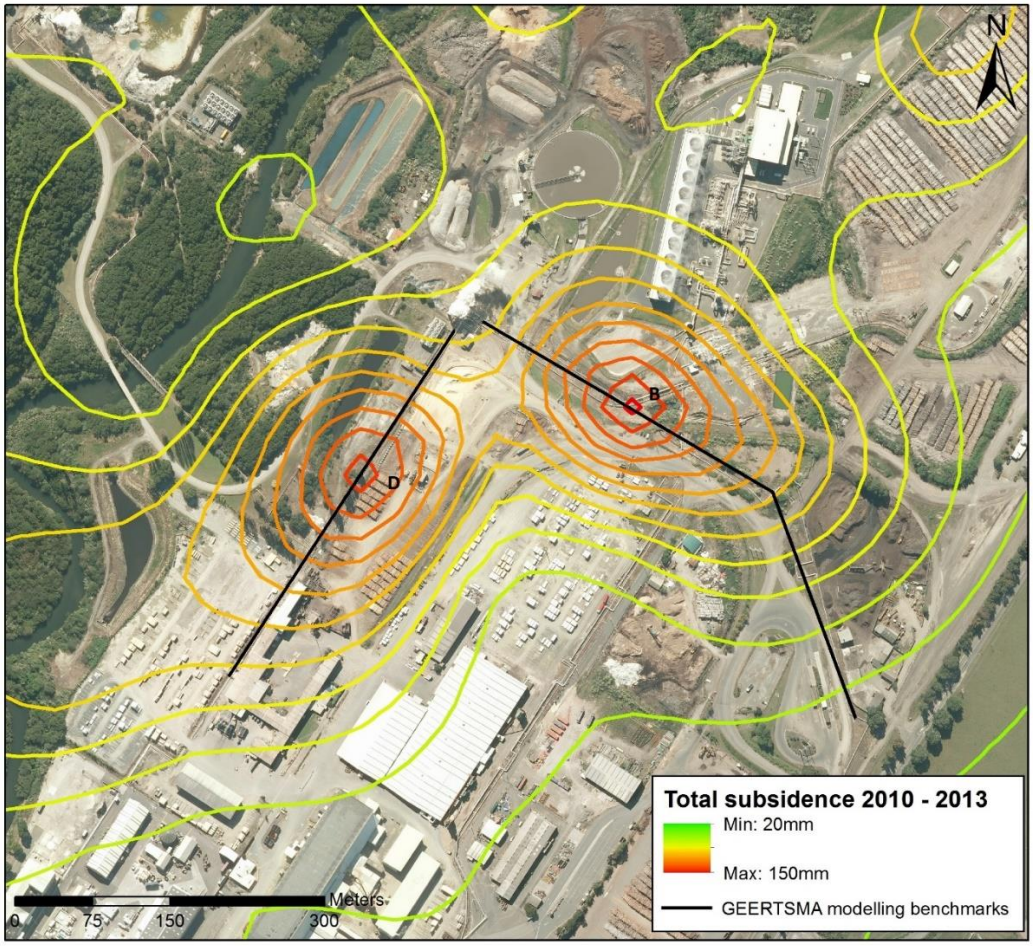

Figure 7.4: Location of Bowls B and D identified with cumulative 2010-2013 subsidence with possible location of new benchmarks for Geertsma analysis along existing geothermal pipes.

From a Geertsma model the source depth, formation, and possibly the mechanism for the subsidence can be identified. KGF has parallel developed, well constrained models of the subsurface; the MVS software platform (CTECH, 2014) maintained by Mighty River Power Ltd., the Leapfrog Geothermal model (ARANZ Geo Ltd., 2014b) developed by Milicich et al. (2013b & 2014), and the shallow cover sequences model developed here; using these models it would be simple to identify the unit responsible for subsidence. If identifying the compressing unit responsible for the subsidence did not result in identifying the mechanism responsible for the subsidence a geotechnical investigation could be conducted.

A geotechnical investigation would consist of drilling and coring the centre of Bowls B and D. Of importance is the drilling parameters vs. depth to explain the in-situ properties encountered, these include high rate of penetration, drilling breaks, and coring difficulties; all of which are characteristic of soft formation conditions. Fluid losses recorded alongside depth identifies zones of relatively high permeability and porosity indicating a potentially weak layer. Core should then be wrapped, sealed, and boxed in preparation for laboratory testing, Figure 7.5

shows the decision tree used for the core testing procedures completed on the Tauhara subsidence report (Bromley et al., 2010).

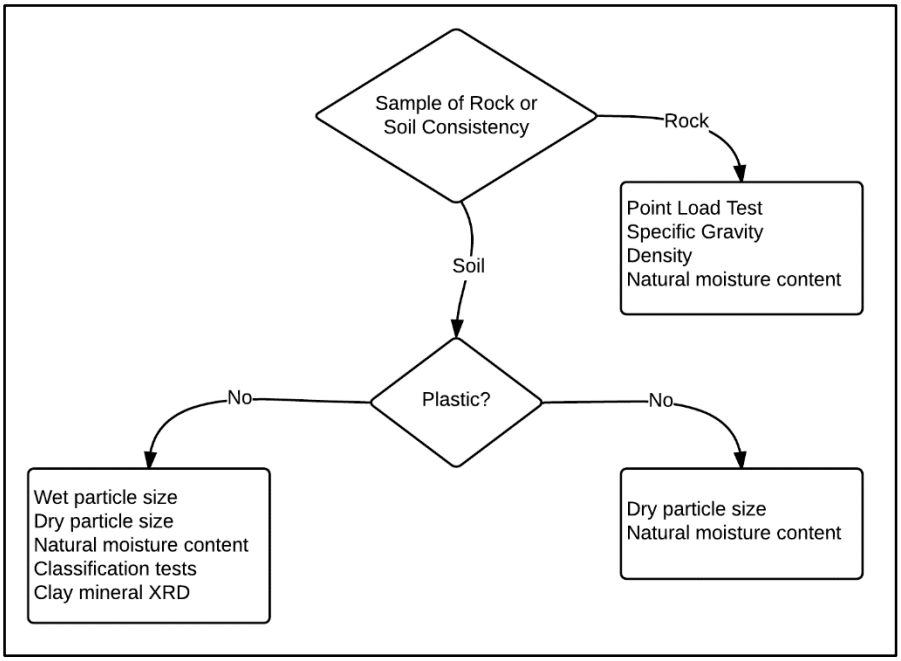

Figure 7.5: Flowchart decision tree of laboratory core testing procedures.

A geotechnical investigation of the subsidence anomalies may define the mechanisms for their presence, however the recovery of soft core is difficult and may be unsuccessful. No approach can be completed with absolute certainty that it will find the mechanisms for the bowls. Current rates of subsidence have a low effect on the surrounding infrastructure, the most affected structure is the KGL cooling towers. Currently the joint opening on the cooling towers is slow and manageable, unless it becomes unmanageable the need to investigate the mechanisms and implementation of a mitigation strategy for the bowls is not present.

7.3 Management of Subsidence across Tasman Mill Site

The development of a subsidence anomaly beneath the Tasman Mill site is of concern to the three operating companies, Norske Skog Tasman (NST), Carter Holt Harvey (CHH) and Svenska Cellulosa Aktiebolaget Hygiene Australasia (SCA), and Mighty River Power Ltd. (MRP) as one of the tappers operating on the geothermal field. The development of an anomaly in the mill area could have a negative effect on the operations of the three operating companies and potentially affect MRP's ability to further develop the KGF resource. MRP has therefore carried out extensive subsidence modelling as per resource consent conditions to evaluate the effect production and injection processes have on ground deformation across KGF

(Geomechanics Technologies, 2013), as well as annual re-levelling surveys of the benchmark network.

From the spatial analysis carried out in Chapter 3 subsidence across the Tasman Mill site has been shown to be part of the broad field wide subsidence bowl. In the most recent survey the field wide bowl covers an area of 17 km^2, defined by the boundary of the -10 mm contour in the survey and differential tilt rates across the mill site are shown to be relatively low, 1.4 mm/100 m/year (Abele & Currie, 2013). Modelling of the cover sequences completed in Chapter 4 revealed the presence of an extrusive rhyolite dome, termed Caxton Formation, beneath the mill site (Fig 4.4). The Caxton Formation is a uniform thickness and is described as a reasonably homogenous formation across the seven production wells (KA41, KA42, KA45, KA46, KA52, PK6, and PK7) in and around the Tasman Mill site. Figure 4.4 shows that the geology beneath the mill site is uniform with no anomalously thick formation that could subside anomalously.

From the benchmark levelling data a detailed analysis of differential subsidence on mill machinery was carried out. Mill machinery with benchmarks on or near the foundations are included in the analysis. This comprised of the NSK paper machines, CHH Lime Kiln 2, CHH recovery boiler, and CHH Digesters 1 and 2. Tilt rates across the NSK paper machine are calculated annually in the Energy Surveys Ltd. report and have been calculated as 1.5 mm/100 m/year for the period 2009-2013 (Abele & Currie, 2013). CHH Lime Kiln 1 differential tilt rates have been calculated between the two benchmarks at the ends of the lime kiln and show an average differential subsidence of 0.6 mm/100 m/year since the installation of the benchmarks in 2007. Differential tilt between the least and most affect benchmarks across the CHH Recovery Boiler are calculated at 2.52 mm/100 m/year. Due to the small footprint of the two digesters only 0. 3mm separates the most deformed and least deformed benchmarks from 2007 – 2012, but due to both being multi-storey ground deformation is amplified at the top of the structure. Results of measurements from the top of the digesters are unavailable, but thought to be within a tolerable range based on ground measurements. Tolerable average differential tilt values across the CHH mill site are believed to be ~2 mm/100 m/year (Derrick Hope, pers. comm., 2014) and all, except for the Recovery Boiler, are less than this amount.

Lime Kiln 2 is considered an indeterminate beam, where the forces acting upon it are constantly changing and unknown due to the material moving through the kiln. Differential tilt affects the force supporting each section of the Lime Kiln potentially deforming it. The kiln is held by

three engineered supports and sits on a trunnion bearing with rollers which allow the kiln to rotate (Figs. 7.6 and 7.7). Potential effects of differential subsidence include premature cracking of rollers and uneven wear across the kiln. The kiln must be kept rotating at all times, if it stops sag occurs between the supports permanently damaging the kiln. Calculated average differential tilt of 0.6 mm/100 m/year would have a negligible to minimal effect on the Lime Kiln.

Figure 7.6: Lime Kiln, support, trunnion and rollers.

Figure 7.7: Lime Kiln rotating drum.

The Recovery Boiler is 1000T top hung boiler with a supporting structure. In April, 2011 pressure parts in the boiler were replaced and CHH took the opportunity to retrofit the supporting structure to meet regulations of Building Act 2004 and NZS 1170.5. The effect of differential tilt on the structure will be for pressure to be placed on the seismic guides (Fig 7.8), significant tilt may cause the guides to perish early due to the added stress placed on them. Considering that Recovery Boiler 2 was constructed in 1967 and has only required re-levelling due to the 1987 Edgecumbe earthquake, subsidence has had little to no effect on the Recovery

Boiler to date. Current subsidence trends should therefore have no effect on the Recovery Boiler in the future.

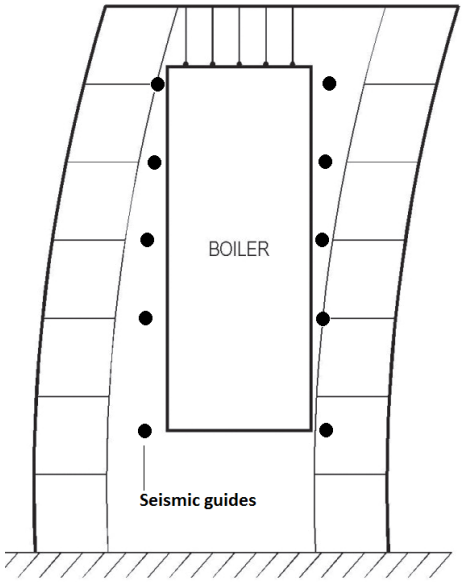

Figure 7.8: Schematic of Recovery Boiler/Building interaction (from Beca Group, 2011).

The Carter Holt Harvey site has 2500 – 3000 pieces of spinning machinery with tolerances that are adjusted during maintenance (Derrick Hope, pers. comm., 6 August, 2014). The vibrations caused by rotating machinery are the most likely cause for tolerances being exceeded; any adjustment required due to differential tilt will then be catered for with regular adjustment as part of a preventative maintenance programme.

Because the subsidence occurring across the mill site is part of the field wide subsidence bowl it is driven by deep reservoir processes related to production and injection effects. Subsidence is on average increasing due to the broadening of the field wide subsidence bowl, shown by the increase in size of the -10 mm contour. However with subsidence rates increasing relatively uniformly and the differential tilt (which causes damage) not increasing, no damage should occur across the mill site in the future based on current trends.

7.4 Mechanisms of Field Wide Subsidence

As already stated in Chapter 3, field wide subsidence is the field wide bowl which is defined by the -10 mm contour drawn from benchmark levelling surveys (see Table 3.2). Because of the size of the bowl field wide subsidence is driven by deep reservoir processes and occurs due to either the contraction or compaction of the reservoir. Compaction occurs when the relative stress on the reservoir increases due to the extraction of fluids and subsequent pressure drawdown. The other mechanism driving the field wide bowl at KGF is thermal contraction of

the reservoir. Thermal contraction occurs because the decrease in temperature of the reservoir results in a contraction of the reservoir rock. The possibility of thermal contraction occurring at KGF was investigated (Allis, 1982a) and found to be illogical as the bulk of the reservoir rock (600 – 1200 m BGL) was close to its original temperature. Since 1982 the reservoir has moved to ~2000 m resulting in a change in the formation and properties of the reservoir (TAOM, 2014). Compaction of the reservoir is unlikely to be primary mechanism driving field wide subsidence because pressure drawdown has been shown to be minimal (<5 bar (see Fig. 3.11)) when compared with other geothermal fields (Allis, 1982a; Narasimhan & Goyal, 1982; Allis, 2000; Hunt & Bromley, 2000; White et al., 2005). Therefore the possibility of thermal contraction being the primary mechanism for field wide subsidence cannot be dismissed and further investigation of the properties of the reservoir rock when heated and cooled is required.

7.5 Future Subsidence

Given the stable operating conditions of KGF since 2009 and the spatially consistent subsidence features occurring, the development of a new subsidence anomaly in the future is unlikely. The datasets analysed here show steady decreasing trends (enthalpy and pressure) and subsidence rates are shown to be steadily increasing due to the broadening of the field wide subsidence bowl however the development of a new subsidence feature requires variable geological conditions that modelling of KGF has shown do not exist except for where current subsidence anomalies are located. Furthermore the large increase in production for the commissioning of KGL did not produce a new anomaly, with sound management any future increases in production should be met with similar results.

The size of the field wide bowl is related to the depth that production is occurring, if production were to go deeper it is likely that this bowl would increase in size. With current production totals and the increasing number of benchmarks being re-levelled it is difficult to predict increases in the size of the bowl, however the field wide bowl has been shown to have no effect on structures which will likely continue to be the case in the future.

Modelling predicts that a ~50% increase in production with 77% reinjection will result in an additional 2.2 mm/year of subsidence and that the development of a new subsidence anomaly because of increased production will not occur. The industry standard is to make long-term projections, and to improve and update these as data becomes available, as per the resource consent conditions (Geomechanics Technologies, 2013). They also add that historical and anticipated subsidence rates at KGF are not excessive nor uncommon for geothermal, oil, and

gas fields around the world. It is noted that other fields experiencing similar or larger rates of subsidence compared to KGF occurred with relatively little or no damage to surface structures. Finally appropriate monitoring (benchmark re-levelling surveys) and model improvements as additional data becomes available should be sufficient to track surface deformation and implement mitigation measures before damage or significant impact occurs to surface structures and operations.

7.6 Considerations for Future Development and Exploitation of Kawerau Geothermal Field

Because of the ongoing subsidence at KGF, careful consideration of the potential subsidence effects must be taken when future development or exploitation is considered. Development of KGF is constrained by a stringent resource consent process involving a hearing panel, council officers from Bay of Plenty Regional, Whakatane District and Kawerau District councils, and submissions from interested parties (which may include existing tappers and industrial users).

Assessments that must be completed as part of the resource consent process for a new development include; environmental effects, cultural impacts, archaeological, air discharge, noise, ecological, erosion and sediment control, thermal features and subsidence monitoring, visual impacts, and sustainability assessments (TAOM, 2014). The environmental effects report compliments and summarises numerous consultancy reports assessing the specific potential effects of a new development and outlines the reasons for requesting consent. Submissions are then requested on the application and a hearing is completed where consent is either granted or refused. Recent applications for further development of KGF include a 45,000 t/day application from Ngāti Tuwharetoa Geothermal Assests Limited (NTGA) and a 15,000 t/day application from Te Ahi O Maui Limited (TAOM).

From the Geomechanics Technologies (2013) report it has been shown that further extraction at KGF will have little effect on the subsidence currently occurring at KGF. Further development is therefore able to go ahead provided resource consent conditions are set within industry standards and based on consents granted to MRP and NTGA. This has been shown to occur with changes made to the TAOM application regarding the injection strategy, where proposed injection was for 200 – 600 mBGL but changed to 1100 mRL to reflect other consents where injection is below production to avoid the rapid return of cool injected fluids into nearby production wells.

Regarding future subsidence and new developments, monitoring through re-levelling surveys is the best method to assess ground deformation along with sound management of the resource. The TAOM development has been approved for a site west of the Onepu Hills and KA22 where it will be unaffected by current subsidence and is predicted to have a minimal effect to ground deformation. KGF is managed as an integrated whole with Bay of Plenty Regional Council developing a single system management plan because one geothermal operation can impact the operation of another or the operations of the Tasman Mill site. All available information indicates that KGF operations are sustainable to the conclusion of current resource consents and likely beyond.

8 Conclusions

8.1 Key Findings

- From annual benchmark re-levelling surveys two types of subsidence features are present at KGF, field wide subsidence and super imposed subsidence anomalies. Field wide subsidence is a broad (17 km^2), low tilt feature driven by reservoir deep processes. Anomalies are smaller, high tilt feature driven by relatively shallow and potentially variable processes.
- Field wide subsidence at KGF has a low potential to cause damage to infrastructure due to its low differential tilt.
- Subsidence anomalies do have the potential to damage infrastructure, but due to the location of the anomalies there is a small amount of infrastructure in proximity to the anomalies.
- Monitored parameters at KGF including pressure and pressure drawdown, production and injection totals, and enthalpy were examined and analysed alongside subsidence. Pressure drawdown is found to be occurring within the reservoir, but when compared with other geothermal fields is a comparably low amount. Shallow pressure drawdown (KA14) near Bowls B and D is extremely low and not enough to explain their presence. Production and injection totals have been approximately stable since 2009 and cannot be correlated with subsidence. Enthalpy is following a general decreasing trend, but is extremely variable. Because of its variable nature and the multiple parameters contributing to its calculation a correlation with subsidence knowing the cause of the decreasing trend is not possible here.
- No one tapper at KGF is responsible for the subsidence occurring. This is because the field is managed as a whole system and the effects of production cannot be traced to one tapper.
- The Recent alluvium is uniformly distributed beneath Tasman Mill site. It consists of pumiceous silts, sands and gravels interspersed with clay lenses, and peat deposits. XRD and laser sizing completed on samples show that no shrink-swell clay is present within the Recent alluvium beneath the mill site and clay particles consist of ~5% of lenses described as having a clay component in engineering geology logs. Evidence shows that lenses with clay are extremely thin (<2 m), are not thick enough, and do not have enough clay in them to cause subsidence. Therefore there is no evidence to date to show that the Recent alluvium has a significant influence on ground deformation across the mill site.
- Modelling shows that the Matahina ignimbrite is thinnest below the mill site, thickening toward KGL power station and beyond. East of the mill and below Bowls B and D are two tongues where the Matahina relative level is deeper than the surrounding area, these are

interpreted as being paleochannels from the Tarawera River or a historic version of it. The possibility that the ignimbrite has channelled the deposition of weaker Recent alluvium that contributes to the subsidence bowls requires a site specific investigation to prove or disprove.

- The Matahina ignimbrite itself is consistently described in well logs with no anomalies that could result in subsidence. The combination of these results in the conclusion that the ignimbrite does not directly contribute to subsidence at KGF but could have channelled the deposition of sediments that could contribute to subsidence.
- The Caxton Formation beneath the current Tasman Mill site is described relatively consistently as a massive to flow banded rhyolite lava. The relatively high thickness of the Caxton Formation compared with the Tahuna Formation combined with the consistent descriptions of Caxton Formation are interpreted that the formation acts as a supporting formation for the Tasman Mill site, preventing anomalous subsidence. Further evidence is that samples of flow banded Caxton Formation had relatively low porosity (12%) and high density (2100 kg/m^3) for its depth and compared to the Tahuna Formation, indicating it is comparably stronger. South of KGL the Caxton Formation is relatively thinner than the Tahuna Formation creating an anomalous thickness of Tahuna Formation.
- The Tahuna Formation underlies the Matahina ignimbrite and Caxton Formation, and is variable in its depth, thickness, and lithology. Where the extrusive Caxton Formation overlies it the Tahuna Formation is relatively much thinner, except beneath Bowls B and D. This led to the hypothesis that the Tahuna Formation is anomalously compressible and the cause of Bowls B and D. Compressibility testing completed on Tahuna and Caxton samples concluded that the Tahuna Formation is approximately twice as compressible as the Caxton Formation and could be contributing to the presence of Bowls B and D but is not compressible enough to be the sole cause of Bowls B and D.
- Two other, untested mechanisms proposed for the presence of Bowls B and D are: 1) The historical presence of a hydrothermal feature such as springs which altered the formations below Bowls B and D to clay, similar to that at Wairakei-Tauhara. No evidence for this mechanism exists in drill holes due to their locations and logged depths, and 2) Brecciation logged at variable depths in the Tahuna and Caxton formations around Bowls B and D results in the presence of the anomalies. A geotechnical investigation with successful core recovery is required to prove or disprove any proposed mechanism.

- Subsidence across the Tasman Mill site is part of the field wide subsidence with low differential tilt values unlikely to disrupt mill operations. Periodic maintenance and adjustment of mill machinery to maintain tolerances should be sufficient to offset any effect of subsidence on mill machinery. The vibration of mill machinery is believed to have a greater impact than the field wide subsidence bowl on the misalignment of machinery.
- Infrastructure affected by Bowls B and D is minimal. TOPP1 and TG1 power stations, located on the bowls edges have relatively small footprints resulting in low tilt values across their foundations. KGL cooling towers have benchmarks installed to monitor deformation occurring along them. Supports of geothermal pipe running through Bowls B and D can be adjusted vertically to mitigate the effects of the anomalies.
- Current subsidence features can be expected to develop at similar rates to those currently occurring.
- All reasonable precautions, modelling, and monitoring is carried out regarding subsidence at KGF. Updates to the data which contributes to modelling is ongoing and expansion to the benchmark network is ongoing in response to the development of subsidence at KGF.
- All catastrophic natural events have a low annual probability of effecting KGF. However the risk present is high due to the large amount of infrastructure and potential for processes to be disrupted by an event.

8.2 Answering the Objectives

1) Spatially analyse the extent of the subsidence and produce a hazard map.

The extent of subsidence at KGF has been shown in Figure 3.3 which shows the cumulative subsidence from 2010 – 2013 benchmark re-levelling surveys. The area covered by the -10 mm/year contour is also stated dating back to the 1998 – 2000 surveys (Table 3.2). Based on the 2010 – 2013 cumulative subsidence map a hazard map for KGF subsidence is created (Fig. 6.6). Key considerations in the hazard map are the amount of subsidence occurring, the likelihood of the development of a new subsidence feature, and the ground tilt occurring. Other hazards are considered to have an extremely low probability of impacting Kawerau as discussed in Chapter 6 and shown in Table 6.4.

2) Define a rate of subsidence for the mill site.

Subsidence across the mill site is analysed in detail in Figure 3.5 which shows the development of subsidence from 2007 – 2013 in annual surveys. Subsidence rates across the mill site vary

from 0 – 5 mm/year in the 2007 – 2008 survey to 10 – 15 mm/year in the 2012 – 2013 survey. Subsidence itself is not the primary concern for mill site operations, instead it is the differential ground tilt which occurs as a result of subsidence. Ground tilt rates across the mill site are shown in Table 3.3 and the average of 0.45 mm/30 m/year (1.5 mm/100 m/year) from 2009 – 2013 is within the 2 mm/100 m/year limit for mill machinery as stated by CHH representatives, and the 1 mm/30 m/year in the NST mill area.

3) Define the contribution to overall subsidence from the cover sequences across the mill complex.

Samples of Recent alluvium are taken from geotechnical borehole G2, samples of Caxton Formation and Tahuna Formation are taken from monitoring well KAM11, and tested for their physical properties to assess the likelihood of the cover sequences to be causing subsidence across the mill site. Results found that the samples did not exhibit properties that would be responsible for subsidence. While the compression of the cover sequences is not the primary mechanism for subsidence across the mill site it is likely that there is a minimal but unknown about of compression within the cover sequences. Due to the heterogeneity of the formations the properties of these formations are likely different beneath Bowls B and D requiring site specific investigation into subsidence at these locations.

4) Define the mechanisms of the subsidence in the mill area

Datasets analysed to define the mechanism for subsidence across the mill site include: benchmark surveys, production and injection masses, pressure and pressure drawdown, enthalpy, KGF boreholes and associated cover sequences modelling, and the geotechnical testing of cover sequences for objective 3. Evidence from all analysis completed concludes that mill site subsidence is part of the broad, low tilt, field wide subsidence bowl which is likely driven by small declines in reservoir pressure and thermal contraction. The likelihood of a high tilt, subsidence anomaly developing across the mill site is virtually nil as the geological conditions for one to develop do not exist based on all evidence present. Furthermore given that one has not developed in 60 years of geothermal exploitation at KGF it is highly unlikely that one should develop in the future.

8.3 Implications for Kawerau Geothermal Field

Implications of this work on the development of Kawerau Geothermal are minimal. Subsidence has been shown to have little potential to disrupt the operations of all concerned parties at KGF

(NST, CHH, MRP, and SCA). Subsidence anomalies have been shown to affect a small amount infrastructure, most of which is monitored closely for damage or has the ability to be adjusted in order to mitigate the effects. Increased exploitation has been modelled to have little effect on ground deformation.

8.4 Limitations

- The most recent benchmark survey (2014) was not available for analysis for this thesis as it had not been processed by Energy Surveys Ltd. This however was expected as it was the case in Mackenzie (2011) where the most recent survey was unavailable.
- The availability of samples for testing the main hypothesis, that the Tahuna Formation is anomalously compressible when compared with the overlying Caxton Formation, was one of the biggest limitations of this work. One sample of each formation was obtained, but not from the subsidence bowls. Samples were of the same formation but from different locations meaning properties are likely different than examined here.
- Because only one sample of each formation was available the testing procedure involved multiple tests on the same sample. While vertical effective stresses in testing were kept well below lithostatic stresses the results show development of plastic strain, due to the compression of clays within the sample and possibly microfractures induced in the sample and closure of pores. This has the potential to alter the properties of the samples. The solution for this was that both Caxton and Tahuna formation samples were tested with the same method across all tests and given time for any elastic strain rebound to occur between tests, however any plastic deformation is unrecoverable.
- Because the core obtained from KGF was not able to be overcored the compressibility of the formations could not be tested using the typical methods. The procedure developed to test the compressibility of the material was able to compare the properties of the two formations tested here but the results cannot be compared to other compressibility tests.

8.5 Future works and Recommendations

Presented below are future works investigating the mechanisms of subsidence at KGF. Some could be completed with current material available provided in is in a satisfactory condition, while others require new material to be drilled:

- The installation and levelling of benchmarks through Bowls B and D at a spacing of <10 m for the purpose of completing a more detailed Geertsma analysis to calculate the potential source depth for the formation for the bowls.
- Following the Geertsma analysis a geotechnical investigation will be required to confirm compressing unit(s) and analyse the properties of the compressing material causing subsidence. Drilling and sampling of Bowls A, B and D with the geotechnical properties of samples tested to confirm the source formation(s), and mechanism(s) driving the bowls.
- The development of a methodology to test the compressive strength of weak rock that is unable to be overcored.
- An analysis of thermal contraction of KGF formations. As discussed thermal contraction of the Basement Greywacke is most likely the driving mechanism for the field wide subsidence bowl. Can the properties of the greywacke be better defined in subsidence modelling to better constrain the models?
- Furthermore are other deep KGF formations undergoing thermal contraction and what is the contribution of these to subsidence?
- Identification of the mechanisms for brecciation within the KGF wells. This would aid in calculating the probability of hydrothermal eruptions at KGF and better constrain the stratigraphy by being able to model the brecciation once the mechanism is known.
- Increased benchmark coverage of CHH mill site; particularly the CHH pulp machines which are not currently covered, and the installation and monitoring of benchmarks on the four corners of TG1 and TOPP1 power stations.
- An analysis of the stresses occurring on the geothermal pipes located through Bowls B and D to aid in the adjustment of the pipes and keep stresses within design limits.

References

Abele, M. & Currie, S. (2012). Kawerau Geothermal Field – Report on the August 2012 Subsidence Levelling Survey (p. 87). Taupo, New Zealand.

Abele, M. & Currie, S. (2013). Kawerau Geothermal Field – Report on the July 2013 Subsidence Levelling Survey (p. 136). Taupo, New Zealand.

Allaby, M. (2008). A Dictionary of Earth Sciences (Third edition., p. 672). Oxford University Press.

Allis, R. G. (1982). Comparison of Subsidence at Wairakei, Broadlands and Kawerau Fields, New Zealand. *Proceedings 8th Workshop Geothermal Reservoir Engineering*, 183–188.

Allis, R. G. (1982b). Mechanism of Induced Seismicity at the Geysers Geothermal Reservoir, California. *Geophysical Research Letters*, *9*(6), 629–632.

Allis, R. G., Christenson, B. W., Nairn, I. A., Risk, G. F., & White, S. P. (1993). The Natural State of Kawerau Geothermal Field. *Proceedings 15th Geothermal Workshop*, 227–233.

Allis, R. G. (1997). Natural State and Response to Development of Kawerau Geothermal Field, New Zealand. *Geothermal Resources Council Transaction*, *21* (October), 3–10.

Allis, R. G. (2000). Review of subsidence at Wairakei field, New Zealand. *Geothermics*, *29*, 455–478.

Allis, R., Bromley, C., & Currie, S. (2009). Update on subsidence at the Wairakei–Tauhara geothermal system, New Zealand. *Geothermics*, *38*(1), 169–180.

Anderson, H., & Webb, T. (1989). The rupture process of the 1987 Edgecumbe earthquake, New Zealand. *New Zealand Journal of Geology and Geophysics*, *32*(1), 43–52.

Anderson, R. L., Ratcliffe, I., Greenwell, H. C., Williams, P. A., Cliffe, S., & Coveney, P. V. (2010). Clay swelling — A challenge in the oilfield. *Earth-Science Reviews*, *98*(3-4), 201–216.

ARANZ Geo Ltd., 2014. http://www.leapfrog3d.com/products/leapfrog-geo

ARANZ Geo Ltd., 2014b. http://www.leapfrog3d.com/products/leapfrog-geothermal

Armienta, M. A., Rodríguez, R., Ceniceros, N., Cruz, O., Aguayo, A., Morales, P., & Cienfuegos, E. (2014). Groundwater quality and geothermal energy. The case of Cerro Prieto Geothermal Field, México. *Renewable Energy*, *63*, 236–254.

Ashwell, P.A. (2014) Controls on the rhyolite dome eruptions in the Taupo Volcanic Zone. Unpublished PhD thesis, University of Canterbury, Christchurch, New Zealand.

Bay of Plenty Regional Council (BOPRC). (2013). Resource Consent No. 67335. http://www.boprc.govt.nz/media/322067/67335-final-decision-with-appendices.pdf. Retrieved 1/02/2015. (p. 45).

Bay of Plenty Regional Council (BOPRC). (2014). 2011/12 LiDAR capture season LAS files for Kawerau Region. Obtained 9 July, 2014.

Bailey, R. A., & Carr, R. G. (1994). Physical geology and eruptive history of the Matahina Ignimbrite, Taupo Volcanic Zone, North Island, New Zealand. *New Zealand Journal of Geology and Geophysics*, *37*(3), 319–344.

Beanland, S., Berryman, K. R., & Blick, G. H. (1989). Geological investigations of the 1987 Edgecumbe earthquake, New Zealand. *New Zealand Journal of Geology and Geophysics*, *32*(1), 73–91.

Beca Group. (2011). CHH Tasman Mill No. 2 Recovery Boiler. http://www.nzsee.org.nz/wp-content/uploads/2013/05/Recovery-Bolier-FINAL.pdf

Begg, J. G., & Mouslopoulou, V. (2010). Analysis of late Holocene faulting within an active rift using lidar, Taupo Rift, New Zealand. *Journal of Volcanology and Geothermal Research*, *190*(1-2), 152–167.

Berryman, K., & Beanland, S. (1989). Evaluation of seismic hazard in the Rangitaiki Plains, New Zealand. *New Zealand Journal of Geology and Geophysics*, *32*(1), 185–190.

Bloomer, A. (2011). Kawerau Direct Heat Use: Historical Patterns and Recent Developments. In *New Zealand Geothermal Workshop*.

Bloomer, A. & Currie, S. (2001). Effects of geothermal induced subsidence. *Proceeding 23rd NZ Geothermal Workshop*.

Bignall, G., & Milicich, S. D. (2012). *Kawerau Geothermal Field: Geological Framework* (p. 35). Taupo, New Zealand.

Bromley, Chris. (2014). Geophysicist – GNS Science, Wairakei, New Zealand. Personal Communication Wednesday 10th September.

Bromley, C. (2014) NZGW 2014; New Zealand Geothermal Progress: Celebrating success through the test of time. Keynote 7: Wednesday 26 November, 2014.

Bromley, C., Lynne, B., Currie, S., Ramsey, G., Rosenberg, M., Pender, M., Lee, S.-G. (2010). *Tauhara Stage II Geothermal Project: Subsidence Report*. GNS Science Consultancy Report 2010/151. (p.163).

Bromley, C., Brockbank, K., Glynn-Morris, T., Rosenberg, M., Pender, M., O'Sullivan, M., & Currie, S. (2013). Geothermal subsidence study at Wairakei – Tauhara, New Zealand. In *Institution of Civil Engineers Geotechnical Engineering* Vol. 166, 211–223.

Bromley, C. J., Currie, S., Jolly, S., & Mannington, W. (2015). Subsidence : an Update on New Zealand Geothermal Deformation Observations and Mechanisms. In *World Geothermal Congress* Vol. 1, 19–25.

Bronswijk, J. J. B. (1988). Modelling of Water Balance, Cracking and Subsidence of Clay Soils. *Journal of Hydrology*, *97*, 199–212.

Bruno, M. S. (1992). Subsidence-Induced Well Failure. *SPE Drilling Engineering*, 8. Retrieved from http://www.terralog.com/article/SPE 20058_Subsidence-Induced Well Failure.pdf

Browne, P. R. L. (1979). Minimum age of the Kawerau geothermal field, North Island, New Zealand. *Journal of Volcanology and Geothermal Research*, *6*, 213–215.

Carroll, L. D., Gamble, J. A., Houghton, B. F., Thordarson, T., & Higham, T. F. G. (1997). A radiocarbon age determination for Mount Edgecumbe (Putauaki) volcano, Bay of Plenty, New Zealand. *New Zealand Journal of Geology and Geophysics*, *40*(4), 559–562.

Clark, J. (2014). Previously Kawerau Project Geologist, now Geology Manager and Fuel Supply Manager for Mighty River Power Ltd. Personal Communication throughout 2014.

Clark, J.P., Askari, M, and Wong, C, (2014). Kawerau geothermal Limited 2013 Annual Report. For Bay of Plenty Regional Council. (p.84).

Cole, J. W. (1990). Structural control and origin of volcanism in the Taupo volcanic zone, New Zealand. *Bulletin of Volcanology*, *52*(6), 445–459.

Cole, J. W., Spinks, K. D., Deering, C. D., Nairn, I. A., & Leonard, G. S. (2010). Volcanic and structural evolution of the Okataina Volcanic Centre; dominantly silicic volcanism associated with the Taupo Rift, New Zealand. *Journal of Volcanology and Geothermal Research*, *190*(1-2).

Cole, J. W., Deering, C. D., Burt, R. M., Sewell, S., Shane, P. A. R., & Matthews, N. E. (2014). Okataina Volcanic Centre, Taupo Volcanic Zone, New Zealand: A review of volcanism and synchronous pluton development in an active, dominantly silicic caldera system. *Earth-Science Reviews*, *128*, 17.

CTECH, 2014. http://www.ctech.com/products/mvsevs-product-suite/mvs/

Darby, D. J., Hodgkinson, K. M., & Blick, G. H. (2000). Geodetic measurement of deformation in the Taupo Volcanic Zone, New Zealand: The north Taupo network revisited. *New Zealand Journal of Geology and Geophysics*, *43*(2), 157–170.

Dowrick, D. J., & Rhoades, D. A. (1993). Damage Cost for Commercial and Industrial Property as a Function of Intensity in the 1987 Edgecumbe Earthquake. *Earthquake Engineering and Structural Dynamics*, *22*, 869 – 884.

Edbrooke, S.W. (compiler), 2005. Geology of the Waikato area: scale 1:250,000. Institute of Geological & Nuclear Sciences 1:250,000 geological map 4. Institute of Geological & Nuclear Sciences Limited, Lower Hutt, New Zealand.

Eysteinsson, H. (2000). Elevation and Gravity Changes at Geothermal Fields on the Reykjanes Peninsula, SW Iceland. In *World Geothermal Congress* Vol. 1976, 559–564.

Ferris, J. (2005). Mineral Catalysis and Prebiotic Synthesis: Montmorillonite-Catalyzed Formation of RNA. *Elements* vol. 1, 145-149.

Geomechanics Technologies. (2013). *Analysis of Surface Deformations Induced by Geothermal Operations at the Kawerau Field: Evaluation of Additional Shallow Extraction Operations (2TAOM4_8) and Comparison to Take Scenarios S0 and S2B. January 10, 2013.* (p. 50).

Geonet (2014). *GeoNet Active Faults Database.* http://maps.gns.cri.nz/website/af/. Retrieved 8 December, 2014.

Geonet (2015). *GeoNet Quake Search.* http://quakesearch.geonet.org.nz/. Retrieved 15 January, 2015.

Geri, G., Rossi, A. I., & Toro, B. (1985). Crustal Deformation and Gravity Changes during the first Ten Years of Exploitation Travale-Radicondoli Geothermal Field, Italy. *Geothermics*, *14*(2), 273–285.

Glowacka, E., Gonzalez, J., & Fabriol, H. (1999). Recent Vertical Deformation in Mexicali Valley and its Relationship with Tectonics, Seismicity, and the Exploitation of the Cerro Prieto Geothermal Field, Mexico. *Pure and Applied Geophysics*, *156*(11), 591–614.

Glowacka, E., Gonzalez, J., & Nava, F. A. (2000). Subsidence in Cerro Prieto Geothermal Field, Baja California, Mexico. In *Proceedings World Geothermal Congress 2000* 591–596.

Glowacka, E., Sarychikhina, O., Suárez, F., Nava, F. A., Farfan, F., Cossio, G. D. D., & Arthur, M. A. G. (2010). Anthropogenic Subsidence in the Mexicali Valley, B.C., Mexico, Caused by the Fluid Extraction in the Cerro Prieto Geothermal Field, and the Role of Faults. *Proceedings World Geothermal Congress*, (April), 2–5.

Grim, R. E. (1968). *Clay Mineralogy* (Second., p. 574). McGraw-Hill Book Company.

Hatton, J. W. (1970). Ground Subsidence of a Geothermal Field during Exploitation. *Geothermics*, *2*, 1–3.

Heap, M. J., & Faulkner, D. R. (2008). Quantifying the evolution of static elastic properties as crystalline rock approaches failure. *International Journal of Rock Mechanics and Mining Sciences*, *45*(4), 564–573.

Heap, M. J., Vinciguerra, S., & Meredith, P. G. (2009). The evolution of elastic moduli with increasing crack damage during cyclic stressing of a basalt from Mt. Etna volcano. *Tectonophysics*, *471*(1-2), 153–160.

Hodge, W. C., & Macfarlane, M. (1988). Effect of the Edgecumbe Earthquake on Mechanical and Process Equipment at the Tasman Mill. *Bulletin of the New Zealand National Society for Earthquake Engineering*, *21*(3), 161–173.

Hodgson, K. A., & Nairn, I. A. (2005). The c. AD 1315 syn-eruption and AD 1904 post-eruption breakout floods from Lake Tarawera, Haroharo caldera, North Island, New Zealand. *New Zealand Journal of Geology and Geophysics*, *48*(3), 491–506.

Hope, Derrick. Engineering Manager at Carter Holt Harvey Tasman Pulp and Paper. Personal communication, 6 August, 2014.

Hotson, Joe. Norske Skog Tasman. Discussion Wednesday 6th August, 2014.

Hunt, T. M., & Bromley, C. J. (2000). Some Environmental Changes Resulting from the Development of Ohaaki Geothermal Field, New Zealand. In *World Geothermal Congress* (pp. 621–626). Kyushu - Tohoku, Japan.

Itoi, R., Inagaki, H., Tanaka, T., & Iwasaki, T. (2014). Effects of Low Temperature Water Inflow into Wellbore at Shallow Feedzone of Production Well on Steam-Water Two-Phase. In *36th New Zealand Geothermal Workshop*. 24–27.

Jurado-Chichay, Z., & Walker, G. P. L. (2000). Stratigraphy and dispersal of the Mangaone Subgroup pyroclastic deposits, Okataina Volcanic Centre, New Zealand. *Journal of Volcanology and Geothermal Research*, *104*(1-4), 319–380.

Keiding, M., Árnadóttir, T., Jónsson, S., Decriem, J., & Hooper, A. (2010). Plate boundary deformation and man-made subsidence around geothermal fields on the Reykjanes Peninsula, Iceland. *Journal of Volcanology and Geothermal Research*, *194*(4), 139–149.

Kilgour, G. N. (2008). *Geology of Kawerau Monitoring Well KAM11* (p. 4). GNS Science Letter report (confidential) LR2008/305LR.

King, R. J. (2009). Minerals explained 49: Kaolinite. *Geology Today*, *25*(2), 75–78.

Kissling, W. M., & Weir, G. J. (2005). The spatial distribution of the geothermal fields in the Taupo Volcanic Zone, New Zealand. *Journal of Volcanology and Geothermal Research*, *145*(1-2), 136–150.

Kosloff, D., Scott, R. F., & Scranton, J. (1980). Finite Element simulation of Wilmington Oil Field subsidence: I. Linear Modelling. *Tectonophysics*, *65*, 339–368.

Leonard, G. S., Begg, J. G., Wilson, C. J. N., & (compilers). (2010). *Geology of the Rotorua Area* (1 sheet + p. 102): Institute of Geological and Nuclear Sciences 1:250,000 Geological Map 5. Lower Hutt, New Zealand. GNS Science.

Lippmann, M. J., Truesdell, A. H., Rodríguez, M. H., & Pérez, A. (2004). Response of Cerro Prieto II and III (Mexico) to exploitation. *Geothermics*, *33*(3), 229–256.

Long Beach California (2014). Historical – Oil Operations – Wilmington Oil Field. Retrieved 10/3/2014 from http://www.longbeach.gov/oil/about/historical.asp

Macdonald, W. J. P., & Muffler, L. J. P. (1972). Recent geophysical exploration of the Kawerau geothermal field, North Island, New Zealand. *New Zealand Journal of Geology and Geophysics*, *15*(3), 303–317.

Mackenzie, H. T. (2011). *Determining the origin of localised subsidence features in the Kawerau Geothermal Field, Bay of Plenty, New Zealand*. Unpublished MSc thesis. University of Canterbury. p.276.

Mayuga, M. N., & Allen, D. R. (1969). Subsidence in the Wilmington Oil Field, Long Beach, California, U.S.A. In *Tokyo Symposium on Land Subsidence*.

Milicich, S. D. (2013a). *Aspects of the Chronology, Structure and Thermal History of the Kawerau Geothermal Field*. Victoria University of Wellington.

Milicich, S. D. (2013b). *Kawerau Geothermal Field Well Logs*. GNS Science Report 2013/06, August, 2013, (p.33).

Milicich, S. D., Bardsley, C., Bignall, G., & Wilson, C. J. N. (2014). 3-D interpretative modelling applied to the geology of the Kawerau geothermal system, Taupo Volcanic Zone, New Zealand. *Geothermics*, *51*, 344–350.

Milicich, S. D., Wilson, C. J. N., Bignall, G., Pezaro, B., & Bardsley, C. (2013a). Reconstructing the geological and structural history of an active geothermal field: A case study from New Zealand. *Journal of Volcanology and Geothermal Research*, *262*, 7-24.

Milicich, S. D., Wilson, C. J. N., Bignall, G., Pezaro, B., Charlier, B. L. A., Wooden, J. L., & Ireland, T. R. (2013b). U–Pb dating of zircon in hydrothermally altered rocks of the Kawerau Geothermal Field, Taupo Volcanic Zone, New Zealand. *Journal of Volcanology and Geothermal Research*, *253*, 97–113.

Moritz, L. (1995). *Geotechnical Properties of Clay at Elevated Temperatures.* Swedish Geotechnical Institute. Report 47. (p. 69).

Mossop, A., & Segall, P. (1997). Subsidence at The Geysers Geothermal Field, N. California from a comparison of GPS and levelling surveys. *Geophysical Research Letters*, *24*(14), 1839–1842.

Nagel, N. B. (2001). Compaction and Subsidence Issues within the Petroleum Industry: From Wilmington to Ekofisk and Beyond. *Physics and Chemistry of the Earth, Part A: Solid Earth and Geodesy*, *26*(1), 3–14.

Nairn, I.A. (1993). Volcanic hazards at Okataina Centre. 3rd ed. [Palmerston North, NZ]: Ministry of Civil Defence. *Volcanic hazards information series 2.* 29, [1].

Nairn, I. A. (1995). The probability and likely effects of a future eruption at Mt Edgecumbe (Putauaki). Report prepared for Bay of Plenty Regional Council.

Nairn, I.A. (2002). Geology of the Okataina Volcanic Centre, 1:50,000. *Institute of Geological and Nuclear Sciences Geological Map 25.*

Nairn, I. A., & Beanland, S. (1989). Geological setting of the 1987 Edgecumbe earthquake, New Zealand. *New Zealand Journal of Geology and Geophysics*, *32*(1), 1–13.

Nairn, I. A., & Wiradiradja, S. (1980). Late Quaternary Hydrothermal Explosion Breccias at Kawerau Geothermal Field, New Zealand. *Bulletin Volcanologique*, *43*(1), 1–13.

Narasimhan, T. N., & Goyal, K. P. (1982). Subsidence due to geothermal fluid withdrawl. *Engineering Geology*.

National Energy Authority (NEA). (2015). Geothermal. http://www.nea.is/geothermal/. Retrieved 30/01/2015.

NZGS. (2005). Field Description of Rock and Soil. Guideline for the Field Classification of Soil and Rock for Engineering Purposes. NZ Geotechnical Society Inc, December, 2005. www.nzgeotechsoc.org.nz

Power, W. (compiler) (2013). *Review of Tsunami Hazard in New Zealand (2013 Update),* GNS Science Consultancy Report 2013/131. (p. 222).

Puente, I., & De La Peña, A. (1979). GEOLOGY OF THE CERRO PRIETO GEOTHERMAL FIELD. *Geothermics*, *8*, 155–175.

Read, E. (2014). Japanese buy CHH pulp, paper business. http://www.stuff.co.nz/business/industries/9981357/Japanese-buy-CHH-pulp-paper-business.

Read, S. A. L., Barker, P. R., & Reyes, A. G. (2001). Consolidation Properties of Huka Falls Formation - Linkages to subsidence at Ohaaki and Wairakei. *Proceeding 23rd NZ Geothermal Workshop*, 57–62.

Read, S., & Kilgour, G. (2009). *Kawerau Geothermal Project, Monitoring Well KAM11. Engineering geological logs of cored sections of well* (p. 22). GNS Science Letter report (confidential) LR2009/359LR.

Rosenberg, M. D., Bignall, G., & Rae, A. J. (2009). The geological framework of the Wairakei–Tauhara Geothermal System, New Zealand. *Geothermics*, *38*(1), 72–84.

Rowland, J. V., & Sibson, R. H. (2001). Extensional fault kinematics within the Taupo Volcanic Zone, New Zealand: Soft-linked segmentation of a continental rift system. *New Zealand Journal of Geology and Geophysics*, *44*(2), 271–283.

Rissmann, C. F. W. (2010). *Using Surface Methods to Understand the Ohaaki Hydrothermal Field, New Zealand*. University of Canterbury. PhD. (p.151).

Sarychikhina, O., Glowacka, E., Mellors, R., & Vidal, F. S. (2011). Land subsidence in the Cerro Prieto Geothermal Field, Baja California, Mexico, from 1994 to 2005. *Journal of Volcanology and Geothermal Research*, *204*(1-4), 76–90.

Sanyal, S. K., & Enedy, S. L. (2011). Fifty Years of Power Generation at the Geysers Geothermal Field, California – The Lessons Learned. In *Thirty-Sixth Workshop on Geothermal Reservoir Engineering*.

Sinclair Knight Merz. (SKM) (2005). *Kawerau Subsidence Review - Geotechnical Investigation Report* (p. 15). Confidential report.

Sparks, R. S. J. (2003). Forecasting volcanic eruptions. *Earth and Planetary Science Letters*, *210*(1-2), 1–15.

Spinks, K., Powell, T., Siega, C., & Bardsley, C. (2010). Mighty River Power's Resource and Development Strategy at Kawerau Geothermal Field, New Zealand. In *World Geothermal Congress*.

Steiner, A. (1968). Clay Mineral in Hydrothermally Altered Rocks at Wairakei, New Zealand. *Clay and Clay Mineral, vol. 16, pp. 193-213.*

Studt, F. E. (1958). Geophysical Reconnaissance at Kawerau, New Zealand. *New Zealand Journal of Geology and Geophysics*, *1*(2), 219–246.

T.A.O.M. Limited. (2014). Resource Consent Hearing. *Te Ahi O Maui Limited Partnership (TAOM) to: Take, use and discharge geothermal fluid from the Kawerau Geothermal Field and to establish a power-station and associated activities for the production of electricity, and for other "cascade" uses.* (pp. 1–25).

Transpower. (2014). *Transmission map: North Island.* Transmission Network as at July 2014. https://www.transpower.co.nz/sites/default/files/uncontrolled_docs/transmission-map-north-island.pdf.

Truesdell, A. H., & Lippmann, M. J. (1998). Effects of Pressure Drawdown and Recovery on the Ciero Prieto Beta Reservoir in the CP-III Area. In *Twenty-Third Workshop on Geothermal Reservoir Engineering*. 90–99.

Ulusay, R., & Hudson, J. A. (2007). *The Complete ISRM Suggested Methods for Rock Characterization Testing and Monitoring: 1974-2006* (p. 628). Ankara, Turkey.

Wallace, P. (2011). *Hydraulic Modelling of the Rangitaiki Plain.* Report prepared for Bay of Plenty Regional Council. January, 2011. (p. 134).

Wallace, L. M., Beaven, J., McCaffrey, R., & Darby, D. (2004). Subduction zone coupling and tectonic block rotations in the North Island, New Zealand. *Journal of Geophysical Research*, *109*(B12), B12406.

Wardman, J., Stewart, C., Wilson, T., & Sword-Daniels, V. (2012a). *Impact assessment of the May 2010 eruption of Pacaya volcano, Guatemala* (p. 85).

Wardman, J. B., Wilson, T. M., Bodger, P. S., Cole, J. W., & Johnston, D. M. (2012b). Investigating the electrical conductivity of volcanic ash and its effect on HV power systems. *Physics and Chemistry of the Earth, Parts A/B/C*, *45-46*, 128–145.

White, P. J., Lawless, J. V, Terzaghi, S., & Okada, W. (2005). Advances in Subsidence Modelling of Exploited Geothermal Fields. *Proceedings World Geothermal Congress*, (April), 24–29.

Wilson, C. J. N., Houghton, B. F., McWilliams, M. O., Lanphere, M. A., Weaver, S. D., & Briggs, R. M. (1995a). Volcanic and structural evolution of Taupo Volcanic Zone, New Zealand: a review. *Journal of Volcanology and Geothermal Research*, *68*(95), 1–28.

Wilson, C. J. N., Houghton, B. F., Kamp, P. J. J., & McWilliams, M. O. (1995b). An exceptionally widespread ignimbrite with implications for pyroclastic flow emplacement. *Nature*, *378*, 605–607.

Wilson, T. M., Stewart, C., Sword-Daniels, V., Leonard, G. S., Johnston, D. M., Cole, J. W., Barnard, S. T. (2012). Volcanic ash impacts on critical infrastructure. *Physics and Chemistry of the Earth, Parts A/B/C*, *45-46*, 5–23.

Wood, C. P., Brathwaite, R. L., & Rosenberg, M. D. (2001). Basement structure, lithology and permeability at Kawerau and Ohaaki geothermal fields, New Zealand. *Geothermics*, *30*(4), 461–481.

Wyering, L. D., Villeneuve, M. C., Wallis, I. C., Siratovich, P. A., Kennedy, B. M., Gravley, D. M., & Cant, J. L. (2014). Mechanical and physical properties of hydrothermally altered rocks, Taupo Volcanic Zone, New Zealand. *Journal of Volcanology and Geothermal Research*, *288*, 76–93.

Appendices

Sample: G2d

Lithology: Recent Alluvium

Well: G2

Depth: 50.0 – 50.14 m

Description: Pumiceous SILT, trace clay, firm to stiff, light grey, moist.

XRD results:

Sample	Quartz	Albite	Kaolinite
G2d1	60	30	10
G2d2	65	35	trace

Laser sizing results:

Sample	Borehole	Grainsize	Size (um)	Percentage (%)
G2D	G2	Clay	<2	4.00
		Silt	2 – 6	6.97
		Fine Sand	6 – 200	85.77
		Medium Sand	200 – 2000	3.27
	Total			100

Sample: G2e

Lithology: Recent Alluvium

Well: G2

Depth: 50.32 – 50.5

Description: Pumiceous SILT, trace clay, firm to stiff, light grey, moist.

XRD results:

Sample	Quartz	Albite	Kaolinite
G2e1	65	35	trace
G2e2	60	40	trace

Laser sizing results:

Sample	Borehole	Grainsize	Size (um)	Percentage (%)
G2E	G2	Clay	<2	5.13
		Silt	2 – 6	9.63
		Fine Sand	6 – 200	83.23
		Medium Sand	200 – 2000	2.00
	Total			100

Sample: 11E

Lithology: Caxton Formation

Well: KAM11

Depth: 203.8 m BGL

Description: Rhyolite lava: flow banded/spherulitic, pumiceous top, glass at the base, xtl-poor (qz +pl)

Porosity and Density using Saturation and Vernier callipers:

Length (mm)	31.17	**Saturated weight (g)**	358.0
Diameter	82.13	**Sample depth (mCHF)**	203.8
Radius	41.07	**Pore volume (m^3)**	0.0000186
Volume (m^3)	0.000165144	**Porosity (%)**	11.263
Bulk volume (cc)	165.144441957	**Dry density (kg/m^3)**	2055.17
Submerged weight (g)	198.64	**Saturated density (kg/m^3)**	2167.80
Dry weight (g)	339.4		

Porosity and Density using Saturation and Buoyancy:

Saturated density (kg/m^3)	2167.80	**Pore volume (cc)**	18.6
Bulk volume (m^3)	0.00015936	**Porosity (%)**	11.672
Bulk volume (cc)	159.36	**Dry density (kg/m^3)**	2129.77
Pore volume (m^3)	1.9E-05		
Porosity difference between two methods (%)	3.540	**Density difference between two methods (%)**	3.398

XRD results:

Sample	Cristobalite	Albite
11E	65	35

Photomicrographs:

Cross polarised light

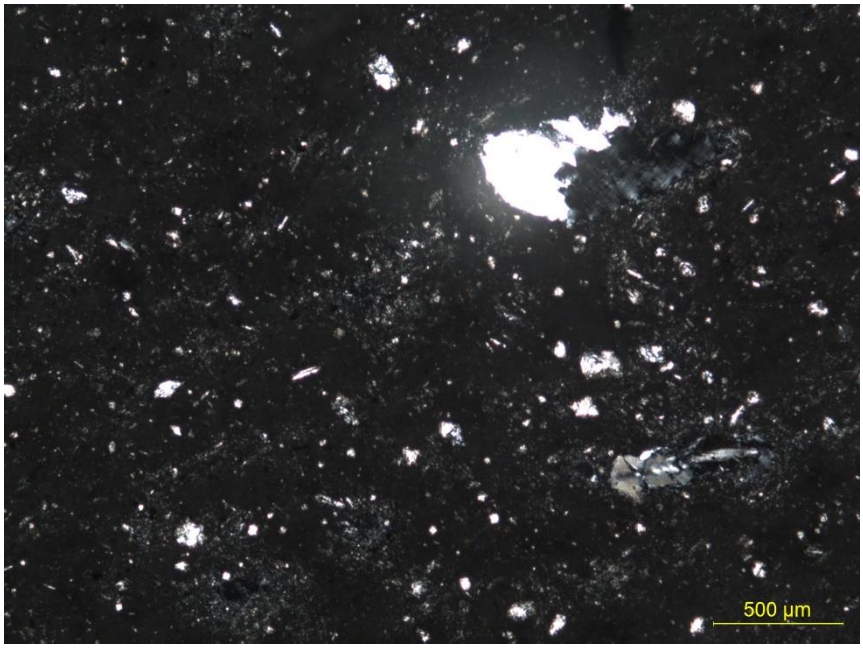

Plain polarised light

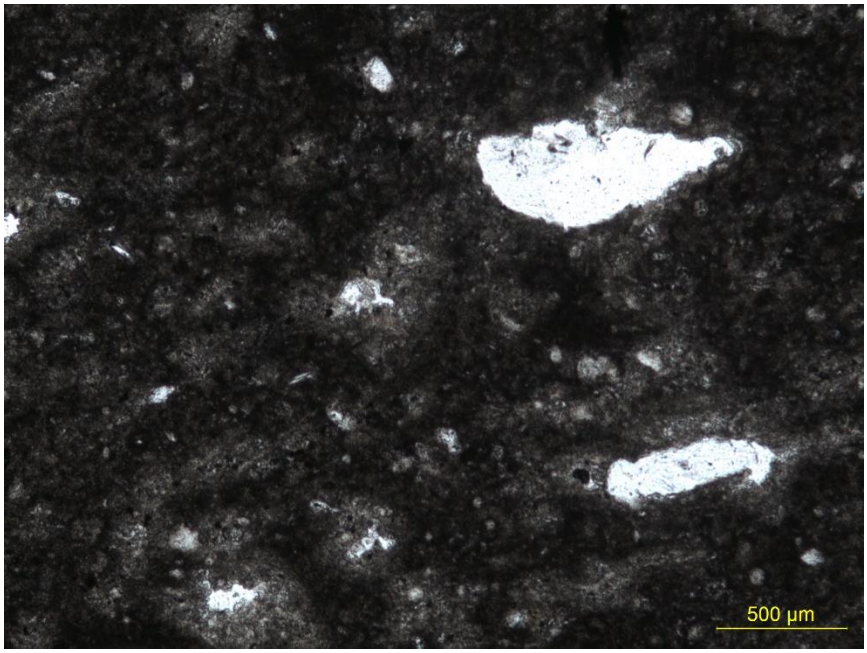

Sample: 11A

Lithology: Tahuna Formation

Well: KAM11

Depth: 426.4 mCHF

Description: Cream to white , non-welded ignimbrite, pumice clasts up to 5cm across which have been intensely altered to clay, lithics up to 2cm across of rhyolite lava, large (up to 2cm across) qz xtal fragments are common along with minor biotite.

Porosity and Density using Saturation and Vernier calipers:

Length (mm)	29.39	**Saturated weight (g)**	292.3
Diameter (mm)	84.02	**Sample depth (mCHF)**	426.4
Radius (mm)	42.01	**Pore volume (m^3)**	0.0000590
Volume (m^3)	0.000162945	**Porosity (%)**	36.208
Bulk volume (cc)	162.945365668	**Dry density (kg/m^3)**	1431.77
Submerged weight (g)	136.08	**Saturated density (kg/m^3)**	1793.85
Dry weight (g)	233.3		

Porosity and Density using Saturation and Bouyancy:

Saturated density (kg/m^3)	1793.85	**Pore volume (cc)**	59
Bulk volume (m^3)	0.00015622	**Porosity (%)**	37.767
Bulk volume (cc)	156.22	**Dry density (kg/m^3)**	1493.41
Pore volume (m^3)	5.9E-05		
Porosity difference between two methods (%)	4.42	**Density difference between two methods (%)**	4.20

XRD results:

Sample	Cristobalite	Albite	Montmorillonite
11A	60	40	10

Photomicrographs:

Cross polarised light

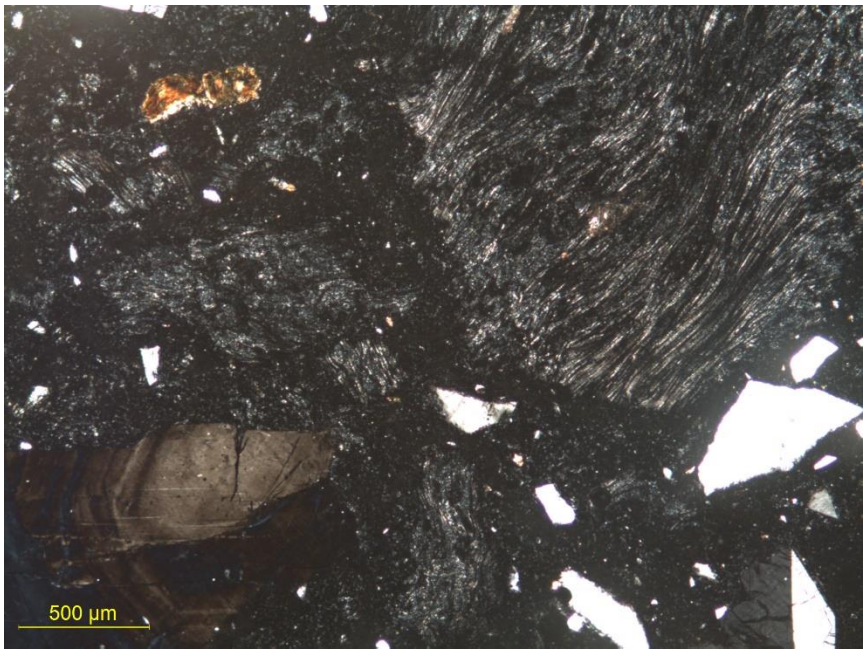

Plain polarised light

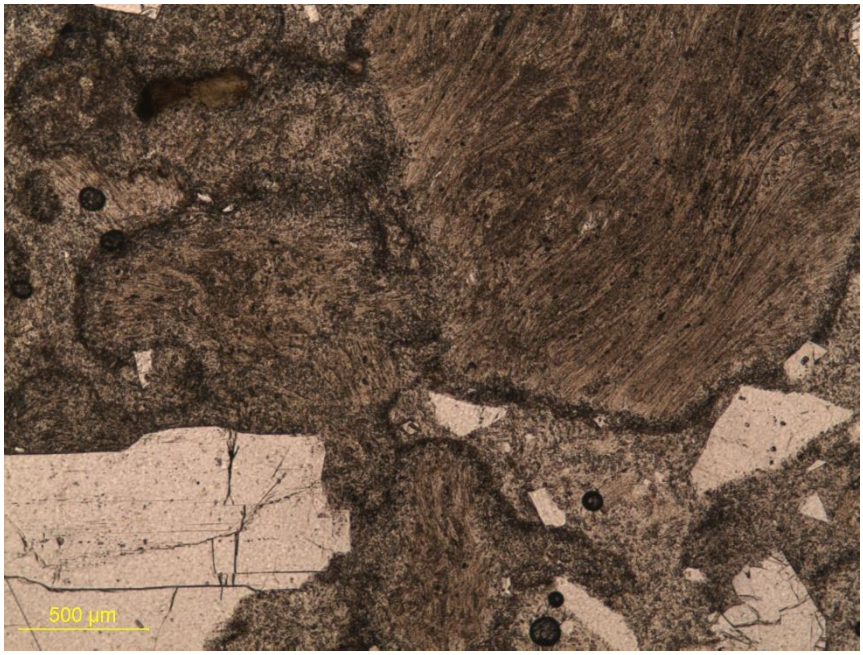

Sample: 37A

Lithology: Tahuna Formation

Well: KA37A

Depth: 160 mCHF

Description: Pumiceous rhyolitic tuff: lithics of rhyolite lava, xtl-poor (qz + pl)

XRD results:

Sample	Quartz	Illite
37A	85	15

Photomicrographs:

Cross polarised light

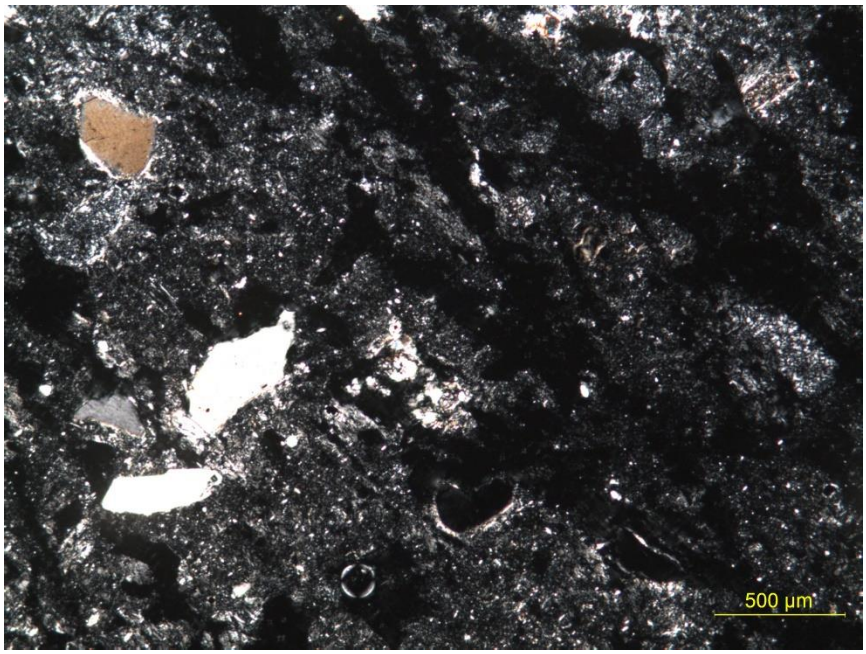

Plain polarised light

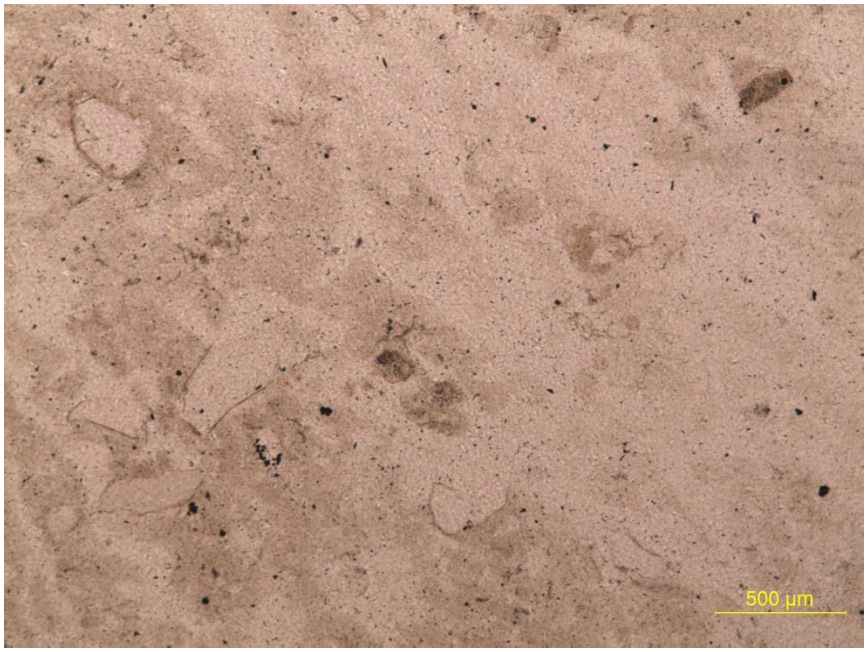

Electronic Appendices

- Electronic Appendix 1 contains the Collar, Survey and Interval tables used to construct the Leapfrog Geo model, Leapfrog Viewer file of the model, and a video showing the construction of the Leapfrog Geo model discussed in Chapter 4.
- Electronic Appendix 2 contains initial details of the samples, laser sizer report, XRD graphs, and raw compressibility testing results used in Chapter 5.